Benha University

Faculty of Engineering

A study to design an ultrasound cylindrical phased array used for hyperthermia treatment

by

Eng. Ayman Soliman Selmy Mohamed

A thesis submitted
in partial fulfillment of the requirements for the
Master degree of Science
in Electrical Engineering Technology

Supervised by

Asoc.Prof. Mahmoud Fathy Mahmoud
Faculty of Engineering
Benha University

Dr. Wael Abdel-Rahman Mohamed
Electrical Engineering Department
Faculty of Engineering
Benha University

2014

The undersigned have examined the thesis entitled '**A study to design an ultrasound cylindrical phased array used for hyperthermia treatment**' presented by **Ayman Soliman Selmy Mohamed**, a candidate for the Master degree of Science in electrical engineering technology and hereby certify that it is worthy of acceptance.

Approved by the Examining Committee:

Prof. Salah Ghazy Ramadan, Benha University

Interior Examiner and Committee Chairperson

Prof. Nahed Hussen Saloma, Cairo University

Exterior Examiner

Asoc Prof. Mahmoud Fathy Mahmoud, Benha University

Thesis Advisor and Examiner

Accepted for Electrical Engineering Department:

Asoc Prof. Ghada Mohamed Amer

Department Chairman

Accepted for the Post Graduate Affairs:

Prof. Hesham Mohamed Elbatsh

Vice Dean for post graduate studies

Accepted for the Faculty:

Prof. Mohammed El-Sayed Basiouny

Dean of the Faculty of Engineering

Abstract

Breast cancer is usually treated with surgery, radiotherapy and chemotherapy. Fever-range hyperthermia treatments (HT) enhance the effect of radiotherapy and chemotherapy in terms of local tumor control and survival rates. Electromagnetic (EM) radiation is commonly used; however there is an increasing interest for using ultrasound (US) due to the larger penetration depth and better focusing capabilities. An adequate applicator for fever-range HT treatment of tumors in the entire intact breast region is not yet available. The purpose of this work is to describe the theoretical design and characterization of an ultrasound cylindrical phased-array applicator. The US applicator is used to compute heating profiles in breast tumors and the results are obtained.

In this thesis, breast models are constructed from human data that is obtained from Computed Tomography (CT) and Magnetic Resonance Imaging (MRI) scans. Design parameters such as frequency, number of physical elements, width of element, kerf (spacing between element), and display angle of ultrasound transducer are optimized to obtain the smallest possible focus. The field ii program will be used for simulating ultrasound transducer fields and ultrasound imaging using linear acoustics. The k-Wave toolbox is developed to show how the nonlinear beam pattern from an ultrasound transducer can be modeled.

List of publications

[1] Ayman S. Selmy, Wael A. Mohamed, and Mahmoud F. M., "A Study to Design an Ultrasound Cylindrical Phased Array Used for Hyperthermia Treatment", J Am Sci, Vol 9, Issue 12, pp.68-76, (2013).

ACKNOWLEDGMENT

I would like to thank my God who shows me the way and makes me able to finish this work.

The help of many people achieved the completeness of this work. First, I would like to thank my supervisor **Asoc.Prof. Mahmoud Fathy Mahmoud** for his help, assistance, and encouragement during the years. No words are sufficient to express my deep gratitude toward my supervisor **Dr. Wael Abdel-Rahman Mohamed** who gives me a lot of time and helpful advices and materials over the years. He was not only my supervisor but also an example I think I will never be in his level.

Also, I would like to thanks to all members of my department of electrical engineering, benha faculty of engineering, benha university for their during last years to finish my works.

I would like to express my heartfelt thanks to my beloved father and mother for her blessings, my wife for her help and my brother's wishes for the successful completion of this work.

Contents

List of Figures

Chapter One: Introduction

1.1 Hyperthermia

In cancer treatment, hyperthermia became important as it increased significantly the therapeutic success and clinical management. Numerous biological and clinical investigations have demonstrated that hyperthermia in the 40-45°C range can significantly enhance clinical responses to radiation therapy, and has potential for enhancing other therapies, such as chemotherapy, immunotherapy and gene therapy [1].

Furthermore, high temperature hyperthermia (greater than 50°C) alone is being used for selective tissue destruction as an alternative to conventional invasive surgery. The degree of thermal enhancement of these therapies is strongly dependent on the ability to localize and maintain therapeutic temperature elevations, due to the often heterogeneous and dynamic properties of tissues, most notably blood perfusion and the presence of thermally significant blood vessels, therapeutic temperature elevations are difficult to spatially and temporally control during these forms of hyperthermia therapy. However, ultrasound technology has significant advantages that allow for a higher degree of spatial and dynamic control of the heating compared to other commonly utilized heating modalities [1].

1.2 Objectives of the Thesis

The aim of this thesis is to study the hyperthermia and its application in the breast cancer.

The following are the thesis objectives:

- To describe the system of imaging using ultrasound.
- To analyze the current therapies of breast cancer.
- To simulate the fetus phantom using field II program and then apply this program to the breast cancer.
- To evaluate the heat distribution in the breast using k-wave toolbox.

1.3 Organization of the Thesis

Chapter 2

In this chapter, the basic characteristics of ultrasound and its parameters are discussed. The system of imagining using ultrasound is described. Types of transducers, modes of imaging, beamforming and image resolution are explained.

Chapter 3

In this chapter, the breast cancer and its relevance to current therapies will be discussed. The histological basis, the ductal carcinoma of no special and special types of breast cancer, tumor grading, the staging of breast cancer and prognostic indices are described. Treatment of breast cancer is considered.

Chapter 4

In this chapter, the analysis of field II program, materials and methodology is discussed. The field II simulation and anatomic phantoms is explained. Finally, the results are obtained.

Chapter 5

In this chapter, the k-wave toolbox is reviewed. The simulation of photoacoustic wave field is discussed. The results are explained with all changing parameters of ultrasound transducers.

Chapter 6

Finally, the conclusions and future works are provided.

1.4 Review of Literatures

Hyperthermia can inhibit the tumor proliferation and in many cases the size of the tumors decreasing by the treatment [2]. The perfusion rate of blood in the tumors is inadequate. This reasoned that same dose of irradiation gives higher temperatures in the tumor than in the surrounding tissues. The surrounding tissues supplied the tumors with blood. The inside of the tumor is necrotized and the intermediate zone is anoxic because the oxygen absence. During the irradiation the aeration intensity of the cells are increasing because the temperature increasing. The oxygen demands of the cells are indirect ratio with the temperature. The chance of survive of the irradiated cells are decreased when the bloods supply can't adapt to the increased cell activity at higher temperatures. Based on these, the cancerous cells will be necrotize because the oxygen absence during ultrasound treatment and the surrounding tissues remains intact. This is the theory of the respiration type hyperthermia. The method is effective, when the temperature of the tumor is between 43-45°C. Between 37- 42°C, the cell proliferation in the tumors increasing. The necessary treatment period usually from half to one hour on 43°C. From 43-46°C, the irradiation period is halved with every centigrade, however the temperatures above 46°C to endangered the surrounding tissues. Based on these, the optimal treatment period is one hour between 42-43,5°C (315-316,5K). In the case of denaturing hyperthermia, the temperature of treatments are over on 43,5°C and the target zones are considerably close and the effect based on the cell protein denaturing. treated cancer cells with ultrasound in water baths with 42°C and concluded that the proliferation of the cells increased to 30min but after decreased [3]. treated prostates with self-tuning ultrasound hyperthermia system with 43-45°C [4]. The advantage of the method is that the control of the ultrasound intensity based on the actual temperatures, and not on the knowledge of heat physical parameters of the tissues. the most effective temperature and period is 43-45°C and 30-60min to the prostate cancer therapy [5]. the application of ultrasound hyperthermia is most reasoned when the patient's has other diseases too (e.g. heart disease) [6]. Examined the tissue ablation effect caused by focused ultrasound with finite element modeling technique [7]. The calculation capable modeling the nonlinear acoustic phenomena and solves the electromechanic and bioheat equations in 2D/3D inhomogeneous elastic and acoustic media. the thermal effect of ultrasound on soft tissues

and these results were applied by Heimburger (1985) [8], for treating deep breast tumors, lung tumors, in eye therapy, and in treating prostate hypertrophy, respectively. Based on the observation of Fry (1993), high intensity focused ultrasound (HIFU) has two types of effect. One of them is the lesion or cut that spreads in a regular way in the focus by way of heat coagulation. The other effect is that vapors are generated in the focus and these vapors rapidly expand towards the ultrasound source. It is proved that due to vaporization a gas body can be formed, or even cavitation may occur inthe tissue range located in the focal point of ultrasound [9]. this can be a factor limiting the intensity of focused coagulate ultrasound applied in hyperthermia. Properties of the tissues are changed by the initial focused ultrasound beam, e.g., the absorption, scattering, focal point are changed. linear models are applied for studying the effect of heat generated in the tissues by ultrasound [10]. Non-linear models based on e.g. the KZK equations [11] were applied by Christopher and Parker (1991).These models calculate the propagation properties of shock waves in body tissues.

Chapter Two: Physics of Ultrasounds

In this chapter, the basic characteristics of ultrasound and its parameters are discussed. The system of imagining using ultrasound is described. Types of transducers, modes of imaging, beamforming and image resolution are explained.

2.1 Basic Characteristics of Ultrasounds

2.1.1 Ultrasound Waves

Ultrasound is becoming increasingly important in medicine both as a diagnostic and therapeutic modality; and is now taking its place as an important diagnostic tool for imaging the breast, then is used for therapeutic the breast cancer.

Ultrasound is a mechanical vibration of matter that perturbs the particles of the medium around their mean positions. The frequency of the excitation is above the audible range, which is usually taken to be 20 kHz, but in practical systems the ultrasound frequencies used are between 2 and 20 MHz‘s. If the medium is elastic, the oscillating particles produce adjacent regions of compression and rarefaction and in this way the vibration initiated at one location can propagate through the medium. The origin of an ultrasound wave is, therefore, the pressure change that occurs when an elastic medium is compressed or expanded. It is this pressure disturbance that propagates and no net displacement of the particles occurs [12].

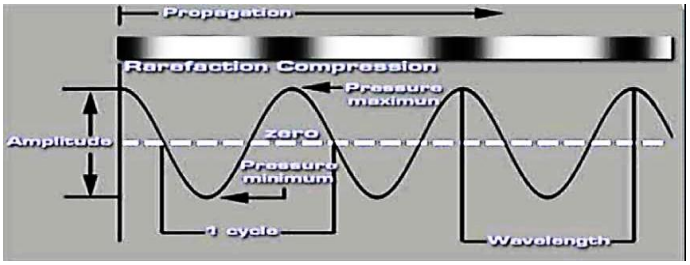

Figure 2.1: Propagation of sound waves [13].

2.1.2 Parameters of Sound Waves

The main parameters and equations of sound waves are:

- The wave length λ (m): is the horizontal length of one cycle of the wave.
- The period T (sec): is the time required for one wave length to pass a certain point.
- The amplitude A (m): is the maximum value of the wave function.
- The frequency f (Hz): is related with the period.

  $$f=1/T \qquad (2.1)$$
- The speed of sound c (m/s): is independent of the above parameters of the sound waves.

  $$ɹ=c/f \qquad (2.2)$$

The acoustic parameters of the medium are its density ρ and adiabatic compressibility κ. It is the local changes in those two parameters that allow sound to propagate. The propagation speed of the disturbance is a property of the medium and is given by:

$$\boldsymbol{c} = \sqrt{\frac{\mathbf{1}}{\boldsymbol{\rho 0 k}}} = \sqrt{\frac{\boldsymbol{B}}{\boldsymbol{\rho 0}}} \qquad (2.3)$$

Where $\rho 0$ is the mean density and B is the adiabatic bulk modulus, assuming no net transfer of energy from the wave to the medium [3]. The speed of sound and the density of various tissues in the human body are given in table 2. 1.

Table 2.1: Approximate densities and sound speeds in human tissues [13].

Medium	Density [kg/m^3]	Speed of sound [m/s]
Air	1.2	333
Lung	0.40×10^3	650
Distilled water	1.00×10^3	1480
Blood	1.06×10^3	1566
Fat	0.92×10^3	1446
Kidney	1.04×10^3	1567
Liver, spleen	1.06×10^3	1566
Muscle	1.07×10^3	1542-1626
Bone	$1.38-1.81\times10^3$	2070-5350
Brain	1.03×10^3	1505-1612

2.1.3 History of Ultrasound

The discovery of high frequency sound waves (ultrasound) was done by Lazzaro Spallanzani. The first mathematical description of sound waves was done in 1877 by Lord Rayleigh. The breakthrough came from Pierre Curie in 1880 with his discovery of piezoelectric effect. So, the reception of ultrasound waves was possible for first time. In 1914, underwater sonar navigation systems for submarines were developed to detect icebergs underwater from 2 miles away. In 1924 first radar (Radio Detection And Ranging system) was invented by Edward Appleton. In 1930s, Ultrasound Metal Flow detectors were constructed in order to check the integrity of the armor plates of battle tanks. In 1940, first claims on the effectiveness of ultrasound as curing modality were made.

The same year Gont and Wedkid presented the first paper that explored the possibility of using ultrasound as a diagnostic tool. So, the history of ultrasound imaging for medical diagnosis starts in the 1950s. Since then, the progress in the field has been enormous moving from the first single-line A mode systems to real-time high resolution images of anatomy and blood-flow.

Nowadays, diagnostic ultrasound is used in more than 25% of all medical imaging clinical procedures. It is used in virtually every medical specialty, with high popularity in obstetrics and cardiology. The great

success of medical ultrasound lies primarily in low cost, mobility, safety, high processing speed and ability to integrate anatomical information with blood velocity monitoring in real-time.

2.2 Description of Basic System of Ultrasound Imaging

2.2.1 Generation of Ultrasound

Before analyzing these steps we have first to mention how the ultrasounds are created. In the figure below we can see the generation of an ultrasound with the use of piezoelectric effect.

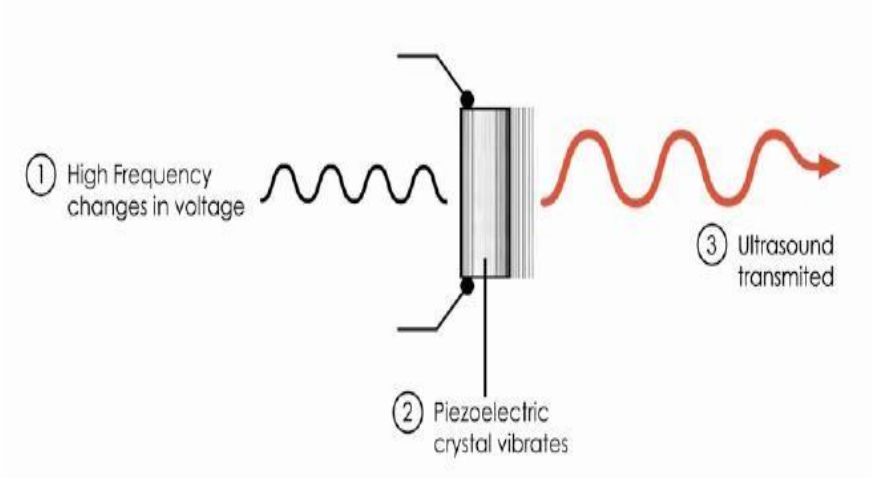

Figure 2.2: Generation of an ultrasound wave with the use of piezoelectric effect [12].

The way that an ultrasound wave is generated in almost all the available transducers is the use of piezoelectric crystal. Piezoelectric comes from the Greek words –Piezo which means "puss of exert pressure" and –electric" which means –electricity". As it is obvious the terms piezoelectric refers to materials which when a voltage is applied on them then convert the signal into pressure oscillations in their surface via mechanical deformations. With the same way if a mechanical force is applied on the material this is then converting into electrical energy.

This way by applying an electrical signal on one piezoelectric material we can monitor it, just by monitoring the voltage at the edges of the material [12-13].

2.2.2 Types of Transducers

In this principle of piezoelectric effect the transducers are based in order to transmit and receive ultrasound waves. In figure 2.3, we can see a schematic of the parts of a typical ultrasound transducer.

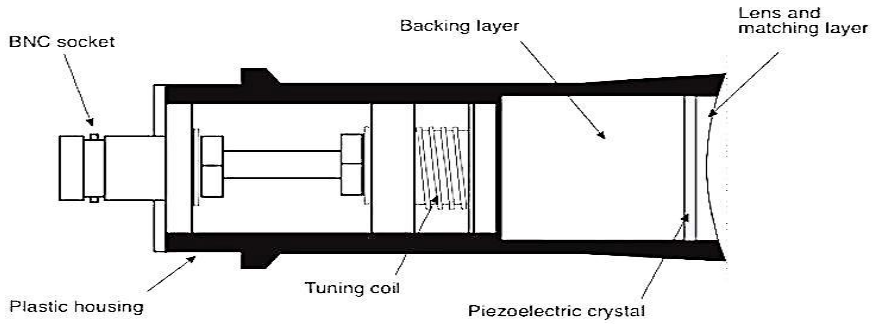

Figure 2.3: Schematic of typical transducer [3].

In order to avoid as possible the mismatch of the importance between the probe and the skin(in order to have low reflection coefficient and more acoustic energy to propagate in the body) a matching layer is used, which can also have a concave shape in order to achieve better focusing of the ultrasound beam. Behind the piezoelectric material is a sound absorbing backing layer is attached to it, in order to limit the mechanical ringing. The drawback with these backing layers is that they absorb a big portion of the backscattered energy and thus reducing the sensitivity of the transducer. This leads into an inevitable trade-off between the sensitivity and the bandwidth of the transducer.

The resonant frequency of the transducer is determined by the thickness of the slab. Ultrasound systems operate in frequency range of 1 to 30 MHz depending on the application. Low range frequencies (1 to 5 MHz) are used in obstetrics, abdominal, liver scans and for cardiac

imaging. Medium range frequencies (5 to 10 MHz) are used for breast scanning, vascular procedures and in pediatrics. Higher frequencies give better resolution, but the penetration depth is small, due to the frequency-dependent tissue attenuation. High frequencies are used in ophthalmology, as well as in intravascular imaging.

In order to reduce the acoustic impedance between the probe and the skin, a matching layer is present. Matching layers can be made flat or have a concave shape for better focusing. In order to limit the mechanical ringing and to provide a short acoustic pulse, sound-absorbing materials are attached to the back of the crystal. Such high impedance backing layers, however, absorb a big portion of the energy reducing sensitivity. Thus, the main trade-off in the design of transducers is that between sensitivity and bandwidth. Air backing yields excellent reflection and high output, but does not dampen the oscillations on the crystal, resulting in narrow-band long pulses. Thus, the design of the backing material depends on the application. For most applications, transducers are designed to have a 50 to 75% relative bandwidth, which is a good compromise between ringing and acoustic output.

The piezoelectric material commonly used in commercial transducers is barium titanate or lead zirconate titanate (PZT) which is piezoceramics. The recent advent of piezocomposites in the transducer technology has improved dramatically the performance. Piezocomposites are new piezoelectric materials resulted from mixing polymers with PZT. Piezocomposites have smaller acoustic impedance and tunable electromagnetically coupling constant, allowing bandwidth higher than 100% without sacrificing sensitivity. High bandwidth is a valuable resource in ultrasound imaging which improves resolution and can improve image quality through techniques such as coded excitation and harmonic imaging [12-13].

The beam shape that is generated by a transducer is determined by the design and construction of the probe. The two main categories are:

- **Flat crystals**: create a straight acoustic beam up to a distance slightly higher than half the wavelength, which then starts diverging.

- Linear arrays: acquire a rectangular image. The most widely used multi-element transducer. Typically, linear array consists of 64 to 256 elements, which are formed by slicing the ceramic into individual elements, each of them having its own electrical connection. The geometry of a linear array is shown in figure 2.4.

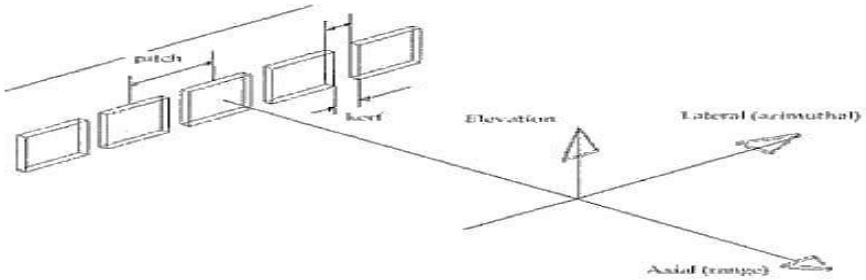

Figure 2.4: Geometry of a linear array and definitions of spatial imaging directions [2].

The center to center distance is called pitch and the gap between elements is the kerf of the array. The direction of the elements is called lateral (or azimuthal). The height of the elements corresponds to the elevation direction and the direction perpendicular to the transducer surface is the axial (or range direction).

In linear array imaging a focused beam can be transmitted into a region of investigation by selecting only the elements that are over the desired region, as shown in figure 2.5. In order to focus at a given depth, the applied delays on the active elements (sub-aperture) must have a concave profile, calculated from geometric optics. This implies that the elements act as omnidirectional point sources. The depth of the transmit focus can vary, by changing the curvature of the delay profile. The same or slightly larger sub- aperture can be

used in reception and similar delay profiles can be applied on the received trades to focus in the same direction. If the received data are stored in memory, several receive focal zones can be applied, or continuous dynamic focusing for every sample. However, only one focal zone is possible in transmit.

In modern scanners, more than one transmit focal zones can be placed at the cost of reducing the frame rate. This is done by transmitting with the same sub-aperture more than once using different focal depths and assembling the received data in depth [12, 13].

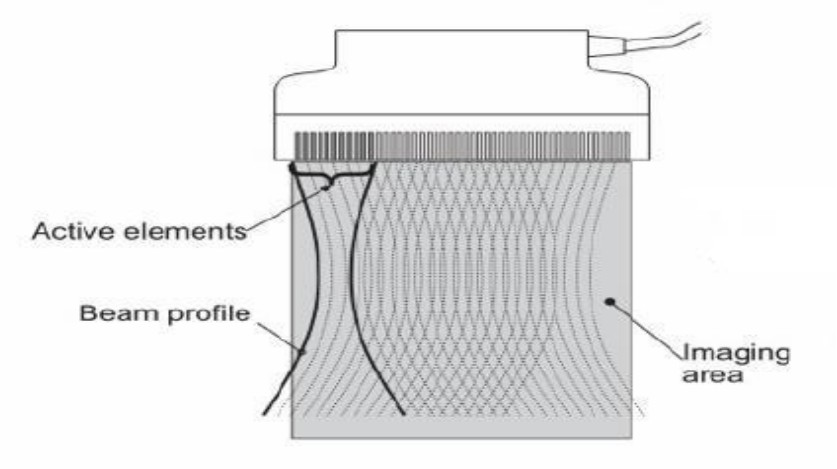

Figure 2.5: Linear array imaging [13].

- Phased arrays: these transducers have the same geometry as the linear arrays, but they have a much smaller footprint and can scan an area much smaller than the size of the aperture. For typical frequencies of 2 to 10 MHz, phased arrays are about 1 to 3 cm long, while the linear arrays are about 10 cm long.

They have a smaller number of elements compared to the linear array, typically 32 to 128 and their pitch is λ/2. It

is possible to scan an area much larger than the size of the aperture in the azimuthal direction.

Phased array imaging essentially implements electronically the scanning process of a mechanically rotating single – element transducer. All elements are used both in transmit and in receive. As in linear array imaging, only a single transmit focus is possible for every emission, while several receive focal zones can be applied. The idealized beam pattern sketched in figure 2.6 corresponds to three different receive foci. Phased arrays are used in cardiology, where there is only a small –acoustic window between the ribs and the labs [12-13].

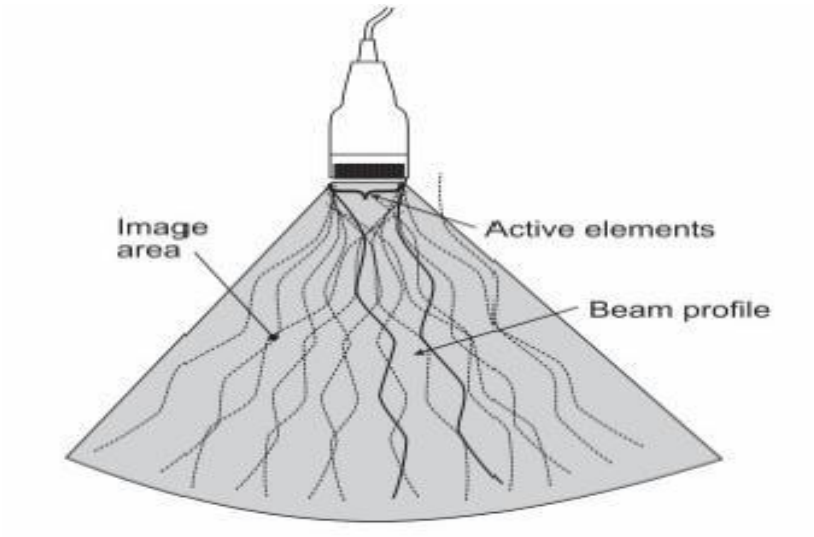

Figure 2.6: Phased array imaging [12].

- **Concave crystals** create a larger imaging region.

  - Convex arrays: in order to scan a sufficiently large region, the array has to be large. An alternative way to

obtain a larger imaging region is to use a rectilinear (or convex) array, in which the elements are placed on a convex surface as shown at the figure 2.7. The method for focusing and scanning is essentially the same as in linear array imaging. In this case, a sector scan is obtained, which is scan converted before display.

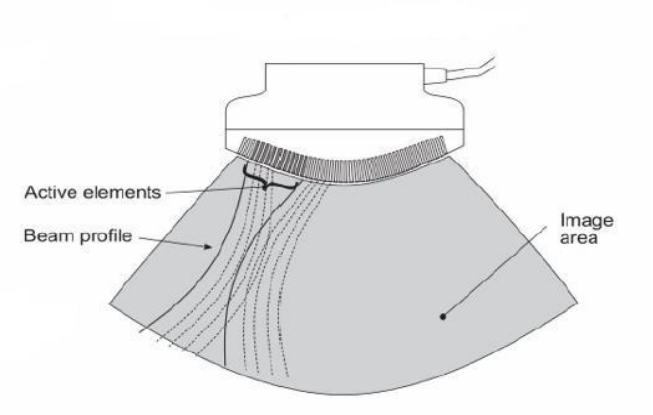

Figure 2.7: Convex array imaging [13].

2.2.3 Basic System Description.

After analyzing the generation of ultrasounds and the types of transducers, we can know analyze briefly the basic system description of medical ultrasound imaging system. The main steps followed are below [12-13].

- Transmission: mainly based on piezoelectric effect with types such as:
  - Single frequency transducers: transmit in one central frequency lower amplitude in near frequencies.
  - Broadband transducers: transmit equal amplitudes in a range of frequencies.

- Multi-frequency transducers: choice of central transmitting frequency.

- Reception: the backscattered echoes carry information about the structures along its propagation path. The echoes are converted to electrical signal based on the inverse piezoelectric effect.

  - Amplitude of echo: reflectivity and scattering strength of the tissue.
  - Time that the echo arrived: depth of the scatterer (average speed the 1540 m/s is used).

- Time gain compensation: is an amplification procedure of the echo, in order to compensate for the severe energy loss from attenuation of ultrasound waves when they propagate through the tissues.

- Envelope detection: after amplification the envelope of echoes is detected. The echoes in an RF signal band-limited to the transducer bandwidth.

- Logarithmic compression: all quantities are expressed in a logarithmic scale in order to decrease the range of echoes, which is very wide. The log- scale in terms of amplitude is calculated by:

$$dB = 20.log\frac{A}{A_0} \qquad (2.4)$$

- Display modes (ways of depict):

  - A-mode: Amplitude Mode was the first mode ever used. Ultrasound pulse is sent to one direction. The backscattered echo was captured and was presented in x-y axis and the amplitude as a function of depth. It is used only to measure distance.

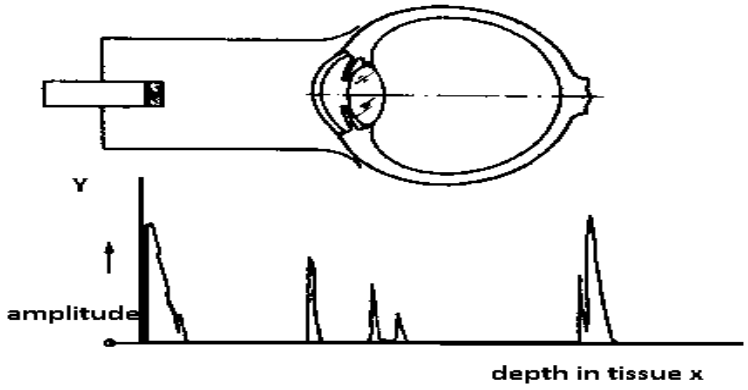

Figure 2.8: Diagram of an A-mode display [13].

- M-mode: Motion Mode is an evolution of A-mode. Provides information about the motion. In the M-mode several lines were emitted in the same direction and the backscattered echo was recorded (A-lines). By acquiring several A-lines and displaying each one side by side, information about the motion was seen. The acquired lines were presented in x-y axis, where x-axis corresponds to time and y-axis to the depth.

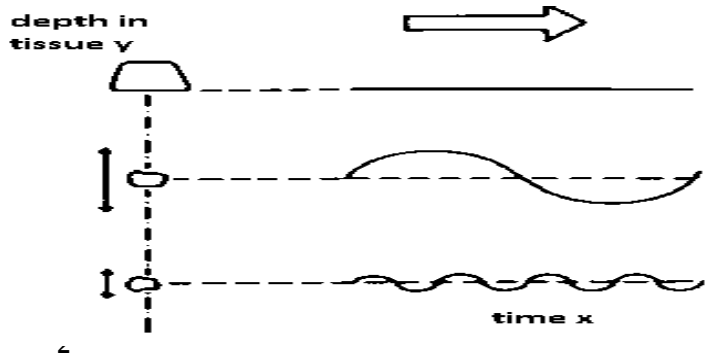

Figure 2.9: Diagram of an M-mode display [13].

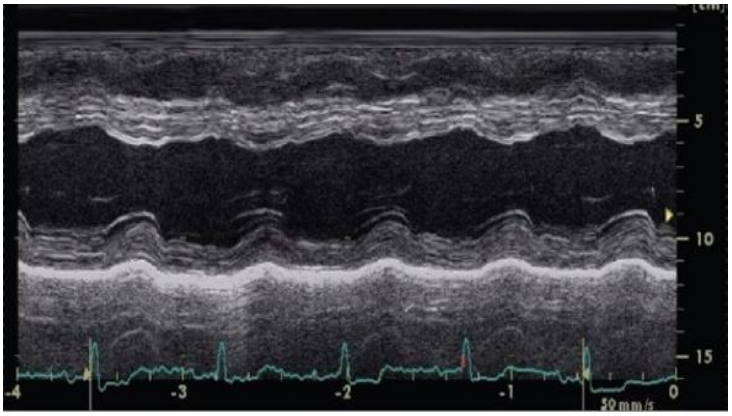

Figure 2.10: Representation of an M-mode display [13].

- B-mode: Brightness Mode is the breakthrough in the field of medical ultrasound. In the B-mode a series of focused fields, lines were transmitted in different direction, acquiring a series of A-lines that covered all the region of interest. The A-lines were then merged missing data were interpolated and a 2D image was created.

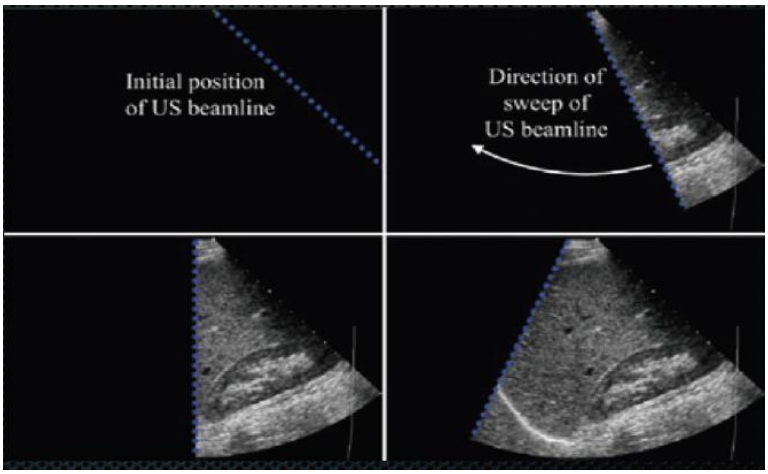

Figure 2.11: Representation of a B-mode display [3].

2.2.4 Properties of Ultrasound Images.

- Beamforming: is the manipulation of the elements of array transducers to enhance focusing and shape directivity of the beam. It is achieved electronically by changing the time delay and the amplitude of the voltage applied on each element. This is done by a beamformer that combines the echoes by delaying and summing those [13].

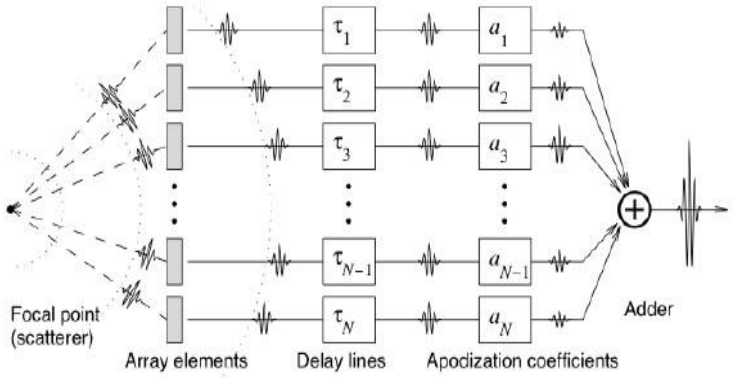

figure 2.13: Beamformer [3].

- Image resolution: is the ability of an imaging system to distinguish between closely-spaced scatterers. In system‘s Point Spread Function (PSF) the resolution is evaluated by the acoustic pulse interrogation of a medium with a single point scatterers places at the focus point. It has mainly three components axial, lateral, elevation [13].

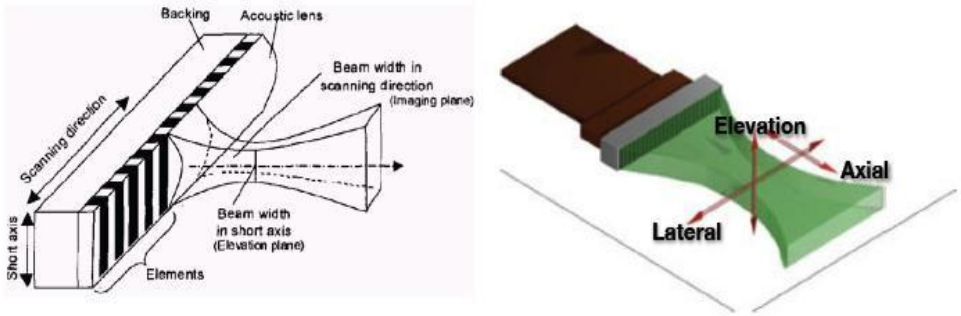

Figure 2.14: Components of image resolution [13].

- Axial resolution: is determined by the duration of the acoustic signal generated on each element, which in turns is determined by the central frequency and the bandwidth of the transducer. Transducers with high bandwidth operating at high frequencies generate short acoustic pulses with good axial resolution [13].

- Lateral (azimuthal) resolution: in general the lateral field of a focused beam consists of a main lobe and decreasing side lobes around the main lobe. The width of main lobe defines the lateral resolution; a beam with a narrow main lobe corresponds to a better lateral resolution. The purpose of the beamformer is to achieve a lateral resolution for a large axial distance around the focal point (depth of focus). In qualitative terms, lateral resolution is inversely proportional to the aperture size (i.e. a large aperture can yield more focused fields.

  More precisely, it is proportional at a first order approximation to the f-number, the ratio between axial focal distance and aperture size. Thus, acoustic fields can be focused more strongly close to the transducer. In order to obtain an ultrasound image with desirable uniform focusing characteristics, a beamform can, for instance, maintain a constant f-number, by updating constantly the delays and re-focus the beam for every depth with approximately constant lateral resolution and depth focus.

  Lateral resolution is also inversely proportional to the transmitted frequency. Therefore, migrating to higher frequencies improves lateral resolution, but reduces the penetration depth due to attenuation. The lateral side lobes of the field degrade image quality by masking weaker scatterers present at the lateral extend of a strong reflector. They can be reduced by applying apodization across the aperture, which can also vary with depth (dynamic apodization) [13].

- Elevation resolution: resolution in elevation is not directly visible in an ultrasound image, since it is the resolution on a plane orthogonal to the imaging plane. Similar to the lateral resolution, it is associated with the active acoustic aperture in that dimension. Linear arrays are often called one-dimensional arrays, since elements are positioned in one row along the azimuthal direction. Since there is only one element in the elevation direction, the beam characteristics outside the image plane cannot be controlled with the beamformer, and echoes coming outside the imaging plane degrade image quality. Commonly 1-D arrays built with concave-shaped elements in the elevation direction, in order to achieve a single focus.

2.3 Safety of Ultrasound

Because of the vast exposure of the general population to diagnostic ultrasound, any question of the possibility of harmful effects becomes very important. This is especially true for exposures of the fetus to ultrasound. In 1991, the US Government‘s Food and Drug Administration (FDA) began allowing the intensity of ultrasound used to scan the fetus to increase to 7.7 times its previous value, if manufacturers agreed to build new output displays into the ultrasound systems. While scientists have conducted many studies to try to determine whether there were any effects of ultrasound on the fetus, virtually all of these studies are of people exposed to ultrasound before the output levels were allowed to increase. Based on their concerns about the theoretical effects of ultrasound on the developing fetus, researchers have conducted epidemiological studies looking for associations between ultrasound exposure and various traits, particularly with problems in brain development, growth, and childhood cancers [15].

Even when an increase in a particular trait is associated, or linked, with ultrasound exposure in an epidemiological study, does not necessarily mean that ultrasound is the cause of the increase in the

trait. So far, there is published data on whether or not in utero ultrasound scans can be linked to any of these traits: low Apgar scores at birth, birth defects, speech or hearing disorders, diminished height or weight in childhood, birth defects, chromosomal abnormalities, childhood cancers, and developmental problems including learning disabilities. There is no conclusive evidence that any of these traits were caused by the in utero ultrasound exposure experienced by these children. However, there is evidence from some of these studies linking some of these traits to ultrasound exposure-evidence which needs further investigation in order to be sure that the more intense ultrasound used today could not be causing these effects. Many of the epidemiological studies only tracked a small number of people, rendering their conclusions less powerful. One way to get a bigger picture in cases like this is to review a whole group of studies that track a particular trait, in order to increase the number of people under consideration [15].

2.3.1 Standardization in Diagnostic Ultrasound

It is very important the subject of standardization in diagnostic ultrasound. The International Electrotechnical Commission (IEC) is included since it is the parent world standards organization. The IEC Subcommittee 29D (Ultrasonics Working Group on Medical Applications) is currently circulating a draft standard entitled –Methods of Measuring the Performance of Ultrasonic Pulse-Echo Diagnostic Equipment.

There are basically three types of standards:

1. Fundamental standards,
2. Engineering standards, and
3. User oriented operational standards.

1. Fundamental Standards:

Measurements of fundamental quantities such as the peak and average acoustic intensity in an ultrasound beam are often very difficult to perform. However, such measurements are presently being made at a number of institutions and should soon result in calibrated secondary standards for engineering measurements. There is no unanimity about the best method for measuring ultrasound intensity. Currently, the following techniques are being examined.

 Radiation Force: a method for measuring average intensity which uses the change in force (typically measured in micrograms) recorded as the deflection of a reflecting or absorbing target with incident ultrasound.

 Calorimetry: a classical method for measuring average power using the change in temperature due to ultrasound absorption in a fluid.

 Capacitive Transducers*:* a method for measuring both peak and average intensities using the modulation of the spacing of a charged parallel plate capacitor by an incident sound wave.

 Transducer Reciprocity Calibration*:* well-known method in sonar which allows a simple measurement of peak and average intensities provided the reciprocity parameters are known and are not seriously complicated by the near field diffraction pattern.

 Optical Diffraction*:* a method for measuring the peak and average intensity using the Debye- Sears effect.

Since no single technique is clearly superior, it seems certain that, some combination of these methods mill result I calibrating secondary standard piezoelectric transducers for research and engineering measurement.

2. Engineering Standards:

These standards are normally intended for measurements on subsystems to be performed by manufacturers and calibration centers. Traditional engineering methods and standards for measuring gain, bandwidth, noise level, electrical leakage, etc., are available. With the exception of the ultrasonic transducer and its radiation pattern, this area of standardization is well advanced, although the measurements can become tedious and, therefore, may be neglected unless mandated by law.

3. User Oriented Operational Standards:

Methods for checking the performance of complex ultrasound systems on a daily or weekly basis may literally be a matter of life or death. Whereas an oscilloscope out of calibration may mean the repeat of a test for an engineer, it may result in missed diagnosis with irretrievable results for the physician. Standards for use by the hospital technologist must be simple and easy to use since they will often be used by people with little or no background in science or engineering (in many larger hospitals, biomedical engineering technicians are just now filling this gap). The test must use a simple low cost device and should test the whole system as a "black box" to avoid manufacturers 'complaints. The traditional method in medicine is to employ a "phantom" or a standard object to be scanned [16].

Chapter Three: Breast Cancer and Hyperthermia Therapy

3.1 Introduction

Breast cancer is a type of cancer originating from breast tissue, most commonly from the inner lining of milk ducts or the lobules that supply the ducts with milk [17]. Cancers originating from ducts are known as ductal carcinomas, while those originating from lobules are known as lobular carcinomas. Breast cancer occurs in humans and other mammals. While the overwhelming majority of human cases occur in women, male breast cancer can also occur [18].

The benefit versus harms of breast cancer screening is controversial. The characteristics of the cancer determine the treatment, which may include surgery, medications (hormonal therapy and chemotherapy), radiation and/or immunotherapy[19]. Surgery provides the single largest benefit, and to increase the likelihood of cure, several chemotherapy regimens are commonly given in addition. Radiation is used after breast-conserving surgery and substantially improves local relapse rates and in many circumstances also overall survival [20].

Worldwide, breast cancer accounts for 22.9% of all cancers (excluding non-melanoma skin cancers) in women [21]. In 2008, breast cancer caused 458,503 deaths worldwide (13.7% of cancer deaths in women) [21]. Breast cancer is more than 100 times more common in women than in men, although men tend to have poorer outcomes due to delays in diagnosis [22-23].

Prognosis and survival rates for breast cancer vary greatly depending on the cancer type, stage, treatment, and geographical location of the patient. Survival rates in the Western world are high [22]. For example, more than 8 out of 10 women (84%) in England diagnosed with breast cancer survive for at least 5 years [18]. In developing countries, however, survival rates are much poorer.

3.1.1 Signs and Symptoms

The first noticeable symptom of breast cancer is typically a lump that feels different from the rest of the breast tissue. More than 80% of breast cancer cases are discovered when the woman feels a lump [24]. The earliest breast cancers are detected by a mammogram [25]. Lumps found in lymph nodes located in the armpit [24]. Can also indicate breast cancer.

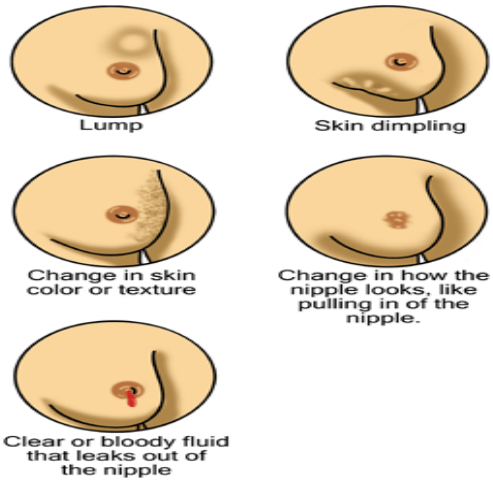

Figure 3.1 Early signs of breast cancer [24].

Indications of breast cancer other than a lump may include thickening different from the other breast tissue, one breast becoming larger or lower, a nipple changing position or shape or becoming inverted, skin puckering or dimpling, a rash on or around a nipple, discharge from nipple/s, constant pain in part of the breast or armpit, and swelling beneath the armpit or around the collarbone [26]. Pain ("mastodynia") is an unreliable tool in determining the presence or absence of breast cancer, but may be indicative of other breast health issues [24-25].

Inflammatory breast cancer is a particular type of breast cancer which can pose a substantial diagnostic challenge. Symptoms may resemble a breast inflammation and may include itching, pain, swelling, nipple inversion, warmth and redness throughout the breast, as well as an orange-peel texture to the skin referred to as peau d'orange [24]. The absence of a discernible lump may delay detection dangerously.

Occasionally, breast cancer presents as metastatic disease-that is, cancer that has spread beyond the original organ. The symptoms caused by metastatic breast cancer will depend on the location of metastasis. Common sites of metastasis include bone, liver, lung and brain [28]. Unexplained weight loss can occasionally herald an occult breast cancer, as can symptoms of fevers or chills. Bone or joint pains can sometimes be manifestations of metastatic breast cancer, as can jaundice or neurological symptoms. These symptoms

are called non-specific, meaning they could be manifestations of many other illnesses [29].

3.1.2 Risk Factors

The primary risk factors for breast cancer are female sex and older age [30]. Other potential risk factors include: lack of childbearing or lack of breastfeeding. Higher levels of certain hormones, [31-32]. Certain dietary patterns and obesity.

3.1.3 Pathophysiology

Breast cancer, like other cancers, occurs because of an interaction between an environmental (external) factor and a genetically susceptible host. Normal cells divide as many times as needed and stop. They attach to other cells and stay in place in tissues. Cells become cancerous when they lose their ability to stop dividing, to attach to other cells, to stay where they belong, and to die at the proper time.

3.1.4 Diagnosis

Most types of breast cancer are easy to diagnose by microscopic analysis of a sample or biopsy of the affected area of the breast. There are, however, rarer types of breast cancer that require specialized lab exams.

The two most commonly used screening methods, physical examination of the breasts by a healthcare provider and mammography, can offer an approximate likelihood that a lump is cancer, and may also detect some other lesions, such as a simple cyst [33]. When these examinations are inconclusive, a healthcare provider can remove a sample of the fluid in the lump for microscopic analysis (a procedure known as fine needle aspiration, or fine needle aspiration and cytology-FNAC) to help establish the diagnosis. The needle aspiration may be performed in a healthcare provider's office or clinic using local anaesthetic if required. A finding of clear fluid makes the lump highly unlikely to be cancerous, but bloody fluid may be sent off for inspection under a microscope for cancerous cells. Together, physical

examination of the breasts, mammography, and FNAC can be used to diagnose breast cancer with a good degree of accuracy.

Other options for biopsy include a core biopsy or vacuum-assisted breast biopsy [34]. Which are procedures in which a section of the breast lump is removed; or an excisional biopsy, in which the entire lump is removed Very often the results of physical examination by a healthcare provider, mammography, and additional tests that may be performed in special circumstances (such as imaging by ultrasound or MRI) are sufficient to warrant excisional biopsy as the definitive diagnostic and primary treatment method.

3.1.5 Prevention

Women may reduce their risk of breast cancer by maintaining a healthy weight, drinking less alcohol, being physically active and breastfeeding their children [35]. These modifications might prevent 38% of breast cancers in the US, 42% in the UK, 28% in Brazil and 20% in China [35]. The benefits with moderate exercise such as brisk walking are seen at all age groups including postmenopausal women [35-36]. Marine omega-3 polyunsaturated fatty acids appear to reduce the risk.

Removal of both breasts before any cancer has been diagnosed or any suspicious lump or other lesion has appeared (a procedure known as prophylactic bilateral mastectomy) may be considered in people with BRCA1 and BRCA2 mutations, which are associated with a substantially heightened risk for an eventual diagnosis of breast cancer [37-38].

The selective estrogen receptor modulators (such as tamoxifen) reduce the risk of breast cancer but increase the risk of thromboembolism and endometrial cancer [39]. There is no overall change in the risk of death [39]. The benefit of breast cancer reduction continues for at least five years after stopping a course of treatment with these medications [40].

3.1.6 History

Because of its visibility, breast cancer was the form of cancer most often described in ancient documents [41]. Because autopsies were rare, cancers of the internal organs were essentially invisible to ancient medicine. Breast cancer, however, could be felt through the skin, and in its advanced state often developed into fungating lesions: the tumor would become necrotic (die from the inside, causing the tumor to appear to break up) and ulcerate through the skin, weeping fetid, dark fluid [41].

The oldest description of cancer was discovered in Egypt and dates back to approximately 1600 BC. The Edwin Smith Papyrus describes 8 cases of tumors or ulcers of the breast that were treated by cauterization. The writing says about the disease, "There is no treatment." [42]. for centuries, physicians described similar cases in their practices, with the same conclusion. Ancient medicine, from the time of the Greeks through the 17th century, was based on humoralism, and thus believed that breast cancer was generally caused by imbalances in the fundamental fluids that controlled the body, especially an excess of black bile. Alternatively, patients often saw it as divine punishment. In the 18th century, a wide variety of medical explanations were proposed, including a lack of sexual activity, too much sexual activity, physical injuries to the breast, curdled breast milk, and various forms of lymphatic blockages, either internal or due to restrictive clothing[43]. In the 19th century, the Scottish surgeon John Rodman said that fear of cancer caused cancer, and that this anxiety, learned by example from the mother, accounted for breast cancer's tendency to run in families [43].

Although breast cancer was known in ancient times, it was uncommon until the 19th century, when improvements in sanitation and control of deadly infectious diseases resulted in dramatic increases in lifespan. Previously, most women had died too young to have developed breast cancer [43].

Additionally, early and frequent childbearing and breastfeeding probably reduced the rate of breast cancer development in those women who did survive to middle age [43].

Because ancient medicine believed that the cause was systemic, rather than local, and because surgery carried a high mortality rate, the preferred treatments tended to be pharmacological rather than surgical. Herbal and mineral preparations, especially involving the poison arsenic, were relatively common.
Breast cancer staging systems were developed in the 1920s and 1930s.

During the 1970s, a new understanding of metastasis led to perceiving cancer as a systemic illness as well as a localized one, and more sparing procedures were developed that proved equally effective. Modern chemotherapy developed after World WarII [44].

The French surgeon Bernard Peyrilhe (1737–1804) realized the first experimental transmission of cancer by injecting extracts of breast cancer into an animal.

In the 1980s and 1990s, thousands of women who had successfully completed standard treatment then demanded and received high-dose bone marrow transplants, thinking this would lead to better long-term survival. However, it proved completely ineffective, and 15–20% of women died because of the brutal treatment [45].

The 1995 reports from the Nurses' Health Study and the 2002 conclusions of the Women's Health Initiative trial conclusively proved that hormone replacement therapy significantly increased the incidence of breast cancer [45].

3.1.7 Tissue Geometry

The incidence of the beam is perpendicular to the tissue layers [46]. The beam transmission surface is

$$S = ab\ [cm^2] \qquad (3.1)$$

where a the width and b the length of transducer in cm. The treated tissue volume is

$$V = Sh\ [cm^3] \qquad (3.2)$$

where S is the surface and h is the tissue thickness in cm. The treated tissue mass is:

$$M = V\rho\ [g] \qquad (3.3)$$

where ρ, g/cm3 the density of tissue.

From the multiplication of treated tissue mass and specific heat C [J/gK], the energy needed for increasing the temperature of the subject tissue by 1K can be calculated in J/K.

3.1.8 Perfusion rate of blood

The knowledge of perfusion rate of blood in the treated tissue volume [46]:

$$\mathrm{gblood/gactuallytissuemass/min\ (BB2)} \quad (3.4)$$

based on the:

$$\mathrm{ml/gtissue/min\ (BB1)} \quad (3.5)$$

connection. The calculation of BB2 requires the knowledge of blood and tissue densities and the treated tissue volume. When using the perfusion rate of blood/minute value, the model assumes that this is the quantity of blood that is present in the subject tissue at any time. Of course, the realistic value may differ from this quantity and this blood quantity changes further during the treatment as a result of the increased perfusion rate and heart rate. Due to this, the perfusion rate of blood is considered by the model as an input parameter, that is it can be adjusted for the individual tissues on the operator window. The length of the path of the sound beam in the blood flowing through the tissues is also a factor of decisive importance.

This means that the height of blood in the irradiated tissue volume determined by the irradiation surface S, cm and the thickness of the specific tissue shall be determined. This corresponds to those assumptions that the

vascular system of the tissues is so dense and the walls of the blood vessels are so thin, that the heat exchange between the tissues and blood can be considered instantaneous. As a consequence of this, it is enough to determine the quantity of blood in the treated tissue volume having a specific surface, and through this to determine the height of the blood body in the tissue, hb, cm with the

$$hb = (BB2/\rho b)/S \qquad (3.7)$$

formula in order to calculate the heat generated in the blood present in the tissue by the irradiated acoustic energy, and to correct the generated heat J/s by heat energy factors representing the quantity of heat transported to, and from, the treated tissues by the perfusion of blood[46].

3.1.9 Intensity connections

In order to determine the different intensity changes, the sound intensity is calculated in the following units of measure: W/cm^2, dB and Np. From the emitted total electric intensity Ie, W=J/s, the initial acoustic intensity Ii can be calculated by using the initial acoustic intensity, W and the electro-acoustic coefficient (η, %) of efficiency according to the equation[46]:

$$Ii=Ie\eta \qquad (3.8)$$

The acoustic intensity per surface unit in W/cm^2 can be calculated from formulae:

$$Is=Ii/S \qquad (3.9)$$

Traditional way of recalculating this variable in dB unit of measure is shown by the equation

$$dB=10\log10(IS/IO) \qquad (3.10)$$

where $I0=10^{-16}$ [W/cm^2].

Recalculation of INp from this equation is described by

$$INp=IdB/8{,}686. \qquad (3.11)$$

Of course, the units of measure can also be recalculated backward using the inverse forms of the appropriate equations. Attenuation caused by the specific tissue volume can be calculated by

$$I=I0e-2\alpha h \qquad (3.12)$$

where INp is the actual Np intensity and I0is the initial intensity expressed in Np, α is the attenuation coefficient (Np/cmMHz), and h is the length of the path of the sound beam in the given medium expressed in cm. From here the model calculates the W/cm^2 intensities for each media backwards through IdB, then it determines the reflections R at the medium interfaces and through this, the transmitted intensity T. If it is assumed that the incidence is perpendicular to the interface between the media, the rate of reflection is

$$R= (Z2-Z1)/ (Z1+Z2) \qquad (3.13)$$

which is a function of the difference between the acoustic hardness (PaS/m) of the media

$$Z=c\rho \qquad (3.14)$$

where c, m/s is the sound velocity, ρ, g/cm^3 is the density, Z1and Z2 are the acoustic hardness of the resultant and receiving media, respectively. From these results the level of relative sound intensity transmitted through the interface can be calculated from

$$T=1-R \qquad (3.15)$$

provided that 1=100%, that is in the absolute acoustic intensity, the acoustic intensity going through the interface between the media in W/cm^2. The heat energy generated in the examined tissue volume can be calculated by the equation

$$dT/dt=2\alpha I/C\rho, [K/s] \qquad (3.16)$$

provided that both the numerator and the denominator of the formula have been corrected by the distance covered and by the treated tissue volume, respectively. By solving this equation to sec K can be arrived at, namely the result show how much the temperature increases in the system in a given period of time where C is the specific heat J/gK of the examined tissue[46].

The reason why the Rayleigh-Sonnerfeld (Goodman, 1968) equation, the equation that handles xyz coordinates was not used in the model is that our goal was to calculate the spatial average temperature of the tissue volume to be treated and the model assumes that the position of the tissue volume to be treated is known, because this is the location where the transducers are focused to. If the calculation was carried out on the basis of the xyz coordinates, the application of the bioheat transfer equation (BHTE) (Pennes, 1948 and Sapareto and Dewey, 1984) would be necessary, although this equation does not deal with the presence of blood vessels and the changes in the perfusion rate of blood that occur during the treatment. The equation systems applied in the model are equivalent with the BHTE system without space coordinates and they take into consideration the input (feed energy) and output (losses) sides of the energy balance. The acoustic intensity reaching the tumor can be calculated as a sum of the residue intensities of all the transducers focused to the tumor, without considering the interferences. Generated heat is determined form this intensity by time units[46].

3.1.10 Main equation

Based on the above, the heat generated by the ultrasound in the individual tissue layers can be calculated from the next equation[46]:

$$\frac{dT}{dt} = \left(\left(\frac{2\alpha tht\big((IinputS) - (It + Icooling)\big)}{Ct\rho tVt} \right) + \left(\frac{2\alpha bhb\big((IinputS) - Ib\big)}{Cb\rho bVb} \right) \right) \left[\frac{K}{s} \right] \qquad (3.18)$$

where b the blood, t the tissue and c the cooling surface, and the result given in K/s. In the equations I_t, W/cm2 is the value of acoustic intensity at the tissue interface. This value shall be multiplied with the irradiated surface (S, cm^2) to calculate the total intensity arriving into a volume element. The symbol of It[J/s] is the heat flow towards the surrounding tissues, $I_{cooling}$ [J/s] towards the cooled transducer surface and the tissue interface located above the subject tissue layer, and Ib[J/s] the heat removed by the blood. The basic

expression that the treatments are carried out by sine waves at a frequency of 1 MHz. The frequency can be adjusted in the model and this results a modification of the attenuation coefficient α, Np/cmMHz [46].

3.1.11 Basic data

The basic data are shown in table 1. Parameters affecting the heat effect of treatment are: the emitted electric intensity, [W]; width and length of the transducer(s), [m]; number of transducers focused to the tumor [pc]; cooling surface of a transducer, [m2]; temperature of the cooling surface, [K]; thickness of skin, muscle and tumor layers, respectively, [m]; coefficient of acoustic efficiency of the transducer, [%].

Table 3.1.Basic data [46]

	Attenuation Coefficient, α [Np/cmMHz]	Sound velocity, c , [m/s]	Specific heat, C, [J/gK]	Heat conductivity, [J/msK]	Density, ρ, [g/cm^3]	Perfusion rate of blood, B1, [ml/g$_{tissue}$/min
Ceramic (c)		2220			7.6	
Electro acoustic coupling (co)		6320			2.7	
Skin (s)	0.24	1720	3.66	0.37	1.01	0.2
Muscle (m)	0.15	1566	3.639	0.55	1.04	0.027
Tumor (t)	0.085	1549	3.9	0.545	1.04	0.25
Blood (b)	0.019	1566	3.89		1.06	

3.1.12 Pink Ribbon

A pink ribbon is the most prominent symbol of breast cancer awareness. Pink ribbons, which can be made inexpensively, are sometimes sold as fundraisers, much like poppies on Remembrance Day. They may be worn to honor those who have been diagnosed with breast cancer, or to identify products that the manufacturer would like to sell to consumers that are interested in breast cancer-usually white, middle-aged, middle-class and upper-class, educated women.

The pink ribbon is associated with individual generosity, faith in scientific progress, and a "can-do" attitude. It encourages consumers to focus on the emotionally appealing ultimate vision of a cure for breast cancer, rather than on the fraught path between current knowledge and any future cures.

Figure 3.2 the pink ribbon symbol [45].

3.2 Hyperthermia Therapy

3.2.1 Introduction

Hyperthermia therapy is a type of medical treatment in which body tissue is exposed to slightly higher temperatures to damage and kill cancer cells or to make cancer cells more sensitive to the effects of radiation and certain anti-cancer drugs [48]. When combined with radiation therapy, it is called

thermoradiotherapy. Whole-body hyperthermia has also been found to be helpful for depression [49].

Local hyperthermia for certain small tumors is generally accepted, similar to surgically removing a tumor. Whole-body hyperthermia is generally considered to be a promising experimental cancer treatment.

Hyperthermia is only useful for certain kinds of cancer, and is not in widespread use. Hyperthermia is most effective when used alongside other therapies, so it is almost always used as an adjuvant therapy [50-51]. The most effective uses are currently being studied.

3.2.2 Mechanism

Hyperthermia may kill or weaken tumor cells, and is controlled to limit effects on healthy cells. Tumor cells, with a disorganized and compact vascular structure, have difficulty dissipating heat.

Hyperthermia may therefore cause cancerous cells to undergo apoptosis in direct response to applied heat, while healthy tissues can more easily maintain a normal temperature. Even if the cancerous cells do not die outright, they may become more susceptible to ionizing radiation therapy or to certain chemotherapy drugs, which may allow such therapy to be given in smaller doses.

Intense heating will cause denaturation and coagulation of cellular proteins, rapidly killing cells within a tumor. More prolonged moderate heating to temperatures just a few degrees above normal can cause more subtle changes. A mild heat treatment combined with other stresses can cause cell death by apoptosis. There are many biochemical consequences to the heat shock response within the cell, including slowed cell division and increased sensitivity to ionizing radiation therapy.

Hyperthermia can kill cells directly, but it's more important use is in combination with other treatments for cancer [52]. Hyperthermia increases blood flow to the warmed area, perhaps doubling perfusion in tumors, while increasing perfusion in normal tissue by ten times or even more [52]. This

enhances the delivery of medications. Hyperthermia also increases oxygen delivery to the area, which may make radiation more likely to damage and kill cells, as well as preventing cells from repairing the damage induced during the radiation session [53].

Cancerous cells are not inherently more susceptible to the effects of heat [52]. When compared in in vitro studies, normal cells and cancer cells show the same responses to heat. However, the vascular disorganization of a solid tumor results in an unfavorable microenvironment inside tumors. Consequently, the tumor cells are already stressed by low oxygen, higher than normal acid concentrations, and insufficient nutrients, and are thus significantly less able to tolerate the added stress of heat than a healthy cell in normal tissue [52].

Mild hyperthermia, which provides temperatures equal to that of a naturally high fever, may stimulate natural immunological attacks against the tumor. However it is also induces a natural physiological response called thermotolerance, which tends to protect the treated tumor [52].

Moderate hyperthermia, which heats cells in the range of 40 to 42 °C, damages cells directly, in addition to making the cells radiosensitive and increasing the pore size to improve delivery of large-molecule chemotherapeutic and immunotherapeutic agents (molecular weight greater than 1,000 Daltons), such as monoclonal antibodies and liposome-encapsulated drugs [52]. Cellular uptake of certain small molecule drugs is also increased [52]. Most local and regional cancer treatments are in this temperature range.

Very high temperatures, above 50 °C (122 °F), are used for ablation (direct destruction) of some tumors. [53]. this generally involves inserting a metal tube directly into the tumor, and heating the tip until the tissue next to the tube has been killed.

3.2.3 Heat Sources

There are many techniques by which heat may be delivered. Some of the most common involve the use of focused ultrasound (FUS or HIFU), infrared

sauna, microwave heating, induction heating, magnetic hyperthermia, infusion of warmed liquids, or direct application of heat such as through sitting in a hot room or wrapping a patient in hot blankets.

3.2.4 Types of Hyperthermia

The computer-controlled short waves are bundled in the tumor or the tumor bed and heated to between 40°C and a maximum of 44°C.

- Local hyperthermia heats a very small area, usually the tumor itself. In some instances, the goal is to kill the tumor by heating it, without damaging anything else. The heat may be created with microwave, radiofrequency, ultrasound energy or using magnetic hyperthermia. Depending on the location of the tumor, the heat may be applied to the surface of the body, inside normal body cavities, or deep in tissue through the use of needles or probes. One relatively common type is radiofrequency ablation of small tumors [51]. This is easiest to achieve when the tumor is on a superficial part of the body, which is called superficial hyperthermia, or when needles or probes are inserted directly into the tumor, which is called interstitial hyperthermia.

- Regional hyperthermia heats a larger part of the body, such as an entire organ or limb. Usually, the goal is to weaken cancer cells so that they are more likely to be killed by radiation and chemotherapeutic medications. This may use the same techniques as local hyperthermia treatment, or it may rely on blood perfusion. In blood perfusion, the patient's blood is removed from the body, heated up, and returned to blood vessels that lead directly through the desired body part. Normally, chemotherapy drugs are infused at the same time. One specialized type of this approach is continuous hyperthermic peritoneal perfusion (CHPP), which is used to treat difficult cancers within the peritoneal cavity (the abdomen), including primary peritoneal mesothelioma and stomach cancer. Hot

chemotherapy drugs are pumped directly into the peritoneal cavity to kill the cancer cells [51].

- Whole-body hyperthermia heats the entire body to temperatures of about 39 to 41 °C. It is typically used to treat metastatic cancer (cancer that spread to many parts of the body). Techniques include infrared hyperthermia domes which include the whole body apart from the head, putting the patient in a very hot room, or wrapping the patient in hot, wet blankets [51].

3.2.5 Treatment

Moderate hyperthermia treatments usually maintain the temperature for about an hour or so [53].

The schedule for treatments depends on the effect desired. After being heated, cells develop resistance to heat, which persists for about three days and reduces the likelihood that they will die from direct cytotoxic effects of the heat [52]. This suggests a maximum treatment schedule of about twice a week [53]. However, if the desired goal is increased radiosensitivity in a poorly oxygenated tumor, rather than directly killing the cells, then application of heat with every radiation treatment is acceptable [52].

3.2.6 Controlling Temperatures

One of the challenges in thermal therapy is delivering the appropriate amount of heat to the correct part of the patient's body. For this technique to be effective, the temperatures must be high enough, and the temperatures must be sustained long enough, to damage or kill the cancer cells. However, if the temperatures are too high, or if they are kept elevated for too long, then serious side effects, including death can result. The smaller the place that is heated and the shorter the treatment time, the lower the side effects.

To minimize damage to healthy tissue and other adverse effects, physicians carefully monitor the temperature of the affected area [51]. The goal is to keep local temperatures under 44 °C (111 °F) to avoid damage to surrounding tissues, and the whole body temperatures fewer than 42 °C (108

°F), which is the upper limit compatible with life. These temperatures compare to the normal human body temperature, taken internally, of about 37.6 °C (99.6 °F).

A great deal of current research focuses on precisely positioning heat-delivery devices (catheters, microwave and ultrasound applicators, etc.) using ultrasound or magnetic resonance imaging, as well as developing new types of nanoparticles that make them particularly efficient absorbers while offering little or no concerns about toxicity to other tissues. Clinicians also hope to use advanced imaging techniques to monitor heat treatments in real time; heat-induced changes in tissue are sometimes perceptible using these imaging instruments.

3.2.7 Adverse Effects

External application of heat may cause blisters, which generally heal quickly, and burns, which do not [53]. All techniques may result in pain or fatigue. Perfusion and moderate or high levels of hyperthermia can cause swelling, blood clots, and bleeding [52]. Whole-body hyperthermia, which is the riskiest treatment, usually results in diarrhea, nausea, vomiting, fatigue, and other symptoms of sunstroke; it may also cause cardiovascular problems [51].

3.2.8 Effectiveness

By itself, hyperthermia is generally ineffective, with only small numbers of patients receiving lasting benefit [53]. However, it may significantly increase the effectiveness of other treatments [53].

When combined with radiation, hyperthermia is particularly effective at increasing the damage to acidic, poorly oxygenated parts of a tumor, [52] and cells that are preparing to divide [53]. Hyperthermia treatment is most effective when provided at the same time, or within an hour, of the radiation [53].

Whole-body hyperthermia cannot safely reach the temperatures necessary to improve the effectiveness of radiation, and thus is not used with radiation, [52] but it may be useful for chemotherapy and immunotherapy [53].

3.2.9 Future Directions

Hyperthermia may be combined with gene therapy, particularly using the heat shock protein 70 promoter [52].

Two major technological challenges make hyperthermia therapy complicated: the ability to achieve a uniform temperature in a tumor, and the ability to precisely monitor the temperatures of both the tumor and the surrounding tissue [52]. Advances in devices to deliver uniform levels of the precise amount of heat desired, and devices to measure the total dose of heat received, are hoped for [53].

In locally advanced adenocarcinoma of middle and lower rectum, regional hyperthermia added to chemoradiotherapy achieved good results in terms of rate of sphincter sparing surgery [54].

Chapter Four: Analysis of Field II, Methodology, and Results

4.1 Introduction

In order to achieve the simulation of region of the breast cancer we use Field II program which was created by a group of technical university of Denmark. Field II is a program for simulating ultrasound transducer fields and ultrasound imaging using linear acoustics. The program is capable of calculating the emitted and pulse-echo fields for both the pulsed and continuous wave for a large number of different transducers. Also any kind of linear imaging can be simulated as well as realistic images of human tissue [57].

4.2 Materials and Methodology

4.2.1 Program Analysis, Organization and Function.

The program consists of a C program and a number of MATLAB m-functions that calls this program. All calculations are performed by the C program and all data is kept by the C program. The Field program system uses the concept of spatial impulse responses as developed by Tupholme and Stepanishen in a series of papers .The approach relies on linear systems theory to find the ultrasound field for both the pulsed and continuous wave. This is done through the spatial impulse response. This response gives the emitted ultrasound field at a specific point in space as function of time, when the transducer is excited by a Dirac delta function. The field for any kind of excitation can then be found by just convolving the spatial impulse response with the excitation function. The impulse response will vary as a function of position relative to the transducer, hence the name spatial impulse response.

The received response from a small oscillating sphere can be found by acoustic reciprocity. The spatial impulse response equals the received response for a spherical wave emitted by a point. The total received

response impulse-echo can, thus, be found by convolving the transducer excitation function with the spatial impulse response of the emitting aperture, with the spatial impulse response of the receiving aperture, and then taking into account the electro-mechanical transfer function of the transducer to yield the received voltage trace. Any excitation can be used, since linear systems theory is used. The result for the continuous wave case is found by Fourier transforming the spatial impulse response for the given frequency. The approach taken here can, thus, yield all the different commonly found ultrasound fields for linear propagation.

A number of different authors have calculated the spatial impulse response for different transducer geometries. But in general it is difficult to calculate a solution, and especially if apodization of the transducer is taken into account. Here the transducer surface does not vibrate as a piston, e.g. the edges might vibrate less than the center. The simulation program circumvents this problem by dividing the transducer surface into squares and the sum the response of these squares to yield the response. Thereby any transducer geometry and any apodization can be simulated.

The time for one simulation is also of major concern. As the squares making up the transducer aperture are small, it is appropriate to use a far field approximation, making simulation simple. Another issue in keeping the simulation time down is to use a low sampling frequency. Often spatial impulse responses are calculated using sampling frequencies in the GHz range due to the sharp discontinuities of the responses. These discontinuities are handled in the Field programs by accurately keeping track of the time position of the responses and use the integrated spatial impulse response as an intermediate step in the calculations. Thereby no energy is lost in the response, which is far more important than having an exact shape of the spatial impulse response. Hereby the Field program usually does better using 100MHz sampling and approximate calculations, than using the exact analytic expression and GHz sampling [56-57].

Field II can simulate all kinds of transducers using linear acoustics. The calculation of the Spatial Impulse Response assumes linearity and any complex-shaped transducer can therefore be divided into smaller apertures

and the response can be found by adding the responses from the sub-apertures. All kinds of ultrasound transducers control dynamically the focusing and the apodization of the transducers.

When the medium becomes complex, solving the wave propagation formula becomes impossible. Modeling becomes more complex inside the body because the ultrasound propagation speed is different for each tissue. It is important to know how the ultrasound wave is generated and the ultrasound wave beam shaped. The simulation method can be used for optimization of the array parameters in the design stage. The purpose of the program is to predict ultrasound fields and thereby make it possible to optimize the geometry, phasing and apodization of an ultrasound [55-57], and [60].

4.2.2 Field II Simulation and Anatomic Phantoms

Field simulation generally follows this type of sequence:

- Define an array.
- Define the Impulse Response of a transducer element of that array.
- Define the waveform of the transmitted signal.
- Define the targets that will be imaging.
- Calculate the scattered response from these targets for each image line position.
- Envelope detection and compress.
- Display the image [55, 58].

The simulations of artificial phantoms are done by simulating and summing the field from a collection of point scatterers. A single RF line in an image can be calculated by summing the response from a collection of scatterers, in which the scattering strength his determined by the density and speed of sound per turbations in the tissue. Homogeneous tissue is, thus, made from a collection of randomly placed scatterers with a scattering strength with a Gaussian distribution. The variance of the distribution is determined by the back scattering cross-section of the particular tissue.

The phantoms typically consist of 100,000 or more scatterers, and simulating 50 to 128 RF line scan take several days depending on the computer used. It is therefore beneficial to split the simulation into concurrently run sessions. This can easily be done by first generating the scatterer's position and amplitude and then storing them in a file. This file can then be used by a number of work stations to find the RF signal for different imaging directions, which are then stored in separate files; one for each RF line. These files are then used to assemble an image. This is the approach used for the simulations shown here. For the1million scatterers it roughly takes 1 hour and 10 minutes for a 3GHz Central Processing Unit (CPU) to generate one RF line, thus, simulating roughly 270 point scatterers per second. The image consists of 128 lines and splitting the simulation over 10 CPU makes it possible to generate the image in a little over 12 hours. The 100 CPU Linux cluster can make the image in roughly 1 hour and 10 minutes.

The anatomic phantoms are attempts to generate images as they will be seen from real human subjects. This is done by drawing a bitmap image of scattering strength of the region of interest. This map then determines the factor multiplied on to the scattering amplitude generated from the Gaussian distribution, and models the difference in the density and speed of sound perturbations in the tissue. Simulated boundaries were introduced by making lines in the scatterer's map along which the strong scatterers were placed. This is marked by completely white lines shown in the scatterer's maps. The model is currently two-dimensional, but can readily be expanded to three dimensions. Currently, the elevation direction is merely made by making a15mm thickness for the scatter positions, which are randomly distributed in the interval. The scatterer map used in this example was based on the optical photos from the Visible Human Project. They were created from scanning a human cadaver with CT and MRI scanners and then subsequently slicing the cadaver into 1mm sections for taking photographs.

4.2.3 Analysis of Routines

The general diagram of the files that we use is below:

We have to mention that firstly we have to initialize Field II with the command field_init via MATLAB [61]. The routines that we have called after are:

- make_scatterers.m

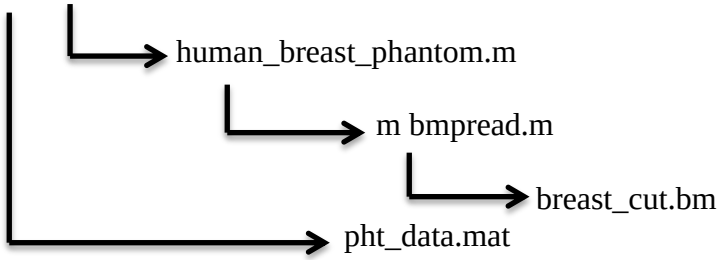

- sim_breast.m

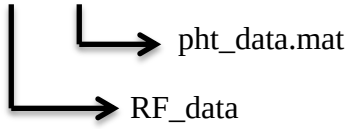

- make_polar.m

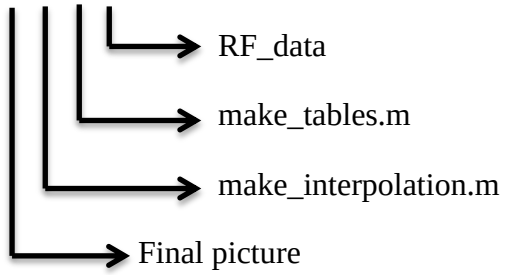

We have three mainly parts:

1- Creation of the phantom

In the first part we have to create the Phantom with the distributed scatterers (1000000 randomly distributed within the Phantom). We use a bmp (8bit) picture of breast. This picture has been created from the normalization according to the 6 different densities of 6 different parts of the breast (water, cerebrospinal fluid, white mater, gray mater, tumor and tumor boundary). So we have a bmp image of scattering strength of the region of interest. The file bmpread.m is used to read the bmp picture of

breast from a disk and returns the indexed image X and associated MAP. The file human_breast_phantom.m creates the phantom. The file make_scatterers.m creates the target points (scatterers N=1000000) randomly distributed within the phantom and makes the file for the scatterers in the phantom with the name pht_data.mat.

2- Simulation

The second part contains the files sim_breast.m that makes the simulation. The simulation is performed and the data is stored in Rf_file (fileRf_data). The data for the scatterers are read from the file pht_data.mat. Here we define the transducer. Here are all the parameters that we need to define for the transducer:

- fo = transducer‘s frequency
- f = focal point
- N = number of elements
- No_lines = number of lines of RF data

3- F i n a l Image

The third part creates the images from the above procedures. The data from file Rf_data are processed to do the polar to rectangular mapping to yield the image. This is done by the routine make_polar.m that creates an image with a dynamic range of 50dB.The parameter that we have changed is the No_lines that must be the same with the number of elements. By calling the routine make_polar.m, this file uses the files make_tables.m and make_interpolation.m to work properly. With this procedure we have the picture.

4.2.4 Results of Simulation in Field II

Before referring the results we have to mention that the study cases have been done according to the combinations of the parameters that can take specific values due to the bibliography, we have a multiple cases.

We will make the scatteres for a simulation and store it in a file for later simulation.

This example shows how a phased array B-mode system scans an image

- This script assumes that the field_init procedure has been called
- Here the field simulation is performed and the data is stored in rf-files; one for each rf-line done.
- The data must then subsequently be processed to yield the image.

    - In the following images, the **bold** letters indicate the parameters that had been studied

- **Generate the transducer apertures for send and receive**

```
f0=3e6;                 % Transducer center frequency [Hz].
fs=100e6;               % Sampling frequency [Hz].
c=1540;                 % Speed of sound [m/s].
lambda=c/f0;            % Wavelength [m].
width=lambda/2;         % Width of element
element_height=7/1000;  % Height of element [m].
kerf=0.0025/1000;       % Kerf [m].
focus=[0 0 70]./1000;   % Fixed focal point [m].
N_elements=32;          % Number of physical elements
Display_angle=80;       % Display angle in degree
FBW= 0.4;               % Fractional bandwidth
```

The output is as following:

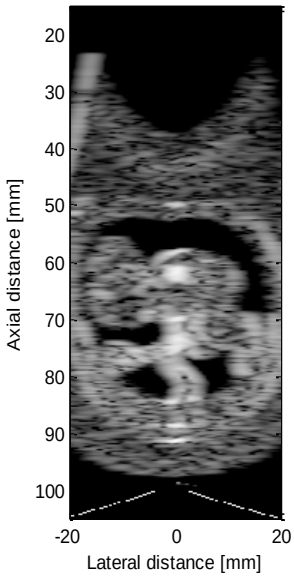

Figure 4.1 the reference fetus photo

Comment: this output will be taken as the reference output where changing the display angle of phantom to 80^{o} in degree.

- **Generate the transducer apertures for send and receive**

```
f0=3e6;                  % Transducer center frequency [Hz].
fs=100e6;                % Sampling frequency [Hz].
c=1540;                  % Speed of sound [m/s].
lambda=c/f0;             % Wavelength [m].
width=lambda/2;          % Width of element
element_height=7/1000;   % Height of element [m].
kerf=0.0025/1000;        % Kerf [m].
focus=[0 0 70]./1000;    % Fixed focal point [m].
N_elements=64;           % Number of physical elements
Display_angle=80;        % Display angle in degree
FBW= 0.4;                % Fractional bandwidth
```

The output is as following:

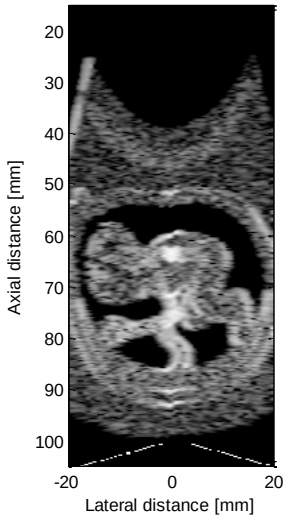

Figure 4.2 the number of physical elements=64 applied on fetus

Comment: in this program the number of physical elements is increased to (64) where the clearance of the fetus phantom is raised and the details are very good.

- **Generate the transducer apertures for send and receive**

```
f0=3e6;                    % Transducer center frequency [Hz].
fs=100e6;                  % Sampling frequency [Hz].
c=1540;                    % Speed of sound [m/s].
lambda=c/f0;               % Wavelength [m].
width=lambda/2;            % Width of element
element_height=7/1000;     % Height of element [m].
kerf=0.0025/1000;          % Kerf [m].
focus=[0 0 70]./1000;      % Fixed focal point [m].
N_elements=16;             % Number of physical elements
Display_angle=80;          % Display angle in degree
FBW= 0.4;                  % Fractional bandwidth
```

The output is as following:

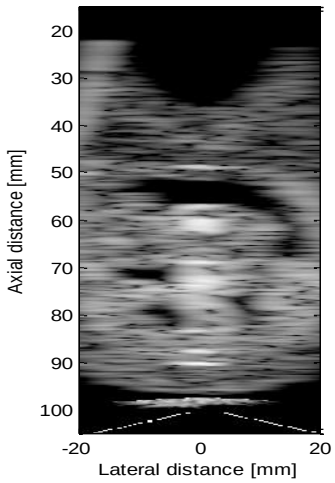

Figure 4.3 the number of physical elements=16 applied on fetus

Comment: in this program the number of physical elements is decreased to (16) where the clearance of the fetus phantom is decreased and the details are very bad.

Conclusion: the number of transducer elements effects on the heat distribution as follows: The higher number of transducer elements, the best focusing point and vice versa. The number of transducer elements ranges according to the most catalogues as follows (16, 32, and 64).

- **Generate the transducer apertures for send and receive**

```
f0=3e6;                 % Transducer center frequency [Hz].
fs=100e6;               % Sampling frequency [Hz].
c=1540;                 % Speed of sound [m/s].
lambda=c/f0;            % Wavelength [m].
width=lambda/2;         % Width of element
element_height=7/1000;  % Height of element [m].
kerf=0 ;                % Kerf [m].
focus=[0 0 70]./1000;   % Fixed focal point [m].
N_elements=32;          % Number of physical elements
Display_angle=80;       % Display angle in degree
FBW= 0.4;               % Fractional bandwidth
```

The output is as following:

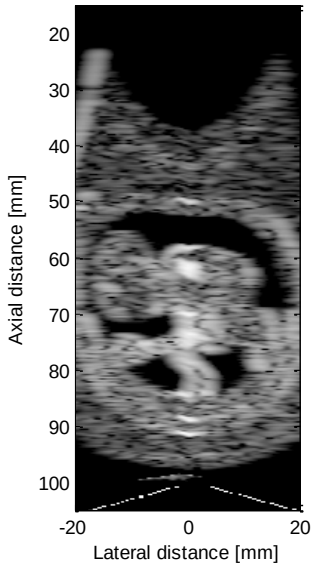

Figure 4.4 the elements spacing = 0 applied on fetus

Comment: in this program the kerf (the elements spacing) is decreased to (0) where the clearance of the fetus phantom is decreased and the details are lower than the reference output.

- **Generate the transducer apertures for send and receive**

```
f0=3e6;                 % Transducer center frequency [Hz].
fs=100e6;               % Sampling frequency [Hz].
c=1540;                 % Speed of sound [m/s].
lambda=c/f0;            % Wavelength [m].
width=lambda/2;         % Width of element
element_height=7/1000;  % Height of element [m].
kerf=0.0050/1000;       %  Kerf [m].
focus=[0 0 70]./1000;   % Fixed focal point [m].
N_elements=32;          % Number of physical elements
Display_angle=80;       % Display angle in degree
FBW= 0.4;               % Fractional bandwidth
```

The output is as following:

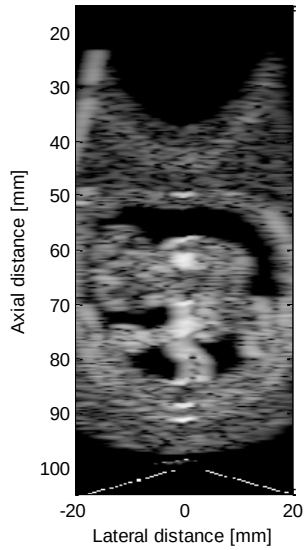

Figure 4.5 the elements spacing = 0.005 mm applied on fetus

Comment: in this program the kerf (the elements spacing) is increased to 0.005 mm where the clearance of the fetus phantom is increased and the details are higher than the reference output.

- **Generate the transducer apertures for send and receive**

```
f0=3e6;                 % Transducer center frequency [Hz].
fs=100e6;               % Sampling frequency [Hz].
c=1540;                 % Speed of sound [m/s].
lambda=c/f0;            % Wavelength [m].
width=lambda/2;         % Width of element
element_height=7/1000;  % Height of element [m].
kerf=0.0100/1000;       % Kerf [m].
focus=[0 0 70]./1000;   % Fixed focal point [m].
N_elements=32;          % Number of physical elements
Display_angle=80;       % Display angle in degree
FBW= 0.4;               % Fractional bandwidth
```

The output is as following:

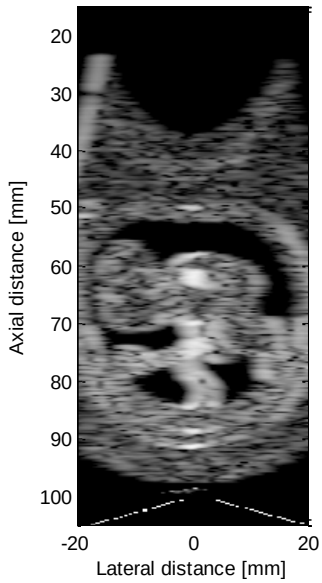

Figure 4.6 the elements spacing = 0.01 mm applied on fetus

Comment: in this program the kerf (the elements spacing) is increased to 0.010 mm where the clearance of the fetus phantom is more increased and the details are higher than the previous output.

- **Generate the transducer apertures for send and receive**

```
f0=0.5e6;                % Transducer center frequency [Hz].
fs=100e6;                % Sampling frequency [Hz].
c=1540;                  % Speed of sound [m/s].
lambda=c/f0;             % Wavelength [m].
width=lambda/2;          % Width of element
element_height=7/1000;   % Height of element [m].
kerf=0.0025/1000;        % Kerf [m].
focus=[0 0 70]./1000;    % Fixed focal point [m].
N_elements=32;           % Number of physical elements
Display_angle=80;        % Display angle in degree
FBW= 0.4;                % Fractional bandwidth
```

The output is as following:

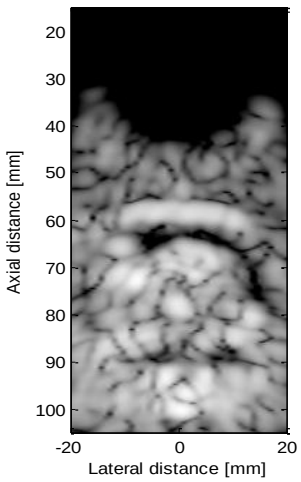

Figure 4.7 the transducer center frequency = 0.5 MHz applied on fetus

Comment: in this program the transducer center frequency is decreased to 0.5 MHz where the clearance of the fetus phantom is decreased and the details are the worst one compared with the reference output.

- **Generate the transducer apertures for send and receive**

```
f0=5e6;                 %  Transducer center frequency [Hz].
fs=100e6;               %  Sampling frequency [Hz].
c=1540;                 %  Speed of sound [m/s].
lambda=c/f0;            %  Wavelength [m].
width=lambda/2;         %  Width of element
element_height=7/1000;  %  Height of element [m].
kerf=0.0025/1000;       %  Kerf [m].
focus=[0 0 70]./1000;   %  Fixed focal point [m].
N_elements=32;          %  Number of physical elements
Display_angle=80;       %  Display angle in degree
FBW= 0.4;               %  Fractional bandwidth
```

The output is as following:

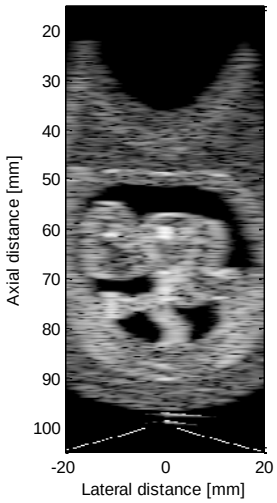

Figure 4.8 the Transducer center frequency = 5 MHz applied on fetus

Comment: in this program the transducer center frequency is increased to 5 MHz where the clearance of the fetus phantom is increased and the details are very good compared with the reference output.

- **Generate the transducer apertures for send and receive**

```
f0=5e6;                 % Transducer center frequency [Hz].
fs=100e6;               % Sampling frequency [Hz].
c=1540;                 % Speed of sound [m/s].
lambda=c/f0;            % Wavelength [m].
width=lambda/2;         % Width of element
element_height=7/1000;  % Height of element [m].
kerf=0.0025/1000;       % Kerf [m].
focus=[0 0 70]./1000;   % Fixed focal point [m].
N_elements=64;          % Number of physical elements
Display_angle=80;       % Display angle in degree
FBW= 0.4;               % Fractional bandwidth
```

The output is as following:

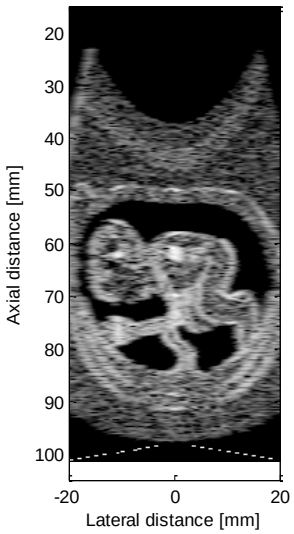

Figure 4.9 the Transducer center frequency = 5 MHz, and the number of physical elements=64 applied on fetus

Comment: in this program the transducer center frequency is increased to 5 MHz and the transducer number of physics element to (64) where the clearance of the fetus phantom is increased and the details are excellent compared with the reference output.

- **Generate the transducer apertures for send and receive**

```
f0=5e6;                 %  Transducer center frequency [Hz].
fs=100e6;               %  Sampling frequency [Hz].
c=1540;                 %  Speed of sound [m/s].
lambda=c/f0;            %  Wavelength [m].
width=lambda/2;         %  Width of element
element_height=7/1000;  %  Height of element [m].
kerf=0.0100/1000;       %  Kerf [m].
focus=[0 0 70]./1000;   %  Fixed focal point [m].
N_elements=32;          %  Number of physical elements
Display_angle=80;       %  Display angle in degree
FBW= 0.4;               %  Fractional bandwidth
```

The output is as following:

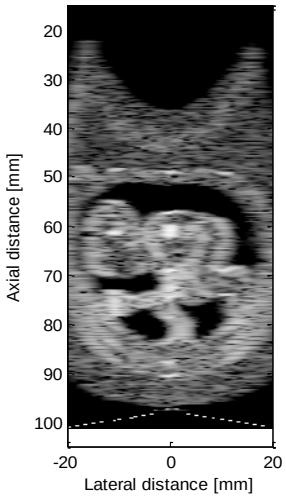

Figure 4.10 the Transducer center frequency = 5 MHz, and the element spacing=0.01 mm applied on fetus

Comment: in this program the transducer center frequency is increased to 5 MHz and the transducer spacing (kerf) to 0.01 mm where the clearance of the fetus phantom is increased and the details are preferred compared with the reference output.

- **Generate the transducer apertures for send and receive**

```
f0=5e6;                 %  Transducer center frequency [Hz].
fs=100e6;               %  Sampling frequency [Hz].
c=1540;                 %  Speed of sound [m/s].
lambda=c/f0;            %  Wavelength [m].
width=lambda/2;         %  Width of element
element_height=7/1000;  %  Height of element [m].
kerf=0.0100/1000;       %  Kerf [m].
focus=[0 0 70]./1000;   %  Fixed focal point [m].
N_elements=64;          %  Number of physical elements
Display_angle=80;       %  Display angle in degree
FBW= 0.4;               %  Fractional bandwidth
```

The output is as following:

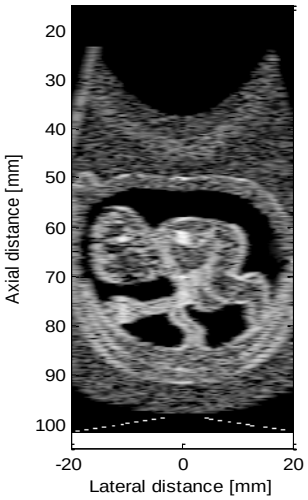

Figure 4.11 the Transducer center frequency = 5 MHz, the number of physical elements=64, and the element spacing=0.01 mm applied on fetus

Comment: in this program the transducer center frequency is increased to 5 MHz, the transducer spacing (kerf) to 0.01 mm, and the transducer number of physical elements to (64) which demonstrates the best output compared with all previous outputs.

- **Generate the transducer apertures for send and receive**

```
f0=3e6;                 % Transducer center frequency [Hz].
fs=100e6;               % Sampling frequency [Hz].
c=1540;                 % Speed of sound [m/s].
lambda=c/f0;            % Wavelength [m].
width=lambda/4;         % Width of element
element_height=7/1000;  % Height of element [m].
kerf=0.0025/1000;       % Kerf [m].
focus=[0 0 70]./1000;   % Fixed focal point [m].
N_elements=32;          % Number of physical elements
Display_angle=80;       % Display angle in degree
FBW= 0.4;               % Fractional bandwidth
```

The output is as following:

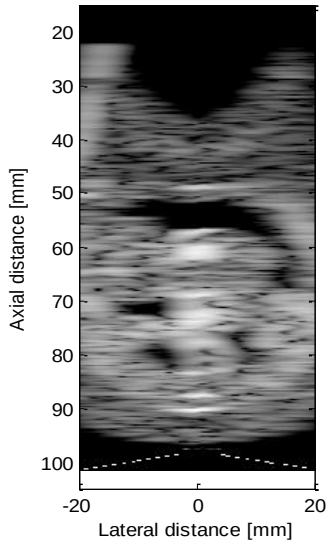

Figure 4.13 the Width of element= lambda/4 applied on fetus

Comment: in this program the width of element is decreased where the clearance of the fetus phantom is slightly increased and the details also aren't preferred compared with the reference output.

- **Generate the transducer apertures for send and receive**

```
f0=3e6;                 % Transducer center frequency [Hz].
fs=100e6;               % Sampling frequency [Hz].
c=1540;                 % Speed of sound [m/s].
lambda=c/f0;            % Wavelength [m].
width=lambda ;          % Width of element
element_height=7/1000;  % Height of element [m].
kerf=0.0025/1000;       % Kerf [m].
focus=[0 0 70]./1000;   % Fixed focal point [m].
N_elements=32;          % Number of physical elements
Display_angle=80;       % Display angle in degree
FBW= 0.4;               % Fractional bandwidth
```

The output is as following:

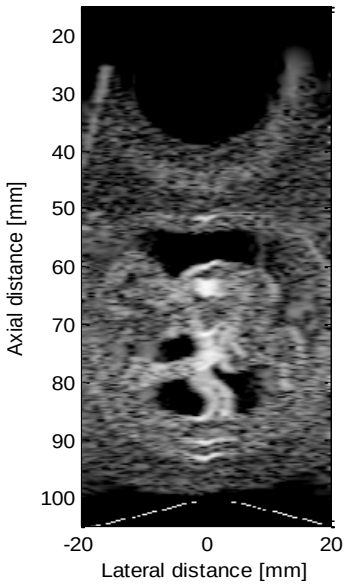

Figure 4.14 the Width of element= lambda applied on fetus

Comment: in this program the width of element is increased where the clearance of the fetus phantom is increased and the details aren't a good compared with the reference output.

- **Generate the transducer apertures for send and receive**

```
f0=3e6;                 % Transducer center frequency [Hz].
fs=100e6;               % Sampling frequency [Hz].
c=1540;                 % Speed of sound [m/s].
lambda=c/f0;            % Wavelength [m].
width=2*lambda ;        % Width of element
element_height=7/1000;  % Height of element [m].
kerf=0.0025/1000;       % Kerf [m].
focus=[0 0 70]./1000;   % Fixed focal point [m].
N_elements=32;          % Number of physical elements
Display_angle=80;       % Display angle in degree
FBW= 0.4;               % Fractional bandwidth
```

The output is as following:

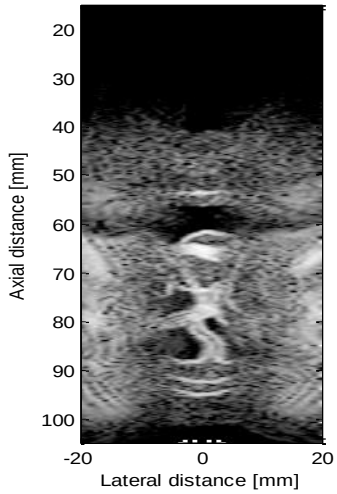

Figure 4.15 the Width of element= 2*lambda applied on fetus

Comment: in this program the width of element is increased where the clearance of the fetus phantom is a very bad compared with the reference output.

Conclusion: in all references, the width of element equal to (lambda/2) and this cleared from previous programs that the best output at this width.

- **Generate the transducer apertures for send and receive**

```
f0=3e6;                 % Transducer center frequency [Hz].
fs=100e6;               % Sampling frequency [Hz].
c=1540;                 % Speed of sound [m/s].
lambda=c/f0;            % Wavelength [m].
width=lambda/2;         % Width of element
element_height=7/1000;  % Height of element [m].
kerf=0.0025/1000;       % Kerf [m].
focus=[0 0 70]./1000;   % Fixed focal point [m].
N_elements=32;          % Number of physical elements
Display_angle=80;       % Display angle in degree
FBW= 0.4;               % Fractional bandwidth
```

The output is as following:

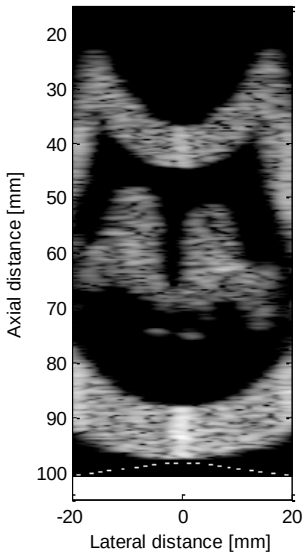

Figure 4.16 the reference breast photo

Comment: this output will be taken as the reference output where changing the display angle of breast phantom to 80^{o} in degree.

- **Generate the transducer apertures for send and receive**

```
f0=3e6;                  % Transducer center frequency [Hz].
fs=100e6;                % Sampling frequency [Hz].
c=1540;                  % Speed of sound [m/s].
lambda=c/f0;             % Wavelength [m].
width=lambda/2;          % Width of element
element_height=7/1000;   % Height of element [m].
kerf=0.0025/1000;        % Kerf [m].
focus=[0 0 70]./1000;    % Fixed focal point [m].
N_elements=64;           %  Number of physical elements
Display_angle=80;        % Display angle in degree
FBW= 0.4;                % Fractional bandwidth
```

The output is as following:

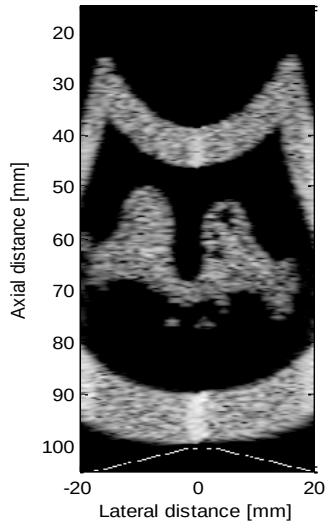

Figure 4.17 the number of physical elements=64 applied on breast

Comment: in this program the number of physical elements is increased to (64) where the clearance of the breast phantom raised and the details are very good.

- **Generate the transducer apertures for send and receive**

```
f0=3e6;                 % Transducer center frequency [Hz].
fs=100e6;               % Sampling frequency [Hz].
c=1540;                 % Speed of sound [m/s].
lambda=c/f0;            % Wavelength [m].
width=lambda/2;         % Width of element
element_height=7/1000;  % Height of element [m].
kerf=0.0025/1000;       % Kerf [m].
focus=[0 0 70]./1000;   % Fixed focal point [m].
N_elements=16;          % Number of physical elements
Display_angle=80;       % Display angle in degree
FBW= 0.4;               % Fractional bandwidth
```

The output is as following:

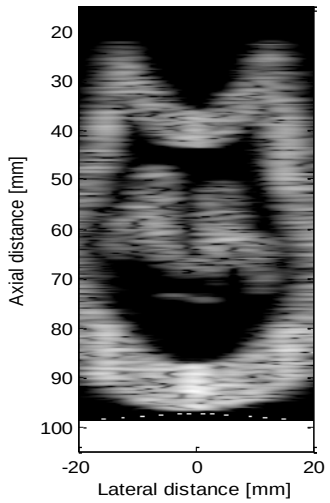

Figure 4.18 the number of physical elements=16 applied on breast

Comment: in this program the number of physical elements is decreased to (16) where the clearance of the breast phantom is decreased and the details are very bad.

Conclusion: the number of transducer elements effects on the heat distribution as follows: The higher number of transducer elements, the best focusing point and vice versa, the number of transducer elements ranges according to the most catalogues as follows (16, 32, and 64).

- **Generate the transducer apertures for send and receive**

```
f0=3e6;                 % Transducer center frequency [Hz].
fs=100e6;               % Sampling frequency [Hz].
c=1540;                 % Speed of sound [m/s].
lambda=c/f0;            % Wavelength [m].
width=lambda/2;         % Width of element
element_height=7/1000;  % Height of element [m].
kerf=0 ;                % Kerf [m].
focus=[0 0 70]./1000;   % Fixed focal point [m].
N_elements=32;          % Number of physical elements
Display_angle=80;       % Display angle in degree
FBW= 0.4;               % Fractional bandwidth
```

The output is as following:

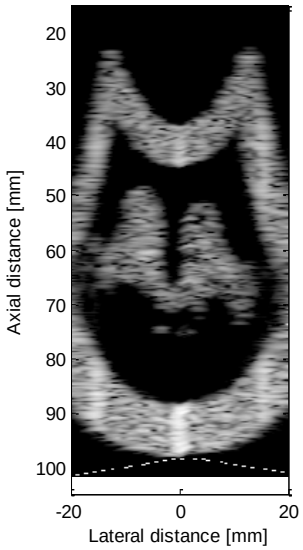

Figure 4.19 the elements spacing = 0 applied on breast

Comment: in this program the kerf (the elements spacing) is decreased to 0 where the clearance of the breast phantom is decreased and the details are lower than the reference output.

- **Generate the transducer apertures for send and receive**

```
f0=3e6;                 % Transducer center frequency [Hz].
fs=100e6;               % Sampling frequency [Hz].
c=1540;                 % Speed of sound [m/s].
lambda=c/f0;            % Wavelength [m].
width=lambda/2;         % Width of element
element_height=7/1000;  % Height of element [m].
kerf=0.0050/1000;       %  Kerf [m].
focus=[0 0 70]./1000;   % Fixed focal point [m].
N_elements=32;          % Number of physical elements
Display_angle=80;       % Display angle in degree
FBW= 0.4;               % Fractional bandwidth
```

The output is as following:

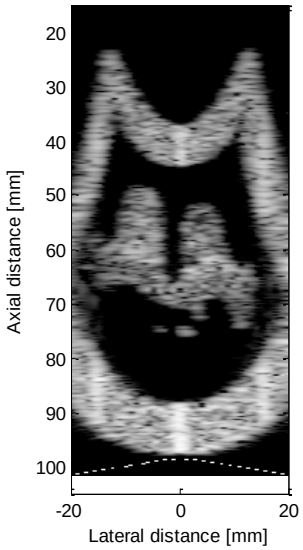

Figure 4.20 the elements spacing =0.005 mm applied on breast

Comment: in this program the kerf (the elements spacing) is increased to 0.005 mm where the clearance of the breast phantom is increased and the details are higher than the reference output.

- **Generate the transducer apertures for send and receive**

```
f0=3e6;                 % Transducer center frequency [Hz].
fs=100e6;               % Sampling frequency [Hz].
c=1540;                 % Speed of sound [m/s].
lambda=c/f0;            % Wavelength [m].
width=lambda/2;         % Width of element
element_height=7/1000;  % Height of element [m].
kerf=0.0100/1000;       % Kerf [m].
focus=[0 0 70]./1000;   % Fixed focal point [m].
N_elements=32;          % Number of physical elements
Display_angle=80;       % Display angle in degree
FBW= 0.4;               % Fractional bandwidth
```

The output is as following:

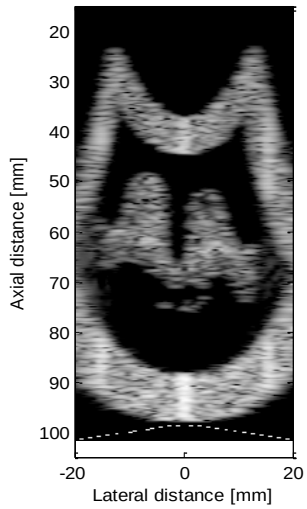

Figure 4.21 the elements spacing = 0.01 mm applied on breast

Comment: in this program the kerf (the elements spacing) is increased to 0.01 mm where the clearance of the breast phantom is more increased and the details are higher than the previous output.

- **Generate the transducer apertures for send and receive**

```
f0=0.5e6;                % Transducer center frequency [Hz].
fs=100e6;                % Sampling frequency [Hz].
c=1540;                  % Speed of sound [m/s].
lambda=c/f0;             % Wavelength [m].
width=lambda/2;          % Width of element
element_height=7/1000;   % Height of element [m].
kerf=0.0025/1000;        % Kerf [m].
focus=[0 0 70]./1000;    % Fixed focal point [m].
N_elements=32;           % Number of physical elements
Display_angle=80;        % Display angle in degree
FBW= 0.4;                % Fractional bandwidth
```

The output is as following:

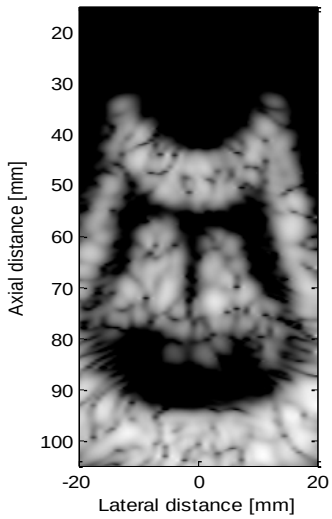

Figure 4.22 the transducer center frequency = 0.5 MHz applied on breast

Comment: in this program the transducer center frequency is increased to 0.5 MHz where the clearance of the breast phantom is decreased and the details are the worst one compared with the reference output.

- **Generate the transducer apertures for send and receive**

```
f0=5e6;                  % Transducer center frequency [Hz].
fs=100e6;                % Sampling frequency [Hz].
c=1540;                  % Speed of sound [m/s].
lambda=c/f0;             % Wavelength [m].
width=lambda/2;          % Width of element
element_height=7/1000;   % Height of element [m].
kerf=0.0025/1000;        % Kerf [m].
focus=[0 0 70]./1000;    % Fixed focal point [m].
N_elements=32;           % Number of physical elements
Display_angle=80;        % Display angle in degree
FBW= 0.4;                % Fractional bandwidth
```

The output is as following:

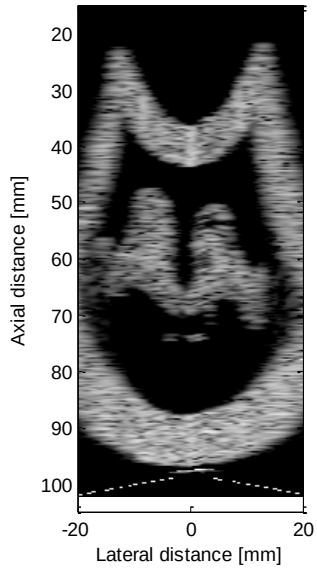

Figure 4.23 the transducer center frequency = 5 MHz applied on breast

Comment: in this program the transducer center frequency is increased to 5 MHz where the clearance of the breast phantom is increased and the details are very good compared with the reference output.

- **Generate the transducer apertures for send and receive**

```
f0=5e6;                 %  Transducer center frequency [Hz].
fs=100e6;               %  Sampling frequency [Hz].
c=1540;                 %  Speed of sound [m/s].
lambda=c/f0;            %  Wavelength [m].
width=lambda/2;         %  Width of element
element_height=7/1000;  %  Height of element [m].
kerf=0.0025/1000;       %  Kerf [m].
focus=[0 0 70]./1000;   %  Fixed focal point [m].
N_elements=64;          %  Number of physical elements
Display_angle=80;       %  Display angle in degree
FBW= 0.4;               %  Fractional bandwidth
```

The output is as following:

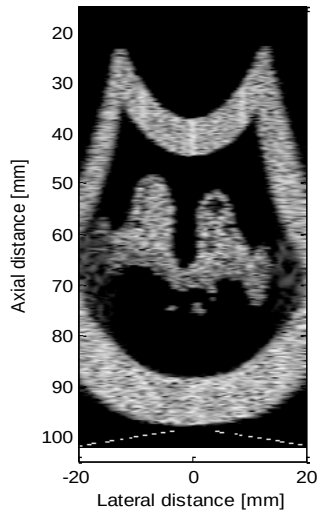

Figure 4.24 the Transducer center frequency = 5 MHz, and the number of physical elements=64 applied on breast

Comment: in this program the transducer center frequency is increased to 5 (MHz) and the transducer number of physics element to (64) where the clearance of the breast phantom is increased and the details are excellent compared with the reference output.

- **Generate the transducer apertures for send and receive**

```
f0=5e6;                 %  Transducer center frequency [Hz].
fs=100e6;               %  Sampling frequency [Hz].
c=1540;                 %  Speed of sound [m/s].
lambda=c/f0;            %  Wavelength [m].
width=lambda/2;         %  Width of element
element_height=7/1000;  %  Height of element [m].
kerf=0.0100/1000;       %  Kerf [m].
focus=[0 0 70]./1000;   %  Fixed focal point [m].
N_elements=32;          %  Number of physical elements
Display_angle=80;       %  Display angle in degree
FBW= 0.4;               %  Fractional bandwidth
```

The output is as following:

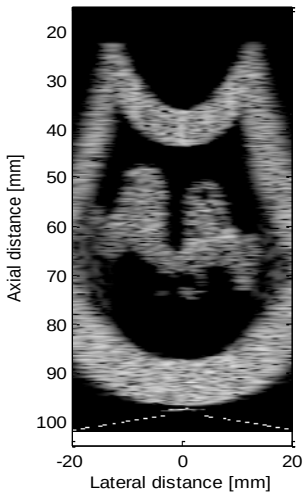

Figure 4.25 the Transducer center frequency = 5 MHz, and the element spacing=0.01 mm applied on breast

Comment: in this program the transducer center frequency is increased to 5 MHz and the transducer spacing (kerf) to 0.01 mm where the clearance of the breast phantom is increased and the details are preferred compared with the reference output.

- **Generate the transducer apertures for send and receive**

```
f0=5e6;                 %  Transducer center frequency [Hz].
fs=100e6;               %  Sampling frequency [Hz].
c=1540;                 %  Speed of sound [m/s].
lambda=c/f0;            %  Wavelength [m].
width=lambda/2;         %  Width of element
element_height=7/1000;  %  Height of element [m].
kerf=0.0100/1000;       %  Kerf [m].
focus=[0 0 70]./1000;   %  Fixed focal point [m].
N_elements=64;          %  Number of physical elements
Display_angle=80;       %  Display angle in degree
FBW= 0.4;               %  Fractional bandwidth
```

The output is as following:

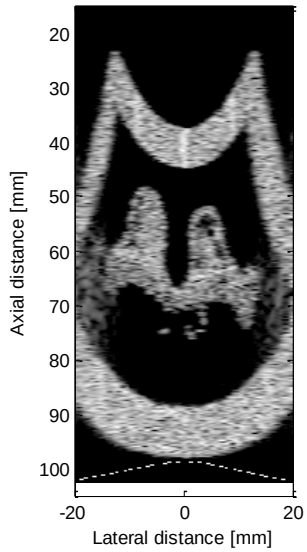

Figure 4.26 the Transducer center frequency = 5 MHz, the number of physical elements=64, and the element spacing=0.01 mm applied on breast

Comment: in this program the transducer center frequency is increased to 5 MHz and the transducer spacing (kerf) to 0.01 mm, and the transducer number of physical elements to (64) which demonstrates the best output compared with all previous outputs.

- **Generate the transducer apertures for send and receive**

```
f0=3e6;                 % Transducer center frequency [Hz].
fs=100e6;               % Sampling frequency [Hz].
c=1540;                 % Speed of sound [m/s].
lambda=c/f0;            % Wavelength [m].
width=lambda/4;         % Width of element
element_height=7/1000;  % Height of element [m].
kerf=0.0025/1000;       % Kerf [m].
focus=[0 0 70]./1000;   % Fixed focal point [m].
N_elements=32;          % Number of physical elements
Display_angle=80;       % Display angle in degree
FBW= 0.4;               % Fractional bandwidth
```

The output is as following:

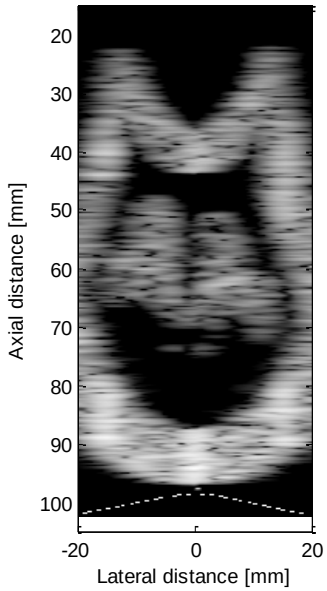

Figure 4.28 the Width of element= lambda/4 applied on breast

Comment: in this program the width of element is decreased where the clearance of the breast phantom is slightly increased and the details also aren't preferred compared with the reference output.

- **Generate the transducer apertures for send and receive**

```
f0=3e6;                 % Transducer center frequency [Hz].
fs=100e6;               % Sampling frequency [Hz].
c=1540;                 % Speed of sound [m/s].
lambda=c/f0;            % Wavelength [m].
width=lambda ;          %  Width of element
element_height=7/1000;  % Height of element [m].
kerf=0.0025/1000;       % Kerf [m].
focus=[0 0 70]./1000;   % Fixed focal point [m].
N_elements=32;          % Number of physical elements
Display_angle=80;       % Display angle in degree
FBW= 0.4;               % Fractional bandwidth
```

The output is as following:

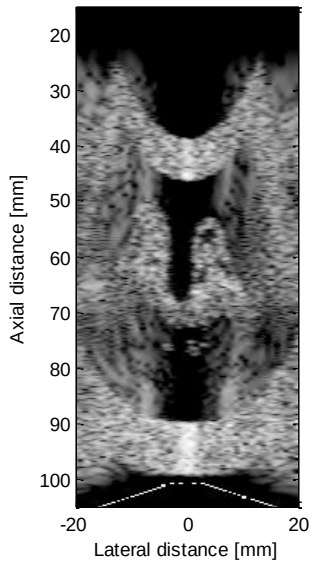

Figure 4.29 the Width of element= lambda applied on breast

Comment: in this program the width of element is increased where the clearance of the breast phantom is increased and the details are good compared with the reference output.

- **Generate the transducer apertures for send and receive**

```
f0=3e6;                 % Transducer center frequency [Hz].
fs=100e6;               % Sampling frequency [Hz].
c=1540;                 % Speed of sound [m/s].
lambda=c/f0;            % Wavelength [m].
width=2*lambda ;        %  Width of element
element_height=7/1000;  % Height of element [m].
kerf=0.0025/1000;       % Kerf [m].
focus=[0 0 70]./1000;   % Fixed focal point [m].
N_elements=32;          % Number of physical elements
Display_angle=80;       % Display angle in degree
FBW= 0.4;               % Fractional bandwidth
```

The output is as following:

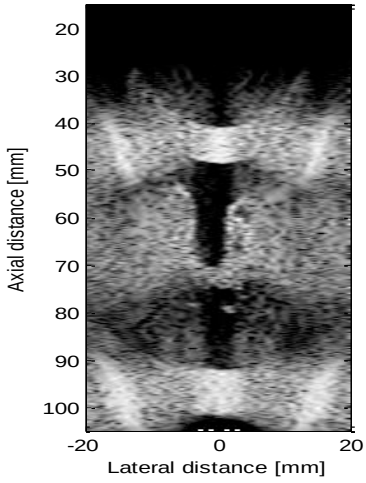

Figure 4.30 the Width of element= lambda applied on breast

Comment: in this program the width of element is more increased where the clearance of the breast phantom is a very bad compared with the reference output.

Conclusion: in all references, the width of element equal to (lambda/2) and this cleared from previous programs that the best output at this width.

- **Generate the transducer apertures for send and receive**

```
f0=3e6;                 % Transducer center frequency [Hz].
fs=100e6;               % Sampling frequency [Hz].
c=1540;                 % Speed of sound [m/s].
lambda=c/f0;            % Wavelength [m].
width=lambda/2;         % Width of element
element_height=7/1000;  % Height of element [m].
kerf=0.0025/1000;       % Kerf [m].
focus=[0 0 70]./1000;   % Fixed focal point [m].
N_elements=32;          % Number of physical elements
Display_angle=80;       % Display angle in degree
FBW= 0.4;               % Fractional bandwidth
```

The output is as following:

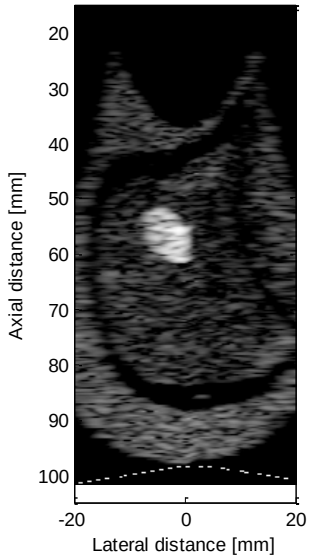

Figure 4.31 the reference breast cancer photo

Comment: this output will be taken as the reference output where changing the display angle of breast phantom to 80^{o} in degree.

- **Generate the transducer apertures for send and receive**

```
f0=3e6;                 % Transducer center frequency [Hz].
fs=100e6;               % Sampling frequency [Hz].
c=1540;                 % Speed of sound [m/s].
lambda=c/f0;            % Wavelength [m].
width=lambda/2;         % Width of element
element_height=7/1000;  % Height of element [m].
kerf=0.0025/1000;       % Kerf [m].
focus=[0 0 70]./1000;   % Fixed focal point [m].
N_elements=64;          %  Number of physical elements
Display_angle=80;       % Display angle in degree
FBW= 0.4;               % Fractional bandwidth
```

The output is as following:

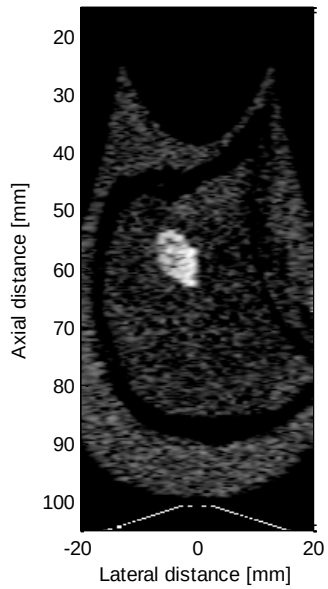

Figure 4.32 the number of physical elements=64 applied on breast cancer

Comment: in this program the number of physical elements is increased to (64) where the clearance of the breast phantom raised and the details are very good.

- **Generate the transducer apertures for send and receive**

```
f0=3e6;                 % Transducer center frequency [Hz].
fs=100e6;               % Sampling frequency [Hz].
c=1540;                 % Speed of sound [m/s].
lambda=c/f0;            % Wavelength [m].
width=lambda/2;         % Width of element
element_height=7/1000;  % Height of element [m].
kerf=0.0025/1000;       % Kerf [m].
focus=[0 0 70]./1000;   % Fixed focal point [m].
N_elements=16;          % Number of physical elements
Display_angle=80;       % Display angle in degree
FBW= 0.4;               % Fractional bandwidth
```

The output is as following:

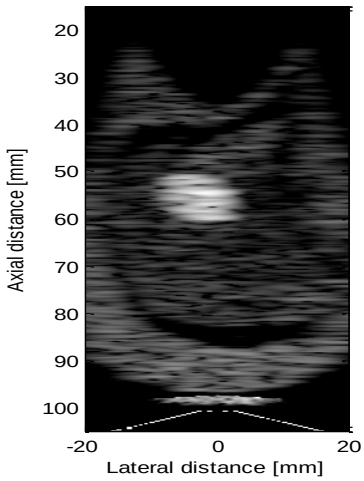

Figure 4.33 the number of physical elements=16 applied on breast cancer

Comment: in this program the number of physical elements is decreased to (16) where the clearance of the breast phantom is decreased and the details are very bad.

Conclusion: the number of transducer elements effects on the heat distribution as follows: The higher number of transducer elements, the best focusing point and vice versa, the number of transducer elements ranges according to the most catalogues as follows (16, 32, and 64).

- **Generate the transducer apertures for send and receive**

```
f0=3e6;                 %  Transducer center frequency [Hz].
fs=100e6;               %  Sampling frequency [Hz].
c=1540;                 %  Speed of sound [m/s].
lambda=c/f0;            %  Wavelength [m].
width=lambda/2;         %  Width of element
element_height=7/1000;  %  Height of element [m].
kerf=0 ;                %  Kerf [m].
focus=[0 0 70]./1000;   %  Fixed focal point [m].
N_elements=32;          %  Number of physical elements
Display_angle=80;       %  Display angle in degree
FBW= 0.4;               %  Fractional bandwidth
```

The output is as following:

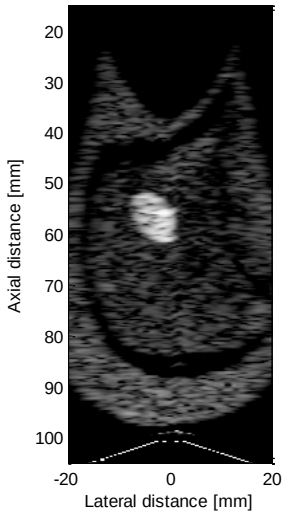

Figure 4.34 the elements spacing = 0 applied on breast cancer

Comment: in this program the kerf (the elements spacing) is decreased to (0) where the clearance of the breast phantom is decreased and the details are lower than the reference output.

- **Generate the transducer apertures for send and receive**

```
f0=3e6;                 % Transducer center frequency [Hz].
fs=100e6;               % Sampling frequency [Hz].
c=1540;                 % Speed of sound [m/s].
lambda=c/f0;            % Wavelength [m].
width=lambda/2;         % Width of element
element_height=7/1000;  % Height of element [m].
kerf=0.0050/1000;       %  Kerf [m].
focus=[0 0 70]./1000;   % Fixed focal point [m].
N_elements=32;          % Number of physical elements
Display_angle=80;       % Display angle in degree
FBW= 0.4;               % Fractional bandwidth
```

The output is as following:

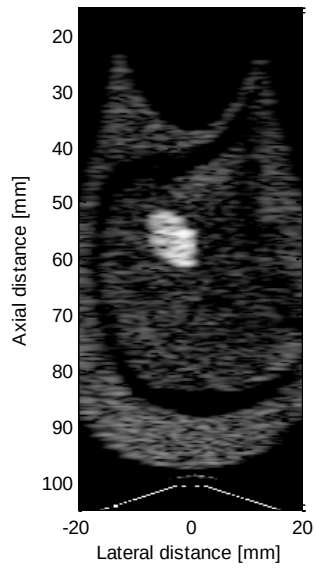

Figure 4.35 the elements spacing = 0.005 mm applied on breast cancer

Comment: in this program the kerf (the elements spacing) is increased to 0.005 mm where the clearance of the breast phantom is increased and the details is higher than the reference output.

- **Generate the transducer apertures for send and receive**

```
f0=3e6;                 % Transducer center frequency [Hz].
fs=100e6;               % Sampling frequency [Hz].
c=1540;                 % Speed of sound [m/s].
lambda=c/f0;            % Wavelength [m].
width=lambda/2;         % Width of element
element_height=7/1000;  % Height of element [m].
kerf=0.0100/1000;       % Kerf [m].
focus=[0 0 70]./1000;   % Fixed focal point [m].
N_elements=32;          % Number of physical elements
Display_angle=80;       % Display angle in degree
FBW= 0.4;               % Fractional bandwidth
```

The output is as following:

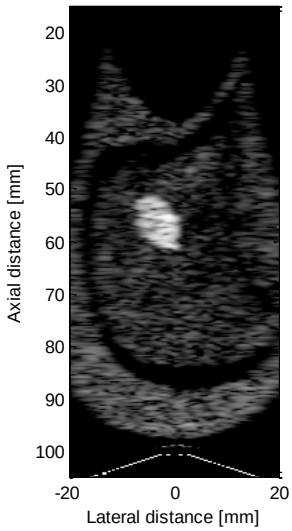

Figure 4.36 the elements spacing = 0.01 mm applied on breast cancer

Comment: in this program the kerf (the elements spacing) is increased to 0.01 mm where the clearance of the breast phantom is more increased and the details are higher than the previous output.

- **Generate the transducer apertures for send and receive**

```
f0=0.5e6;                % Transducer center frequency [Hz].
fs=100e6;                % Sampling frequency [Hz].
c=1540;                  % Speed of sound [m/s].
lambda=c/f0;             % Wavelength [m].
width=lambda/2;          % Width of element
element_height=7/1000;   % Height of element [m].
kerf=0.0025/1000;        % Kerf [m].
focus=[0 0 70]./1000;    % Fixed focal point [m].
N_elements=32;           % Number of physical elements
Display_angle=80;        % Display angle in degree
FBW= 0.4;                % Fractional bandwidth
```

The output is as following:

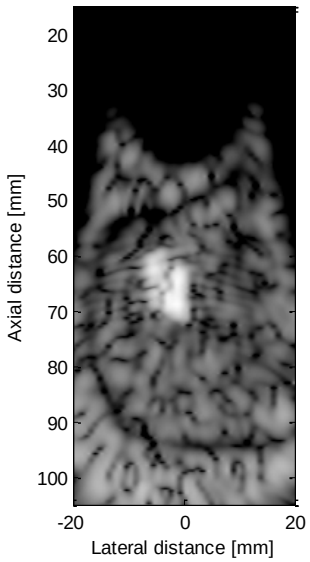

Figure 4.37 the transducer center frequency = 0.5 MHz applied on breast cancer

Comment: in this program the transducer center frequency is increased to 0.5 MHz where the clearance of the breast phantom is decreased and the details are the worst one compared with the reference output.

- **Generate the transducer apertures for send and receive**

```
f0=5e6;                 %  Transducer center frequency [Hz].
fs=100e6;               %  Sampling frequency [Hz].
c=1540;                 %  Speed of sound [m/s].
lambda=c/f0;            %  Wavelength [m].
width=lambda/2;         %  Width of element
element_height=7/1000;  %  Height of element [m].
kerf=0.0025/1000;       %  Kerf [m].
focus=[0 0 70]./1000;   %  Fixed focal point [m].
N_elements=32;          %  Number of physical elements
Display_angle=80;       %  Display angle in degree
FBW= 0.4;               %  Fractional bandwidth
```

The output is as following:

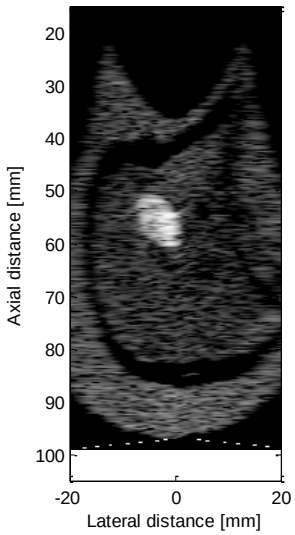

Figure 4.38 the transducer center frequency = 5 MHz applied on breast cancer

Comment: in this program the transducer center frequency is increased to 5 MHz where the clearance of the breast phantom is increased and the details are very good compared with the reference output.

- **Generate the transducer apertures for send and receive**

```
f0=5e6;                 %  Transducer center frequency [Hz].
fs=100e6;               %  Sampling frequency [Hz].
c=1540;                 %  Speed of sound [m/s].
lambda=c/f0;            %  Wavelength [m].
width=lambda/2;         %  Width of element
element_height=7/1000;  %  Height of element [m].
kerf=0.0025/1000;       %  Kerf [m].
focus=[0 0 70]./1000;   %  Fixed focal point [m].
N_elements=64;          %  Number of physical elements
Display_angle=80;       %  Display angle in degree
FBW= 0.4;               %  Fractional bandwidth
```

The output is as following:

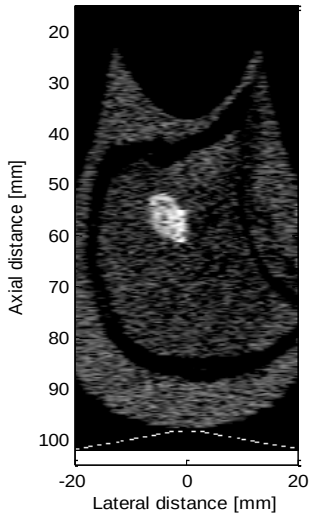

Figure 4.39 the Transducer center frequency = 5 MHz, and the number of physical elements=64 applied on breast cancer

Comment: in this program the transducer center frequency is increased to 5 MHz and the transducer number of physics element to (64) where the clearance of the breast phantom is increased and the details are excellent compared with the reference output.

- **Generate the transducer apertures for send and receive**

```
f0=5e6;                 %  Transducer center frequency [Hz].
fs=100e6;               %  Sampling frequency [Hz].
c=1540;                 %  Speed of sound [m/s].
lambda=c/f0;            %  Wavelength [m].
width=lambda/2;         %  Width of element
element_height=7/1000;  %  Height of element [m].
kerf=0.0100/1000;       %  Kerf [m].
focus=[0 0 70]./1000;   %  Fixed focal point [m].
N_elements=32;          %  Number of physical elements
Display_angle=80;       %  Display angle in degree
FBW= 0.4;               %  Fractional bandwidth
```

The output is as following:

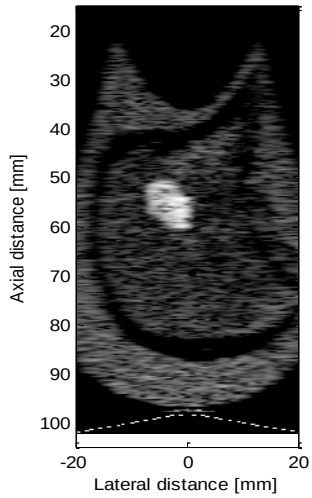

Figure 4.40 the Transducer center frequency = 5 MHz, and the element spacing=0.01 mm applied on breast cancer

Comment: in this program the transducer center frequency is increased to 5 MHz and the transducer spacing (kerf) to 0.01 mm where the clearance of the breast phantom is increased and the details are preferred compared with the reference output.

- **Generate the transducer apertures for send and receive**

```
f0=5e6;                 %  Transducer center frequency [Hz].
fs=100e6;               %  Sampling frequency [Hz].
c=1540;                 %  Speed of sound [m/s].
lambda=c/f0;            %  Wavelength [m].
width=lambda/2;         %  Width of element
element_height=7/1000;  %  Height of element [m].
kerf=0.0100/1000;       %  Kerf [m].
focus=[0 0 70]./1000;   %  Fixed focal point [m].
N_elements=64;          %  Number of physical elements
Display_angle=80;       %  Display angle in degree
FBW= 0.4;               %  Fractional bandwidth
```

The output is as following:

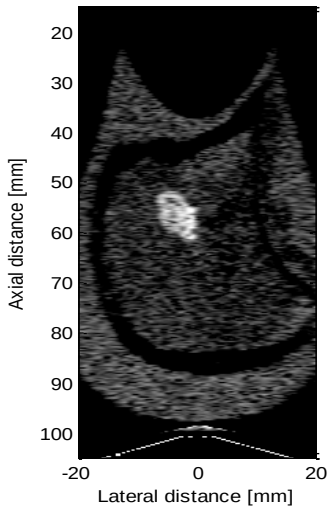

Figure 4.41 the Transducer center frequency = 5 MHz,
The number of physical elements=64, and the element spacing=0.010 mm applied on breast cancer

Comment: in this program the transducer center frequency is increased to 5 MHz and the transducer spacing (kerf) to 0.01 mm, and the transducer number of physical elements to (64) which demonstrates the best output compared with all previous outputs.

- **Generate the transducer apertures for send and receive**

```
f0=3e6;                 % Transducer center frequency [Hz].
fs=100e6;               % Sampling frequency [Hz].
c=1540;                 % Speed of sound [m/s].
lambda=c/f0;            % Wavelength [m].
width=lambda/8;         % Width of element
element_height=7/1000;  % Height of element [m].
kerf=0.0025/1000;       % Kerf [m].
focus=[0 0 70]./1000;   % Fixed focal point [m].
N_elements=32;          % Number of physical elements
Display_angle=80;       % Display angle in degree
FBW= 0.4;               % Fractional bandwidth
```

The output is as following:

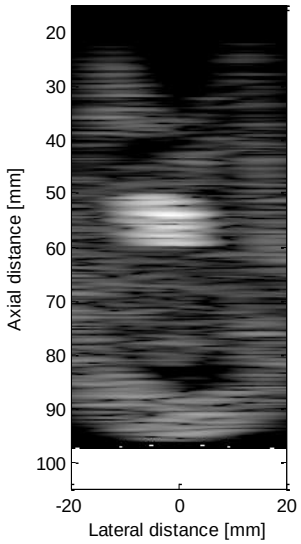

Figure 4.42 the Width of element= lambda/8 applied on breast cancer

Comment: in this program the width of element is decreased where the clearance of the breast phantom is decreased and the details aren't preferred compared with the reference output.

- **Generate the transducer apertures for send and receive**

```
f0=3e6;                 % Transducer center frequency [Hz].
fs=100e6;               % Sampling frequency [Hz].
c=1540;                 % Speed of sound [m/s].
lambda=c/f0;            % Wavelength [m].
width=lambda/4;         % Width of element
element_height=7/1000;  % Height of element [m].
kerf=0.0025/1000;       % Kerf [m].
focus=[0 0 70]./1000;   % Fixed focal point [m].
N_elements=32;          % Number of physical elements
Display_angle=80;       % Display angle in degree
FBW= 0.4;               % Fractional bandwidth
```

The output is as following:

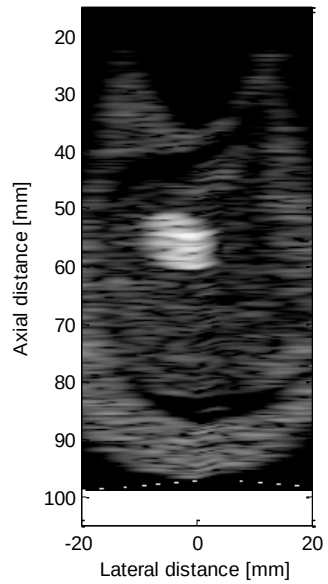

Figure 4.43 the Width of element= lambda/4 applied on breast cancer

Comment: in this program the width of element is decreased where the clearance of the breast phantom is slightly increased and the details also aren't preferred compared with the reference output.

- **Generate the transducer apertures for send and receive**

```
f0=3e6;                 % Transducer center frequency [Hz].
fs=100e6;               % Sampling frequency [Hz].
c=1540;                 % Speed of sound [m/s].
lambda=c/f0;            % Wavelength [m].
width=lambda ;          %  Width of element
element_height=7/1000;  % Height of element [m].
kerf=0.0025/1000;       % Kerf [m].
focus=[0 0 70]./1000;   % Fixed focal point [m].
N_elements=32;          % Number of physical elements
Display_angle=80;       % Display angle in degree
FBW= 0.4;               % Fractional bandwidth
```

The output is as following:

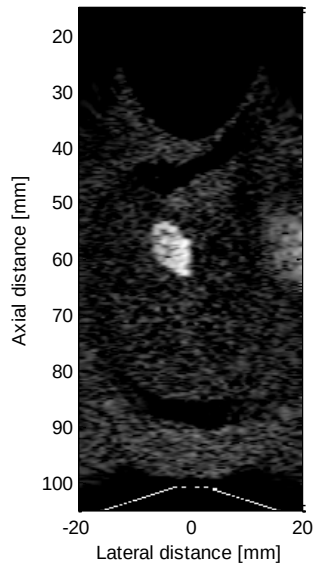

Figure 4.44 the Width of element= lambda/8 applied on breast cancer

Comment: in this program the width of element is increased where the clearance of the breast phantom is increased and the details aren't a good compared with the reference output.

- **Generate the transducer apertures for send and receive**

```
f0=3e6;                 % Transducer center frequency [Hz].
fs=100e6;               % Sampling frequency [Hz].
c=1540;                 % Speed of sound [m/s].
lambda=c/f0;            % Wavelength [m].
width=2*lambda ;        %  Width of element
element_height=7/1000;  % Height of element [m].
kerf=0.0025/1000;       % Kerf [m].
focus=[0 0 70]./1000;   % Fixed focal point [m].
N_elements=32;          % Number of physical elements
Display_angle=80;       % Display angle in degree
FBW= 0.4;               % Fractional bandwidth
```

The output is as following:

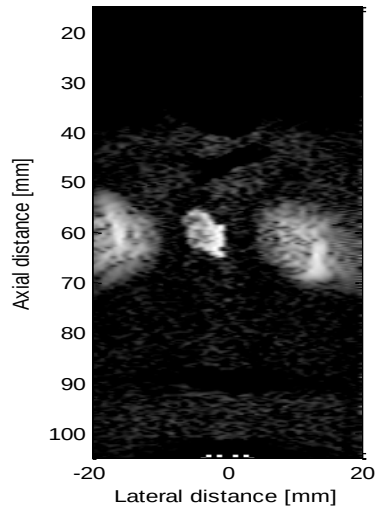

Figure 4.45 the Width of element= lambda applied on breast cancer

Comment: in this program the width of element is more increased where the clearance of the breast phantom is a very bad compared with the reference output.

Conclusion: in all references, the width of element equal to (lambda/2) and this cleared from previous programs that the best output at this width.

Chapter Five: The k-Wave Toolbox analysis

5.1 Overview of Functions

The k-Wave toolbox is designed to make photoacoustic modeling easy and fast. The functions included within the toolbox can be divided into four broad categories:

- The simulation of photoacoustic (or ultrasonic) wave fields.
- The reconstruction of photoacoustic images.
- The creation of geometric shapes.
- Utility and system functions.

The simulation functions compute the time evolution of an acoustic wave field within homogeneous or heterogeneous media in either 1-, 2-, or 3-D. The computations are based on a k-space solution to coupled acoustic equations as discussed in Sec. 2. These functions can also be used for time reversal image reconstruction. The additional image reconstruction functions allow the initial photoacoustic pressure to be estimated from data recorded over a linear (2-D) or planar (3-D) measurement surface. The geometry creation functions allow both Cartesian- and grid-based geometries to be defined, including circles, arcs, disks, spheres, shells, and balls.

The Cartesian-based functions return the geometric coordinates of the particular shape, while the grid-based functions return a binary matrix (i.e., matrix of 1s and 0s) where the 1s correspond to the location of shape. The utility functions are used to perform additional tasks such as grid creation, matrix smoothing, matrix interpolation, file loading, etc. Examples of using many of the functions within the toolbox are given in the following sections.

5.2 Times-Domain Simulation of Photoacoustic Wave Fields

Figure 5.1 illustrates the computational architecture of the simulation functions based on the coupled first-order acoustic equations (kspaceFirstOrder1D, kspaceFirst -Order2D, and kspaceFirstOrder3D). The functions are given information about the discretization of the propagation medium, its acoustic properties, the initial (or time varying) pressure distribution, and the location and characteristics of the measurement surface that detects the ultransonic wave field. These properties are assigned as fields within four input structures; kgrid, medium, source, and sensor. The propagation of the wave field through the medium is then computed step by step, with the pressure values at the sensor elements stored after each iteration. These values are returned when the time loop has completed. A simple example of a 2-D simulation in a heterogeneous layered medium is given here (1-D and 3-D simulations are performed in an analogous fashion):

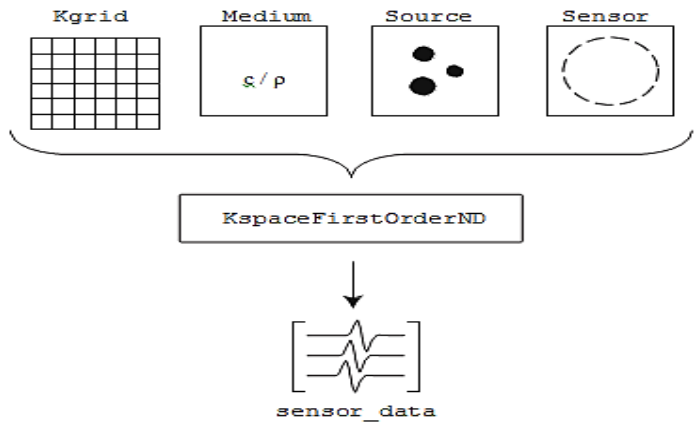

Figure 5.1 Schematic of the architecture of the simulation functions within the k-wave toolbox that are based on coupled first-order acoustic equations for heterogeneous media

```
% create the computational grid
Nx = 256;
Nz = 128;
dx = 50e−6;
kgrid = makeGrid(Nx, dx, Nz, dz);
```

The medium discretization is performed using the utility function makeGrid. The size (dx, dz) and number (Nx, Nz) of pixels in each Cartesian direction are used to calculate the Cartesian and k-space discretizations, and a k-Wave grid structure kgrid encapsulating this information is returned. The discretizations are calculated to satisfy the requirements of the FFT-based spatial derivatives. This structure is used extensively by both the simulation and utility functions within k-Wave. The time-steps used in the simulation are defined by kgrid.t_array, which is set to ‘auto’ by makeGrid. In this case, the time array is automatically calculated within the simulation functions using the utility function makeTime based on the size and properties of the k-space grid and sensible stability criterion.

5.3 The simulation examples to illustrate effective parameters on the ultrasound transducers

These examples show how the nonlinear beam pattern from an ultrasound transducer can be modeled. It builds on the Defining an Ultrasound Transducer and Simulating Transducer Field Patterns examples.

Appendix A shows the temperature scale for the figures from figure 5.2 to figure 5.25 .

This example shows an ultrasound transducer from the above position with the following parameters :

```
source_strength = 1e6;                  % [Pa].
tone_burst_freq = 0.5e6;                % [Hz].
tone_burst_cycles = 5;
transducer.number_elements = 32;        % total number of transducer elements
transducer.element_width = 1;           % width of each element [grid points].
transducer.element_length = 12;         % length of each element [grid points].
transducer.element_spacing = 0;         % kerf width between the elements
transducer.radius = inf;                % radius of curvature of the transducer [m].
```

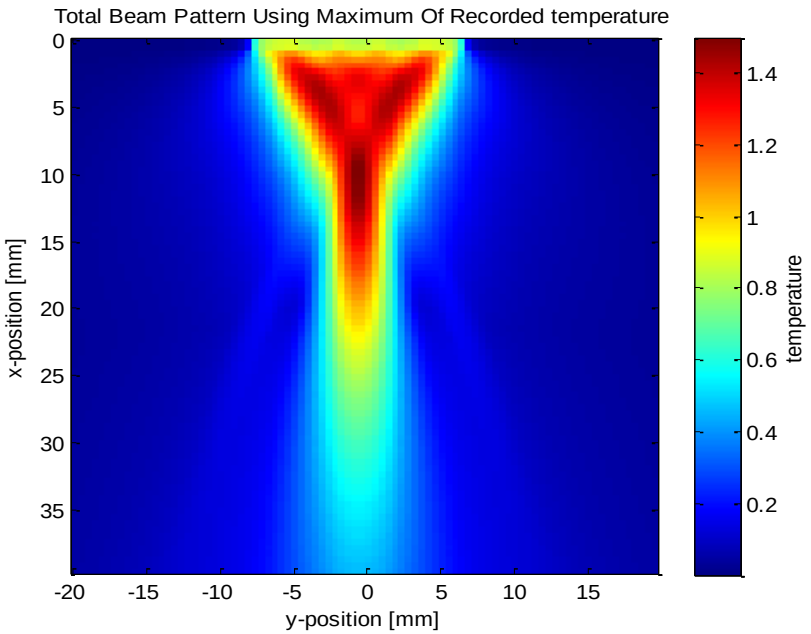

Figure 5.2 heat distribution of ultrasound transducer from above position

Comment : the transducer field pattern as shown demonstrates that the maximum temperature region located at x= [8:13], and y= [-1.5:1.5]. There are other unpreferable two regions at the face region of the transducer.

This example shows an ultrasound transducer from the bottom position with the following parameters :

```
source_strength = 1e6;                  % [Pa].
tone_burst_freq = 0.5e6;                % [Hz].
tone_burst_cycles = 5;
transducer.number_elements = 32;        % total number of transducer elements
transducer.element_width = 1;           % width of each element [grid points].
transducer.element_length = 12;         % length of each element [grid points].
transducer.element_spacing = 0;         % kerf width between the elements
transducer.radius = inf;                % radius of curvature of the transducer [m].
```

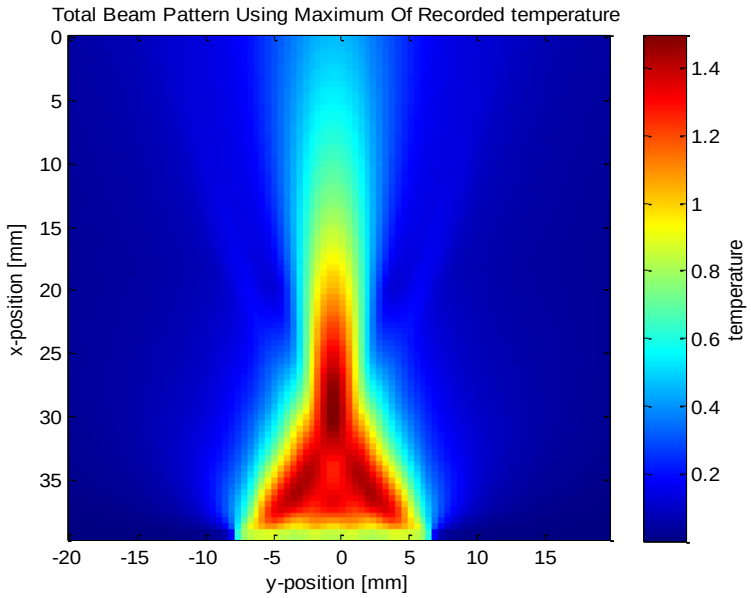

Figure 5.3 heat distribution of ultrasound transducer from bottom position

Comment : this is another transducer where the field pattern is flipped according to the position of transducer, as shown it demonstrates that the maximum temperature region located at x=[27:32], and y=[-1.5:1.5]. There are another unpreferable two regions at the face region of the transducer.

This example shows an ultrasound transducer from the left position with the following parameters :

```
source_strength = 1e6;                  % [Pa].
tone_burst_freq = 0.5e6;                % [Hz].
tone_burst_cycles = 5;
transducer.number_elements = 32;        % total number of transducer elements
transducer.element_width = 1;           % width of each element [grid points].
transducer.element_length = 12;         % length of each element [grid points].
transducer.element_spacing = 0;         % kerf width between the elements
transducer.radius = inf;                % radius of curvature of the transducer [m].
```

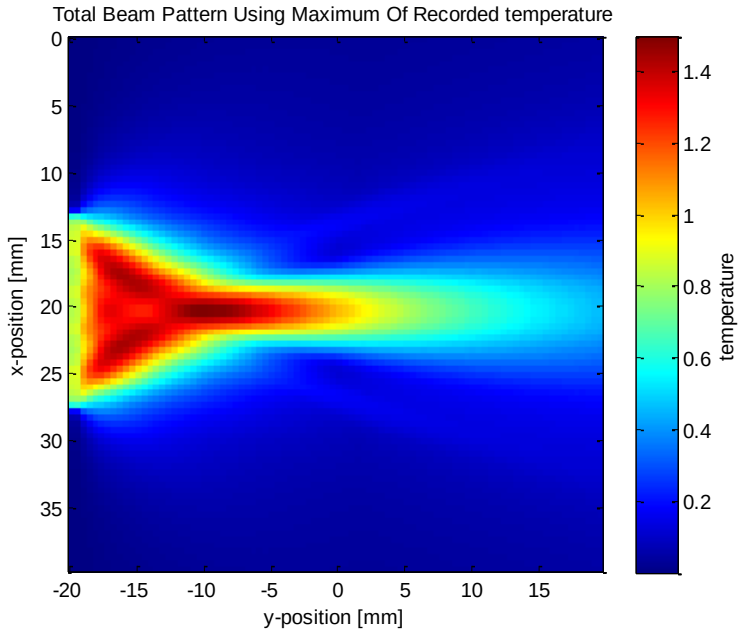

Figure 5.4 heat distribution of ultrasound transducer from left position

Comment : this is another transducer where the field pattern is rotated according to the position of transducer, as shown it demonstrates that the maximum temperature region located at x= [18.5:21.5], and y= [-12:-7]. There are another unpreferable two regions at the face region of the transducer.

This example shows an ultrasound transducer from the right position with the following parameters :

```
source_strength = 1e6;                  % [Pa].
tone_burst_freq = 0.5e6;                % [Hz].
tone_burst_cycles = 5;
transducer.number_elements = 32;        % total number of transducer elements
transducer.element_width = 1;           % width of each element [grid points].
transducer.element_length = 12;         % length of each element [grid points].
transducer.element_spacing = 0;         % kerf width between the elements.
transducer.radius = inf;                % radius of curvature of the transducer [m].
```

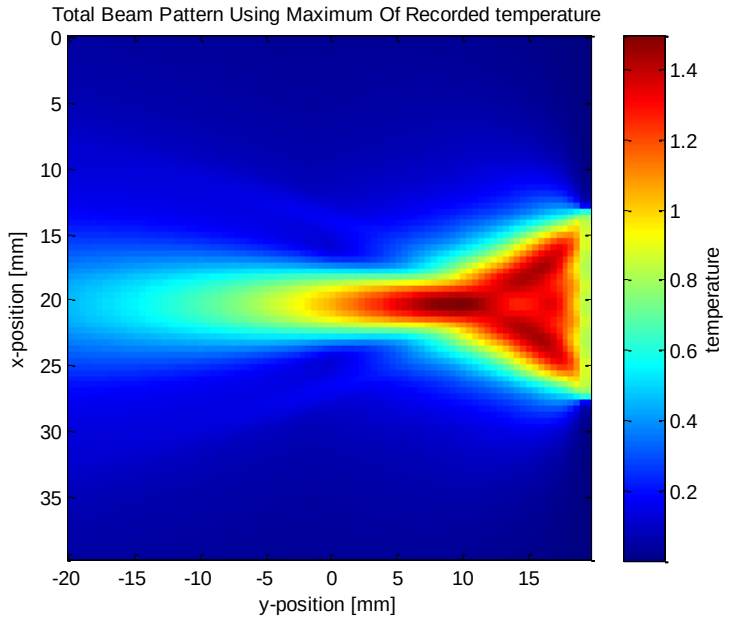

Figure 5.5 heat distribution of ultrasound transducer from right position

Comment : this is another transducer where the field pattern is rotated according to the position of transducer, as shown it demonstrates that the maximum temperature region located at x= [18.5:21.5], and y= [7:12]. There are another unpreferable two regions at the face region of the transducer.

This example shows summation of two ultrasound transducers at horizontal position with the following parameters :

```
source_strength = 1e6;                  % [Pa].
tone_burst_freq = 0.5e6;                % [Hz].
tone_burst_cycles = 5;
transducer.number_elements = 32;        % total number of transducer elements
transducer.element_width = 1;           % width of each element [grid points].
transducer.element_length = 12;         % length of each element [grid points].
transducer.element_spacing = 0;         % kerf width between the elements.
transducer.radius = inf;                % radius of curvature of the transducer [m].
```

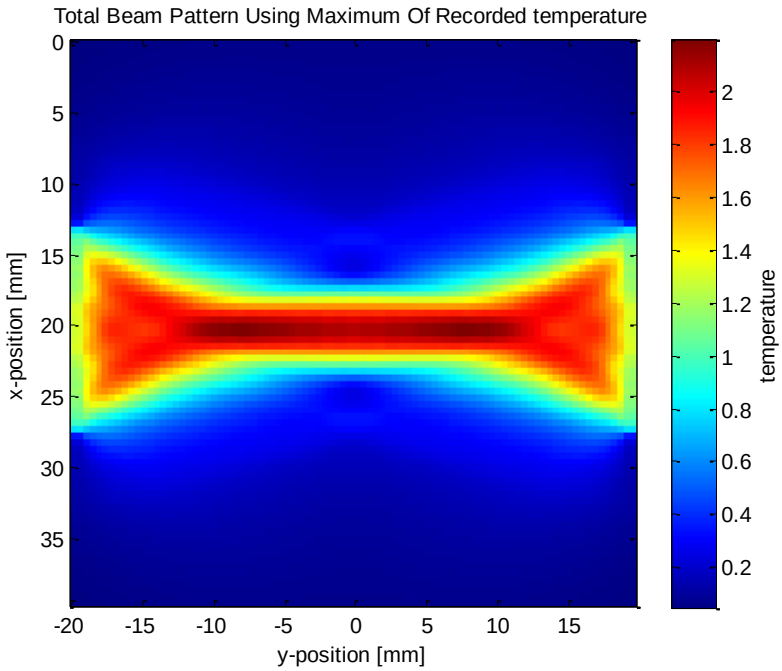

Figure 5.6 heat distribution of two ultrasound transducer at horizontal position

Comment : this field pattern is produced from summation of two ultrasound transducer at the horizontal position, as shown it demonstrates that the maximum temperature region located at x= [18.5:21.5], and y= [-12:12].

This example shows summation of two ultrasound transducers at vertical position with the following parameters :

```
source_strength = 1e6;                  % [Pa].
tone_burst_freq = 0.5e6;                % [Hz].
tone_burst_cycles = 5;
transducer.number_elements = 32;        % total number of transducer elements
transducer.element_width = 1;           % width of each element [grid points].
transducer.element_length = 12;         % length of each element [grid points].
transducer.element_spacing = 0;         % kerf width between the elements
transducer.radius = inf;                % radius of curvature of the transducer [m].
```

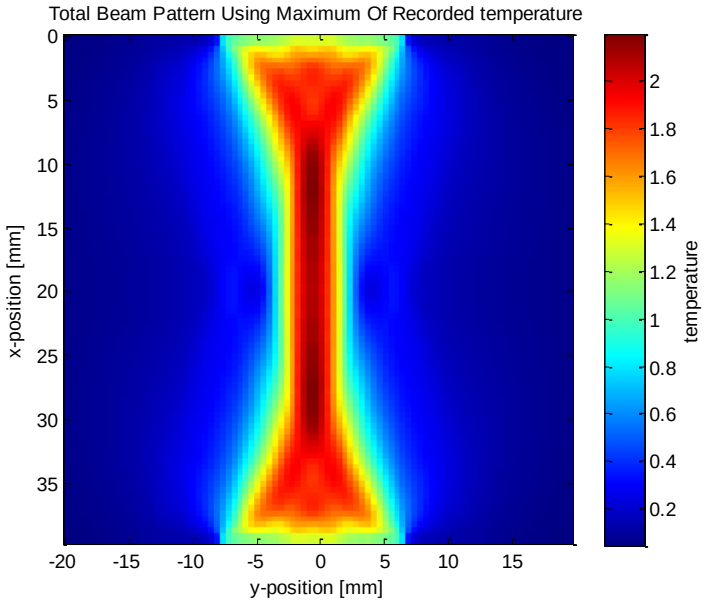

Figure 5.7 heat distribution of two ultrasound transducers at vertical position

Comment : this field pattern is produced from summation of two ultrasound transducer at the vertical position, as shown it demonstrates that the maximum temperature region located at x= [8:32], and y= [-1.5:1.5]..

This example shows summation of four ultrasound transducers at all positions with the following parameters :

```
source_strength = 1e6;                  % [Pa].
tone_burst_freq = 0.5e6;                % [Hz].
tone_burst_cycles = 5;
transducer.number_elements = 32;        % total number of transducer elements
transducer.element_width = 1;           % width of each element [grid points].
transducer.element_length = 12;         % length of each element [grid points].
transducer.element_spacing = 0;         % kerf width between the elements
transducer.radius = inf;                % radius of curvature of the transducer [m].
```

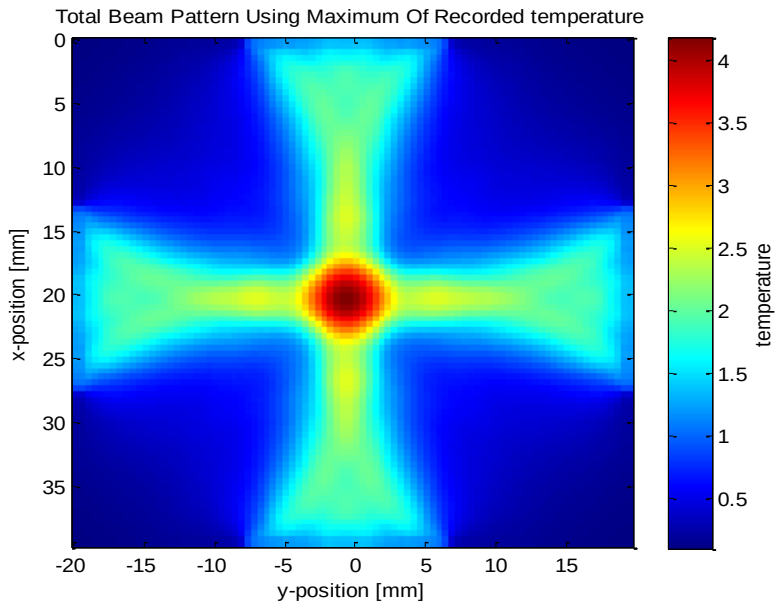

Figure 5.8 heat distributions of four ultrasound transducers and this output will be taken as a reference

Comment : this field pattern is produced from summation of four ultrasound transducers from all positions, as shown it demonstrates that the maximum temperature point located at x= [18:22], and y= [-2:2]. This output will be taken as the reference for all the following programs compared with the k-wave_user_manual.

This example show the output for summation of four transducers as shown where we changed the transducer number elements from 32 to 64 the output is

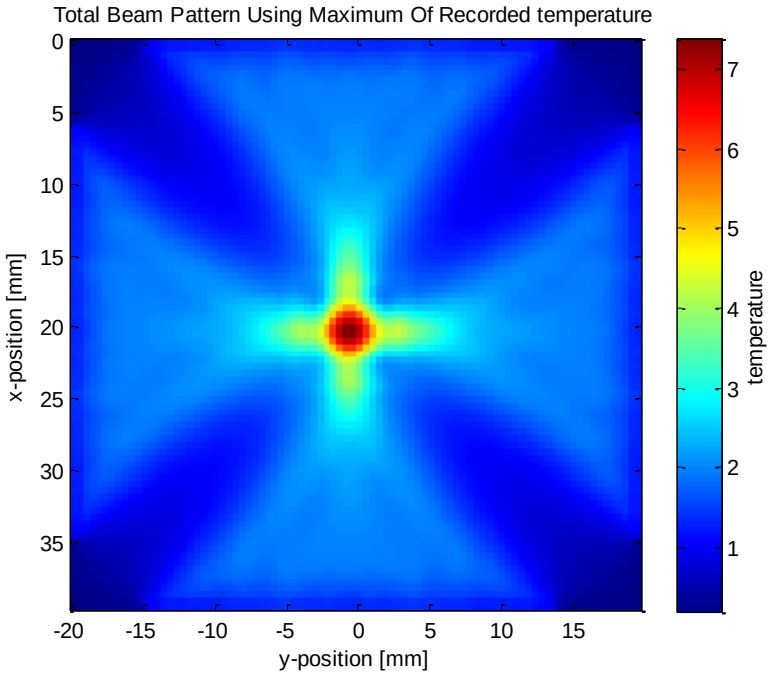

Figure 5.9 heat distributions of four ultrasound transducers where the transducer number elements=64

Comment : this field pattern is produced from summation of four ultrasound transducers from all positions where we increase the transducer number elements, as shown it demonstrates that the maximum temperature point located at x=[19:21], and y=[-1:1]. .

This example show the output for summation of four transducers as shown where the transducer number elements is reduced from 32 to 16 the output is

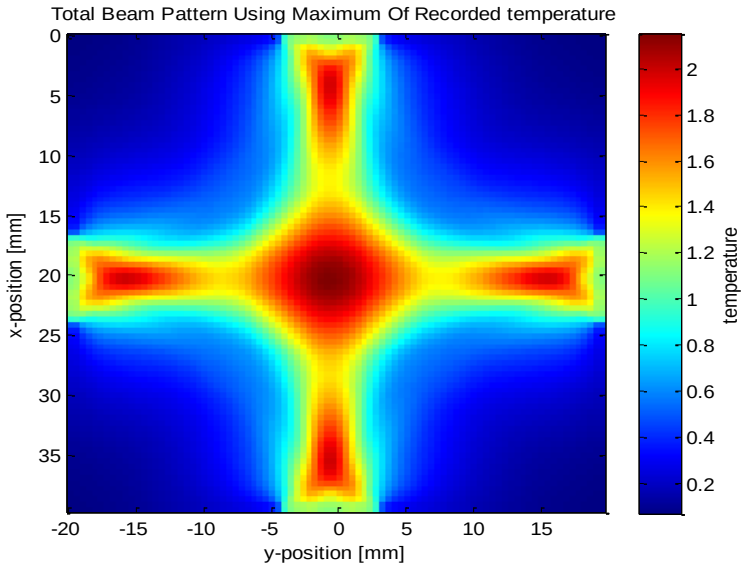

Figure 5.10 heat distributions of four ultrasound transducers where the transducer number elements=16

Comment : this field pattern is produced from summation of four ultrasound transducers from all positions where we decrease the transducer number elements, as shown it demonstrates that the maximum temperature point located at x=[17:23], and y=[-3:3]. There are unpreferable four regions at the face of transducers .

Conclusion: the number of transducer elements effect on the heat distribution as follows:

The higher number of transducer elements, the best focusing point and vice versa.

The number of transducer elements ranges according to the most catalogues as follows (16, 32, 64, and 132)

This example show the output for summation of four transducers as shown where the transducer element length is reduced from 12 to 6 the output is

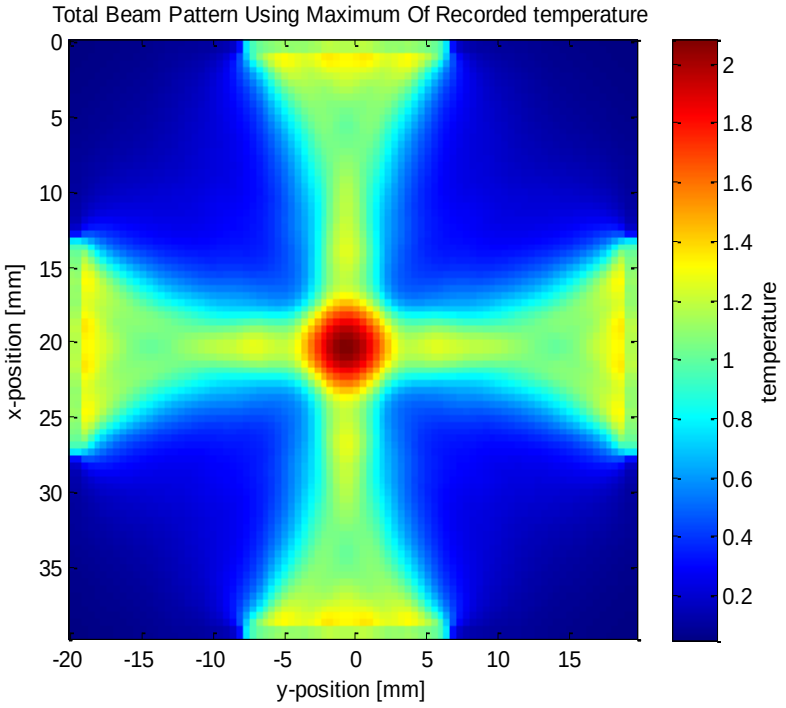

Figure 5.11 heat distributions of four ultrasound transducers where the transducer element length =6

Comment : this field pattern is produced from summation of four ultrasound transducers from all positions where the transducer element length is decreased, as shown it demonstrates that the maximum temperature point located at x=[18:22], and y=[-2:2]. The heat distribution starts very close to the face surface of transducers.

This example show the output for summation of four transducers as shown where the transducer element length is increased from 12 to 18 the output is

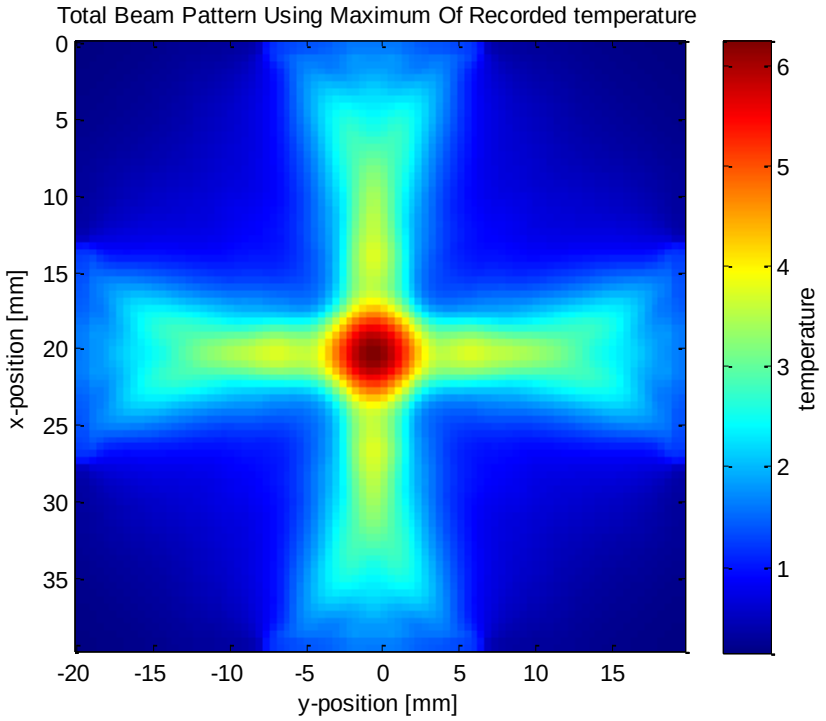

Figure 5.12 heat distributions of four ultrasound transducers where the transducer element length =18

Comment : this field pattern is produced from summation of four ultrasound transducers from all positions where we increase the transducer element length, as shown it demonstrates that the maximum temperature point located at x=[18:22], and y=[-2:2]. The heat distribution starts far from the face surface of transducer.

This example show the output for summation of four transducers as shown where the transducer element length is increased from 12 to 24 the output is

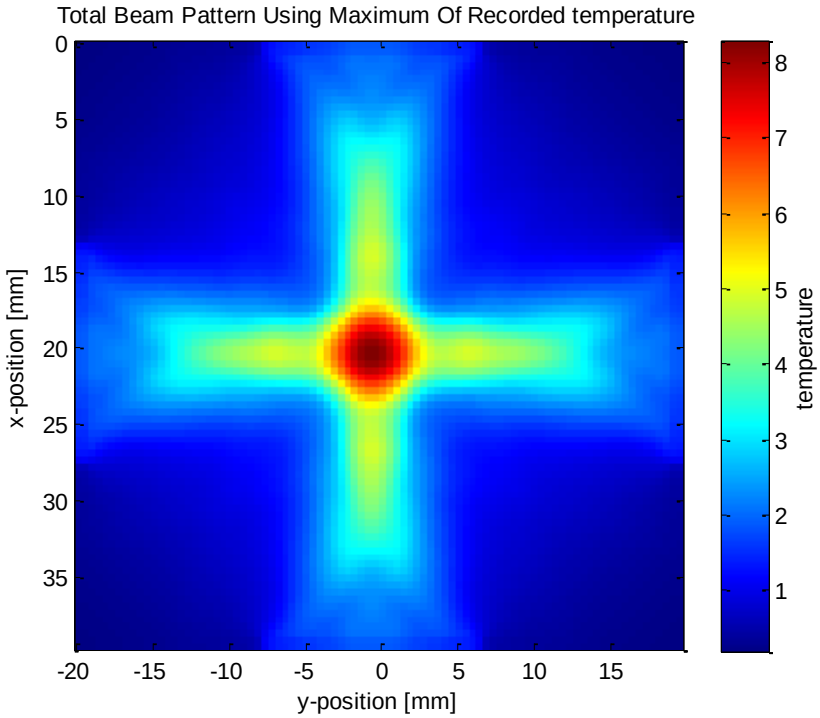

Figure 5.13 heat distributions of four ultrasound transducers where the transducer element length =24

Comment : this field pattern is produced from summation of four ultrasound transducers from all positions where we increase more the transducer element length , as shown it demonstrates that the maximum temperature point located at x=[18:22], and y=[-2:2]. The heat distribution starts more far from the face surface of transducer.

Conclusion: the transducer element length doesn't effects on the focal point of heat distribution but it effect on the starts of heat distribution by increasing or decreasing of the transducer element length .

This example show the output for summation of four transducers as shown where transducer element spacing is increased from 0 to 1 the output is

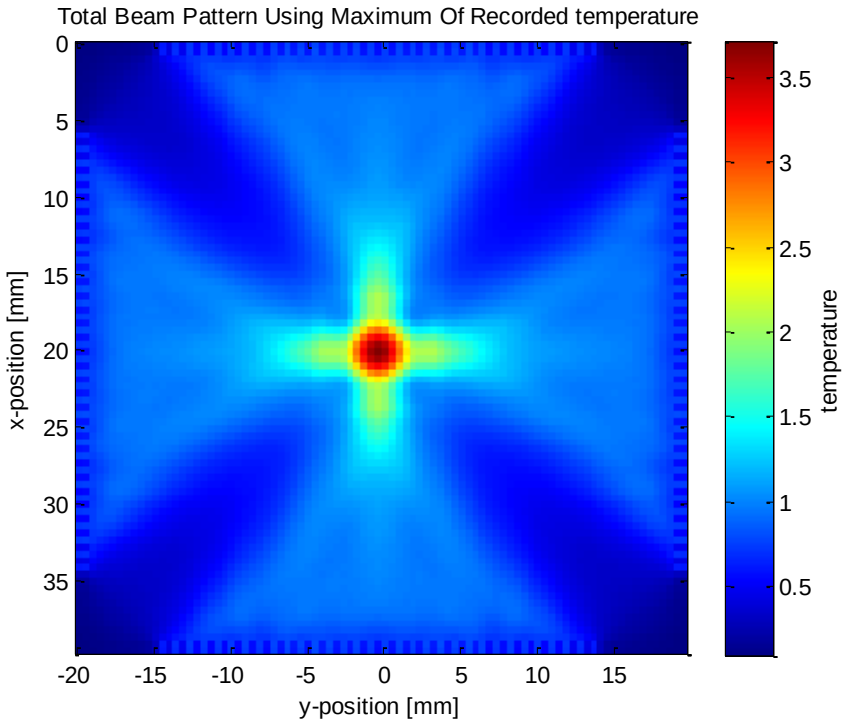

Figure 5.14 heat distributions of four ultrasound transducers where the transducer element spacing =1

Comment : the transducer element spacing means the kerf width between the elements, this field pattern is produced from summation of four ultrasound transducers from all positions where we more increase the transducer element spacing, as shown it demonstrates that the maximum temperature point located at x= [19:21], and y= [-1:1]. This output remembers us when increasing the transducer number elements and this case improve the output.

Conclusion: the transducer element spacing effects on the heat distribution as follows:

The higher transducer element spacing width, the best focusing point and vice versa

This example show the output for summation of four transducers as shown where tone burst frequency is decreased from 0.5 (MHz) to 0.25 (MHz) the output is

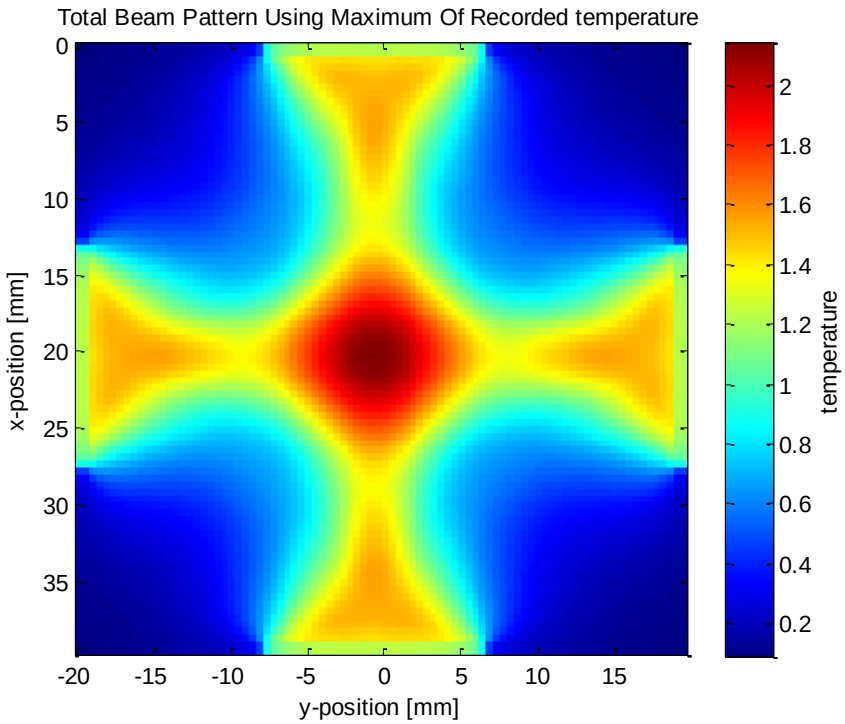

Figure 5.15 heat distributions of four ultrasound transducers where the Tone burst frequency =0.5 MHz

Comment : this field pattern is produced from summation of four ultrasound transducers from all positions where we decrease the tone burst frequency, as shown it demonstrates that the maximum temperature point located at x=[17:23], and y=[-3:3]. This output remembers us when decreasing the transducer number elements.

This example show the output for summation of four transducers as shown Where tone burst frequency is increased from 0.5 (MHz) to 1 (MHz) the output is

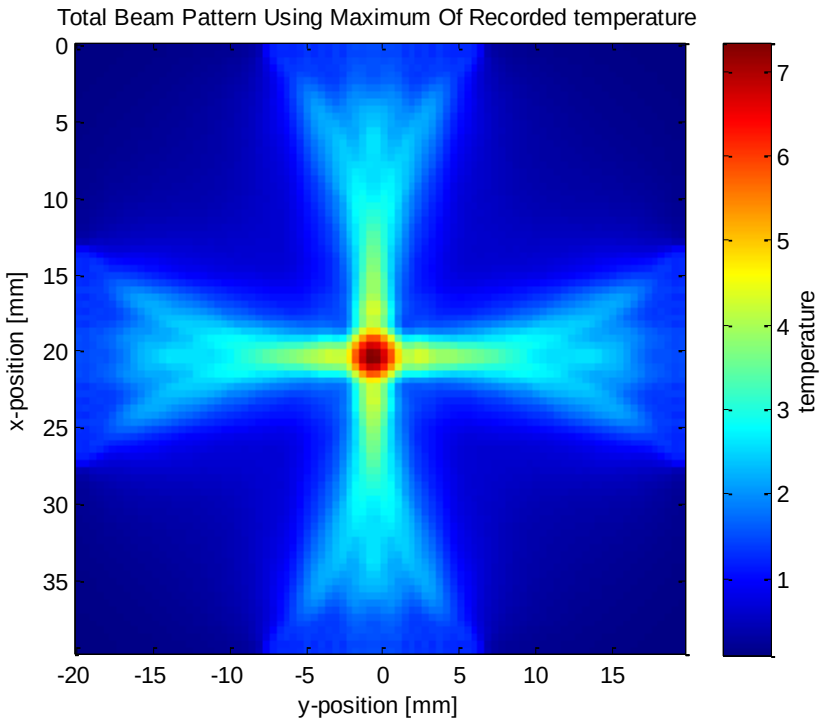

Figure 5.16 heat distributions of four ultrasound transducers where the tone burst frequency =1 MHz

Comment : this field pattern is produced from summation of four ultrasound transducers from all positions where we increase the tone burst frequency, as shown it demonstrates that the maximum temperature point located at x=[19:21], and y=[-1:1]. .

This example show the output for summation of four transducers as shown Where tone burst frequency is increased from 0.5 (MHz) to 2 (MHz) the output is

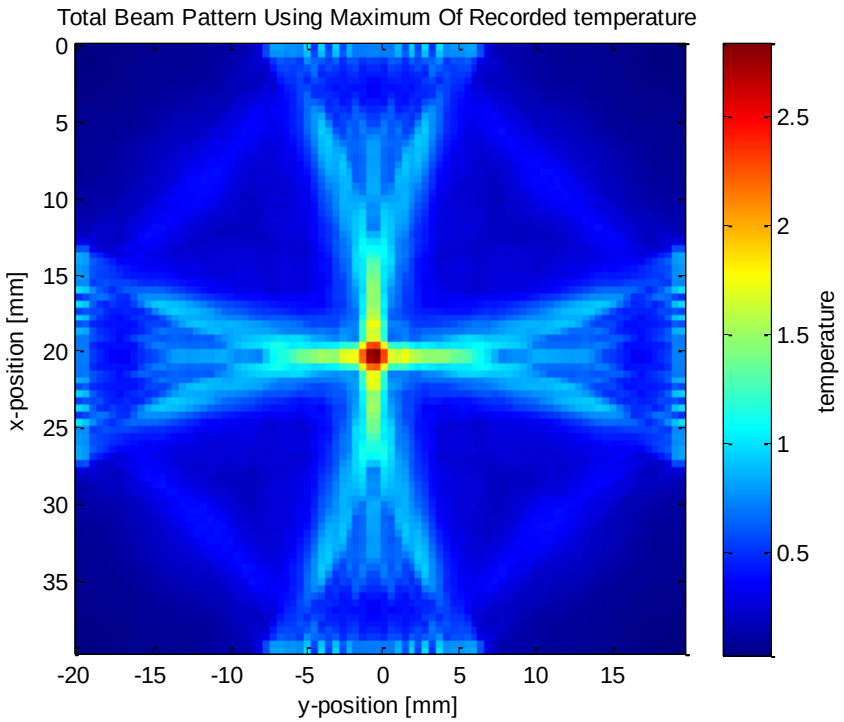

Figure 5.17 heat distributions of four ultrasound transducers where the Tone burst frequency =2 MHz

Comment : this field pattern is produced from summation of four ultrasound transducers from all positions where we increase the tone burst frequency, as shown it demonstrates that the maximum temperature point located at x=[19.5:20.5], and y=[-0.5: 0.5].

This example show the output for summation of four transducers as shown where tone burst frequency is increased from 0.5 (MHz) to 4 (MHz) the output is

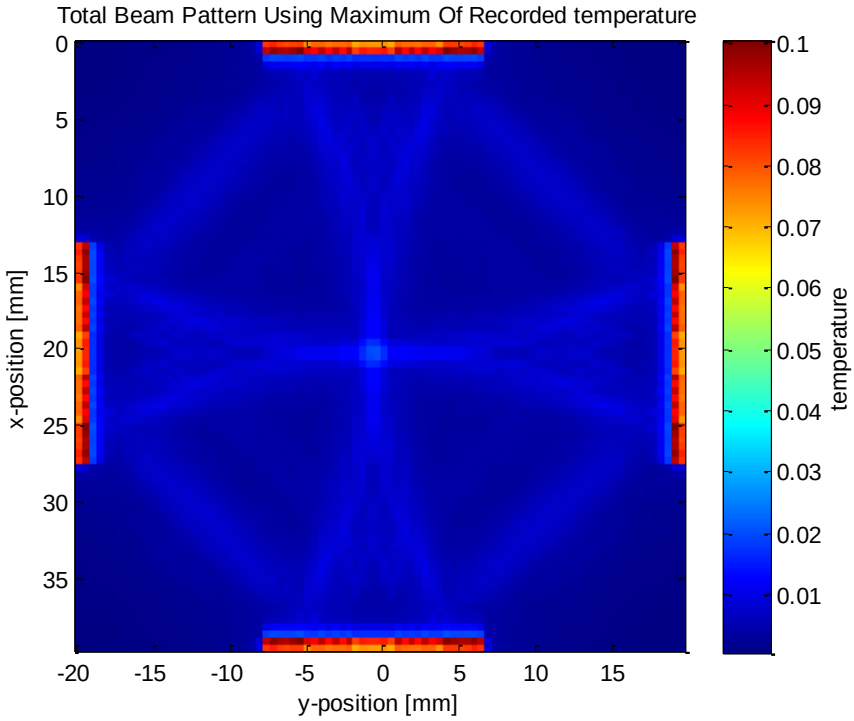

Figure 5.18 heat distributions of four ultrasound transducers where the Tone burst frequency =4 MHz

Comment : this field pattern is produced from summation of four ultrasound transducers from all positions where we more increase the tone burst frequency, as shown it demonstrates that the output is very bad.

Conclusion: tone burst frequency effects on the heat distribution as follows:

The more tone burst frequency, the greater focusing point and vice versa but take care any ultrasound transducer has a limitation of tone burst frequency , we must never go out from this limitation and thus which sudden at the last program.

This example show the output for summation of four transducers as shown where transducer focus distance is increased from 0.020 (m) to 0.160 (m) the output is

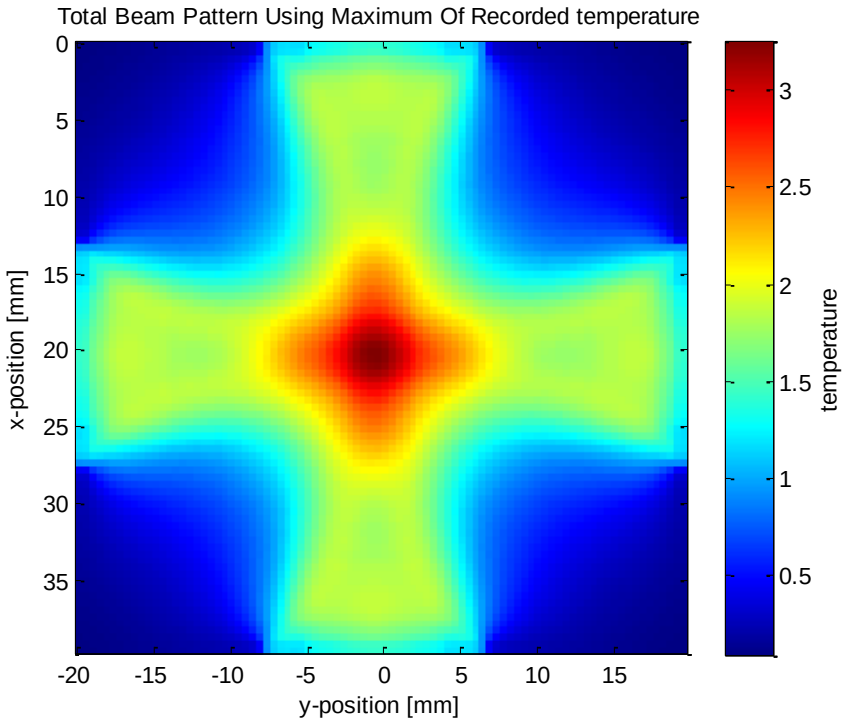

Figure 5.19 heat distributions of four ultrasound transducers where the transducer focus distance =160 mm

Comment : this field pattern is produced from summation of four ultrasound transducers from all positions where we more increase the transducer focus distance, as shown it demonstrates that the maximum temperature region located at x=[17.5:22.5], and y=[-2.5: 2.5].

This example show the output for summation of four transducers as shown where transducer focus distance is increased from 0.02 (m) to 0.08 (m) the output is

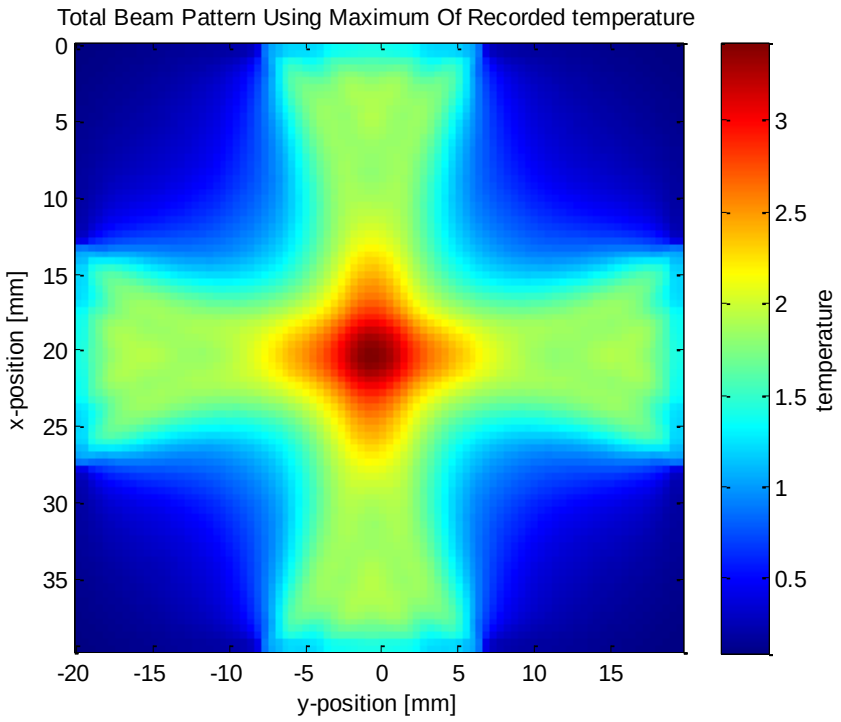

Figure 5.20 heat distributions of four ultrasound transducers where the transducer focus distance =80 mm

Comment : this field pattern is produced from summation of four ultrasound transducers from all positions where we increase the transducer focus distance, as shown it demonstrates that the maximum temperature region located at x=[18:22], and y=[-2: 2], and the output is better than the previous example .

This example show the output for summation of four transducers as shown where transducer focus distance is decreased from 0.020 (m) to 0.005 (m) the output is

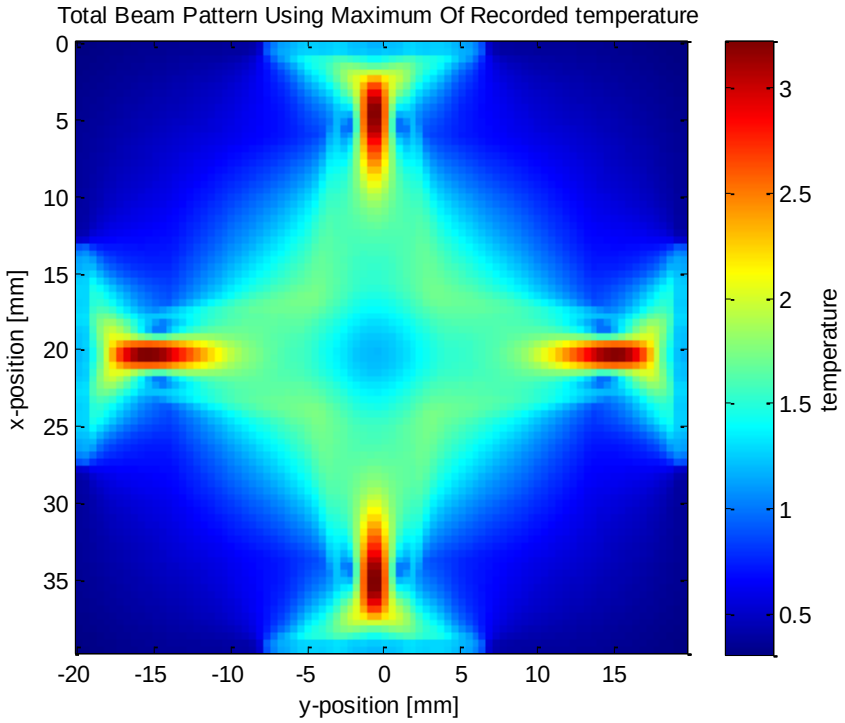

Figure 5.21 heat distributions of four ultrasound transducers where the transducer focus distance =5 mm

Comment : this field pattern is produced from summation of four ultrasound transducers from all positions where we decrease the transducer focus distance, as shown it demonstrates that the maximum temperature point located at four different points, and the output is the worst one compared with all the previous examples.

Conclusion: the transducer focus distance effects on the heat distribution where it focus the output of transducers at a certain point depending on the focus distance , and we limit the output region between x=[0:40], and y=[-20:20]. so the best transducer focus distance to locate the maximum field pattern at the center must be equal (20 mm) .

This example show the output for summation of four transducers as shown Where two parameters are increased such that increasing the transducer number elements from 32 to 64 and increasing tone burst frequency from 0.5 (MHz) to 1 (MHz), the output is

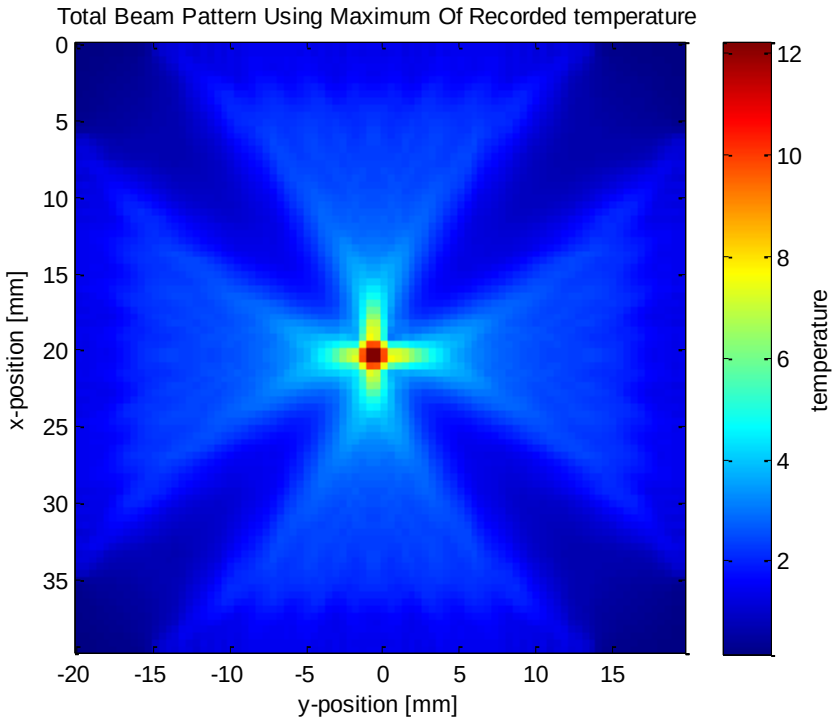

Figure 5.22 heat distributions of four ultrasound transducers
Where the transducer number elements=64 and tone burst frequency=1 MHz

Comment : this field pattern is produced from summation of four ultrasound transducers from all positions where we increase the transducer number elements and the tone burst frequency, the maximum temperature point located at x=[19.5:20.5], and y=[-0.5: 0.5], as shown it demonstrates that the output is very good compared with all previous .

This example show the output for summation of four transducers as shown Where two parameters are increased such that increasing the transducer number elements from 32 to 64 and increasing tone burst frequency from 0.5(MHz) to 2(MHz), the output is

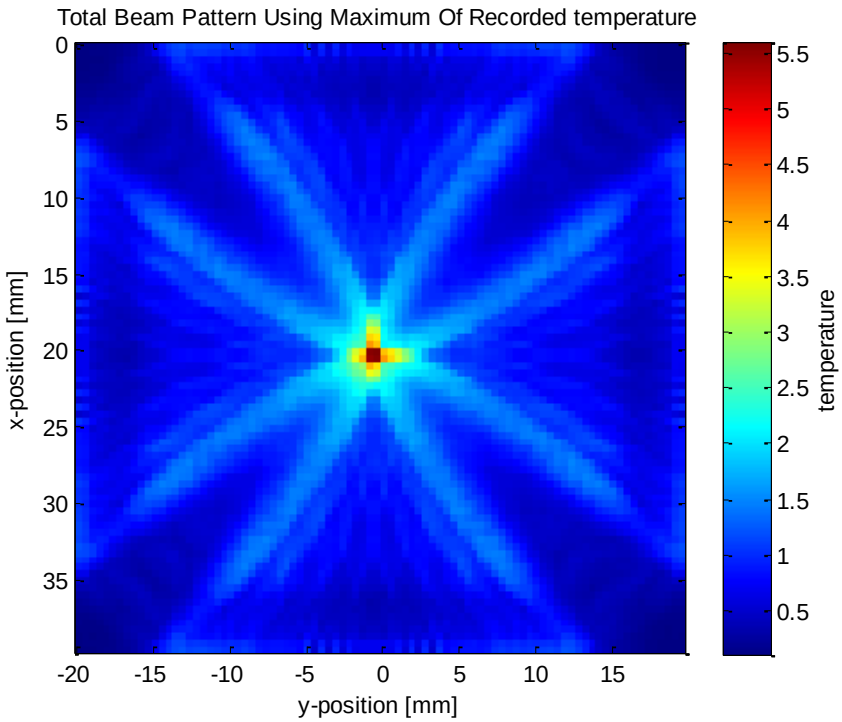

Figure 5.23 heat distributions of four ultrasound transducers
Where the transducer number elements=64 and tone burst frequency=2 MHz

Comment : this field pattern is produced from summation of four ultrasound transducers from all positions where we increase the transducer number elements and more increase the tone burst frequency, the maximum temperature point located at x=[19.6:20.4], and y=[-0.4: 0.4]. as shown it demonstrates that the output is very good compared with all previous .

Conclusion: the more tone burst frequency, the greater focusing point and the more number of transducer element, the best focusing point, when we take this two condition together it will improve the output very good .

This example show the output for summation of four transducers as shown Where two parameters are changed such that increasing the transducer element spacing from 0 to 1 and increasing tone burst frequency from 0.5(MHz) to 1(MHz), the output is

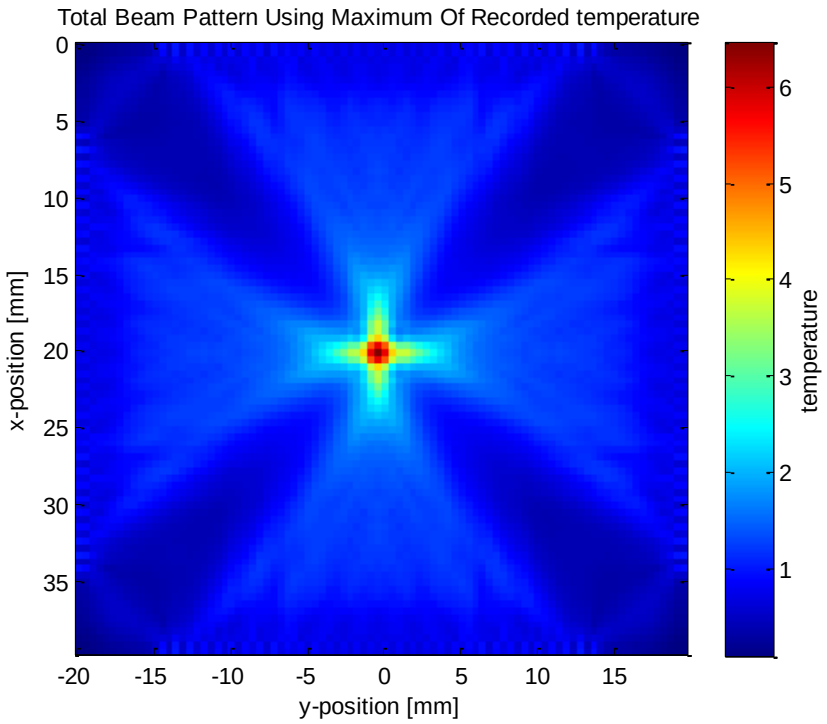

Figure 5.24 heat distributions of four ultrasound transducers
Where the transducer element spacing=1 and tone burst frequency=1 MHz

Comment : this field pattern is produced from summation of four ultrasound transducers from all positions where we increase the transducer element spacing and more increase the tone burst frequency, the maximum temperature point located at x=[19.6:20.4], and y=[-0.4: 0.4]. as shown it demonstrates that the output is very good .

This example show the output for summation of four transducers as shown Where three parameters are changed such that increasing the transducer element spacing from 0 to 1 and increasing tone burst frequency from 0.5(MHz) to 1(MHz),and increasing the transducer number elements from 32 to 64 the output is

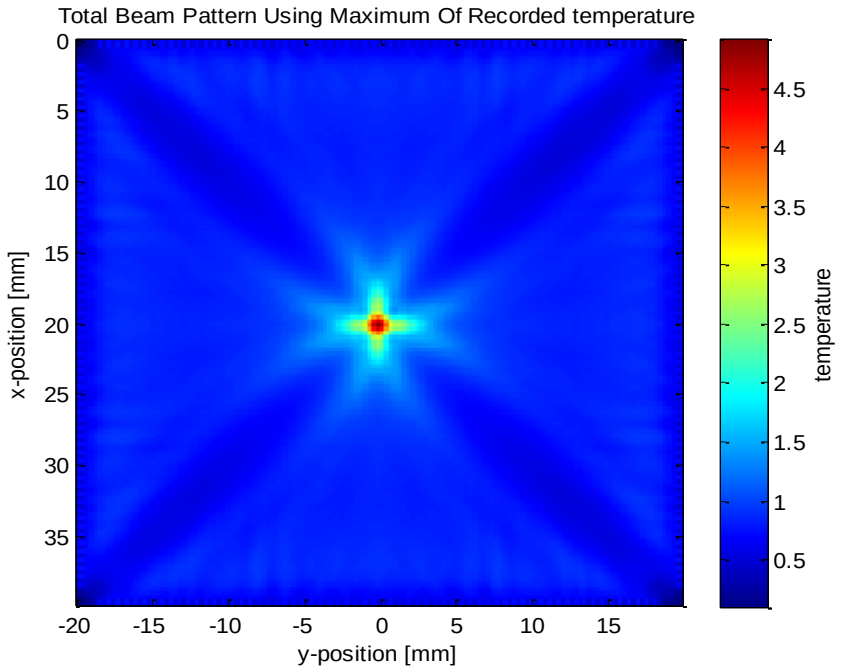

Figure 5.25 heat distributions of four ultrasound transducers where the transducer element spacing=1, the transducer number of elements=64 and tone burst frequency=1 MHz

Comment : this field pattern is produced from summation of four ultrasound transducers from all positions where we increase the transducer element spacing and more increase the tone burst frequency, and increasing the transducer number elements the maximum temperature point located at x=[19.9:20.1], and y=[-0.1: 0.1]. as shown it demonstrates that the output is the best one but take care when we increase the transducer element spacing and the transducer number elements the dimension of the output go out from the total grid point of the field pattern so we must increase and set total number of grid points from 128 to a number which is sufficient to contain the total grid points, we use total number of grid points =178.

From the previous programs we can conclude that:
Each transducer is affected with some parameters which increase or decrease in the heat distribution or the transducer field patterns such as:

- number of transducer elements

  There is a proportional relationship between the number of transducer elements and transducer field patterns where The higher number of transducer elements, the best focusing point and vice versa, and select the required number of transducer elements according to their catalogue which determine them.

- transducer element length

  The transducer element length doesn't affect the focal point of heat distribution but it affects the starts of heat distribution by increasing or decreasing of the transducer element length.

- tone burst frequency

  It is one of the most effected parameters of the ultrasound transducers where there are a proportional relationship between the tone burst frequency and transducer field patterns where the more tone burst frequency, the greater focusing point and vice versa but take care any ultrasound transducer has a limitation of tone burst frequency, we must never go out from this limitation.

- Temperature scale

  Taking into consideration that the range of temperature (35-45 ^{0}C) relative to our k-wave output scale (0 - 5) according to the programs which were created, and the values over 5 on scale means high temperature over 45^{o}C used for ablation so we use the appropriate scale which doesn't out of our range.

Chapter Six: Conclusions and future works

This chapter concludes the thesis by summarizing important observations, contributions and results. It also highlights the future avenues of research that has introduced from the work.

6.1 conclusions

This work represents a study to design an ultrasound cylindrical phased array used for hyperthermia treatment, Hyperthermia (also called thermal therapy or thermotherapy) is a type of cancer treatment in which body tissue is exposed to high temperatures (up to 44°C). Research has shown that high temperatures can damage and kill cancer cells, usually with minimal injury to normal tissues. By killing cancer cells and damaging proteins and structures within cells, hyperthermia may shrink tumors.

We used the cylindrical phased array which is profitable for the breast shape. The ultrasound transducers used have variable parameters which affected the transducer outputs such as the transducer center frequency, the spacing between elements, the transducer number of elements, and the width of elements.

We found that the best output occurs when the transducer number of elements is increased to 64, the transducer element spacing is increased to 1 (grid points), and the tone burst frequency is increased to 2(MHz) which gives more concentration at a certain point such that gives the highest temperature at this point (breast cancer region) of breast and gives lower temperatures at the surrounding regions to keep other cells at the normal condition.

6.2 Future works

Modeling of focusing ultrasound need more study for different positions such that more temperature at any point in the breast. Further study has to be concerned for tumor in brain or any part of the body.

.

References

[1] Osama.M.Hassan, Noha.S.D.Hassan, andYasser.M .kadah," Modeling of Ultrasound Hyperthermia Treatment of Breast Tumors", National Radio Science Conference, 26th, pp. 1-8, (2009).

[2] Mátai, G., " Medical applying of the radio frequency radiations ", Hungarian Science, Vol. 8, pp. 1024-1042, (2002).

[3] Mise, K., Kan, N., Okino," Effect of heat treatment on tumor cells and antitumor effector cells ", Cancer Research, Vol. 50, Issue 19, pp. 6199-6202, (1990).

[4] Lei, S. – Schiano, J. – Smith, N. B., " An adaptive control method for ultrasound prostate hyperthermia ", Proc. Of the IASTED International Conference, November 4-6, Cambridge, MA, USA, (2002).

[5] Hurwitz, M. D., Kaplan, I. D., "Feasibility and patient tolerance of a novel transrectal ultrasound hyperthermia system for treatment of prostatecancer ", Int. J. Hyperthermia, Vol. 17, Issue 1, pp. 31-37, (2001).

[6] Fosmire, H., Hynynen, K., Drach, G. W.," Feasibility and toxicity of transrectal ultrasound hyperthermia in the treatment of locally advanced adenocarcinoma of the prostate ", Int.J. Radiat. Oncol. Biol. Phys. Vol. 26, pp. 253-259, (1993).

[7] Wojcik, G., Mould, Jr., Lizzy, F., "Nonlinear modelling of therapeutic Ultrasound ", IEEE Ultrasonics Symposium Proceedings, pp. 1617-1622, (1995).

[8] Fry, W. J. – Mosberg, W. H. – Barnard, " Production of focal destructive lesions in the central nervous system with ultrasound ", J. Neurosurg. Vol. 11, pp. 471-478, (1954).

[9] Lizzi, F. L. – Coleman, D. J. – Driller, J.- Silverman, "A therapeutic ultrasound system incorporating real-time ultrasonic scanning", In Proc. of the 1986 Ultrasonics Symposium, McAvoy, B. R. (ed.), IEEE, New York,(1987).

[10] Damianou, C. A. – Hynynen. K. – Fan, X., "Evaluation of accurancy of a theoretical model for predicting the necrosed tissue volume during focused ultrasound surgery", IEEE Trans. Ultrason., Ferroelect. And Freq.Control, Vol. 42, pp. 182-187, (1995).

[11] Aanonsen, S. I., " Numerical computation of the nearfield of a finite amplitude sound beam ", Rep. #73, Dept of Mathematics, University of Bergen, (1983).

[12] Dermitzakis Aristides, Master‘s Thesis "Acoustical Behavior of Single Ultrasound Contrast Agent Microbubbles", January 2010.

[13] Dermitzakis Aristides, Presentations for the course, "Ultrasound", Retrieved 2-10-2013.

[14] Susan Katz Miller, " Exposure Criteria for Medical Diagnostic Ultrasound: II. Criteria Based on all Known Mechanisms", National Council on Radiation Protection and Measurements.

[15] Kwan H. Ng, "International Guidelines and Regulations for the Safe Use of Diagnostic Ultrasound in Medicine ", Journal of Medical Ultrasound, Vol 10, Issue 1, PP 5–9, (2002).

[16] Kenneth Erikson, Francis Fry, and Joie Jones, "Ultrasound in Medicine-A Review", IEEE Transactions On Sonics And Ultrasonic, Vol. 21, Issue 3, July (1971).

[17] Sariego, and Jack, "Breast cancer in the young patient", Southeastern Surgical Congress, Vol 76, Issue 12, pp. 1397-1400, (2010).

[18] http://www.nlm.nih.gov/medlineplus/malebreastcancer.html , Retrieved 2-10-2013.

[19] Florescu A, Amir E, Bouganim N, Clemons M, "Immune therapy for breast cancer in 2010-hype or hope?", Current Oncology, Vol 18(1), pp. 9-18, (2011).

[20] Thomas A. Buchholz, "Radiation therapy for early-stage breast cancer after breast-conserving surgery", the new England journal of medicine, Vol 360, Issue 63-70, (2009).

[21] http://en.wikipedia.org/wiki/Breast_cancer#cite_refIARC_GLOBAL_2008_5-1, Retrieved 2-10-2013.

[22] Boyle P., and Levin B., "World Cancer Report", International Agency for Research on Cancer,(2008).

[23] "Male Breast Cancer Treatment", National Cancer Institute, Retrieved 2-10-2013.

[24] Merck Manual of Diagnosis and Therapy ,"Breast Disorders: Breast Cancer", (February 2003).

[25] American Cancer Society, "Cancer Facts & Figures 2007", Retrieved 2-10-2013.

[26] Watson M, "Assessment of suspected cancer", InnovAiT journal, Vol. 1, Issue 2, pp. 94-107, (2008).

[28] Lacroix M, "Significance, detection and markers of disseminated breast cancer cells", Endocrine-related Cancer, Vol 13, Issue 4, pp. 1033-67. (2006).

[29] http://www.cancer.gov/cancertopics/factsheet/Sites-Types/metastatic Retrieved 2-10-2013.

[30] Reeder, JG, Vogel, and VG, "Breast cancer prevention", Cancer treatment and research, Vol 141, PP 149-164, (2008).

[31] Yager JD, "Estrogen carcinogenesis in breast cancer", The new England journal of medicine, Vol 354 (3), PP 270–282, (2006).

[32] Santoro, E., DeSoto, M., and Hong Lee, and J,"Hormone Therapy and Menopause". National Research Center for Women & Families, (2009).

[33] Saslow, D.; Hannan, J.; Osuch, J.; Alciati, M. H.; Baines, C.; Barton, M.; Bobo, J. K.; Coleman, C.; Dolan, M.; Gaumer, G.; Kopans, D.; Kutner, S.; Lane, D. S.; Lawson, H.; Meissner, H.; Moorman, C.; Pennypacker, H.; Pierce, P.; Sciandra, E.; Smith, R.; Coates, R. ,"Clinical breast examination: practical recommendations for optimizing performance and reporting", CA: a cancer journal for clinicians, Vol 54, Issue 6, PP 327–344, (2004).

[34] Yu YH, Liang C, Yuan XZ, "Diagnostic value of vacuum-assisted breast biopsy for breast carcinoma: a meta-analysis and systematic review", Breast cancer research and treatment, Vol 120, Issue 2, PP 469–79, (2010).

[35] http://www.dietandcancerreport.org Retrieved 2-10-2013.

[36] Eliassen AH, Hankinson SE, Rosner B, Holmes MD, Willett WC, "Physical activity and risk of breast cancer among postmenopausal women", Arch. Intern. Med, Vol 170 , Issue 19, PP 1758–1764, (2010).

[37] Hartmann LC, Schaid DJ, Woods JE et al., "Efficacy of bilateral prophylactic mastectomy in women with a family history of breast cancer", the new England journal of medicine, Vol 340 , Issue 2, PP 77–84, (1999).

[38] Meijers-Heijboer H, van Geel B, van Putten WL et al., "Breast cancer after prophylactic bilateral mastectomy in women with BRCA1 and BRCA2 mutations", the new England journal of medicine, Vol 345, Issue 3, PP 159–164, (2001).

[39] Nelson, HD; Smith, ME; Griffin, JC; Fu, R, "Use of medications to reduce risk for primary breast cancer: a systematic review for the U.S. Preventive Services Task Force.", Annals of internal medicine, Vol 158, Issue 8, PP 604–614, (2013).

[40] Cuzick, Jack; Sestak, Ivana; Bonanni, Bernardo; Costantino, Joseph P; Cummings, Steve; DeCensi, Andrea; Dowsett, Mitch; Forbes, John F; Ford, Leslie; LaCroix, Andrea Z; Mershon, John; Mitlak, Bruce H; Powles, Trevor; Veronesi, Umberto; Vogel, Victor; Wickerham, D Lawrence, "Selective oestrogen receptor modulators in prevention of breast cancer: an updated meta-

analysis of individual participant data", The Lancet, Vol 381, Issue 9880, PP 1827–1834, (2013).

[41] Olson, James Stuart, "Bathsheba's breast: women, cancer & history", Baltimore: The Johns Hopkins University Press, PP 9–13, (2002).

[42] http://www.cancer.org/cancer/cancerbasics/thehistoryofcancer/ Retrieved 2-10-2013.

[43] Aronowitz, Robert, "Unnatural history: breast cancer and American society", Cambridge, UK: Cambridge University Press, PP 22–24, (2007).

[44] Marc Lacroix, "A Concise History of Breast Cancer", USA: Nova Science Publishers, PP 59–68, (2011).

[45] Sulik, Gayle A, "Pink Ribbon Blues: How Breast Cancer Culture Undermines Women's Health", USA: Oxford University Press, PP 200–203, (2010).

[46] Bob Riter, "History of Breast Cancer Advocacy", Cancer Resource Center of the Finger Lakes, Retrieved 2-10-2013.

[47] http://www.cancer.gov/dictionary?expand=H Retrieved 2-10-2013.

[48] http://www.ncbi.nlm.nih.gov/pubmed/23820835, Retrieved 2-10-2013.

[49] Current Procedural Terminology, America Medical Association, PP 392, (2012)

[50] http://www.cancer.gov/ , Retrieved 2-10-2013.

[51] Carolyn Freeman; Halperin, Edward C.; Brady, Luther W.; David E. Wazer , "Perez and Brady's Principles and Practice of Radiation Oncology", Philadelphia: Wolters Kluwer Health/Lippincott Williams & Wilkins, PP 637–644, (2008).

[52] Dollinger, Malin, "Everyone's Guide to Cancer Therapy", Revised 5th Edition: How Cancer Is Diagnosed, Treated, and Managed Day to Day. Kansas City, MO: Andrews McMeel Publishing, PP 98–100, (2008).

[53] Maluta S, Romano M, Dall'oglio S, et al., "Regional hyperthermia added to intensified preoperative chemo-radiation in locally advanced adenocarcinoma of middle and lower rectum", Int J Hyperthermia, Vol 26 (2), PP 108–117, (2010).

[54] Laura Onose, Luminta Moraru, Mariana Carmen Nicolae, "Simulation of acoustic fields from medical ultrasound transducers", (2009)

[55] http://dukemil.egr.duke.edu/Ultrasound/k-space/node2.html Retrieved 2-10-2013.

[56] http://field-ii.dk/?news.html Retrieved 2-10-2013.

[57] Jorgen Arendt Jensen, "A model for the propagation and scattering of ultrasound in tissue", (1990)
[58] Jorgen Arendt Jensen, "FIELD: A Program for Simulating Ultrasound Systems", (1996)
[59] Jorgen Arendt Jensen, Darshan ,Gandhi, William D. O'Brien, "Ultrasound fields in an attenuating medium", (1993)
[60] M. Schlaikjer, S. Torp-Pedersen, J. A. Jensen, "Simulation of RF data with tissue motion for optimizing stationary echo canceling filters", (2003)
[61] Jorgen Arendt Jensen, Svetoslav Ivanov Nikolov, "Fast Simulation of Ultrasound Images", (2000).

Appendix A

Temperature scale

The range of temperature (35-45 ^{0}C) relative to our k-wave output scale (0 - 5) according to the programs which were created, and the values over 5 on scale means high temperature over 45^{o}C used for ablation so we use the appropriate scale which doesn't out of our range.

The following table shows the values of temperatures corresponding to the written scale in the figures which were introduced at chapter five from figure 5.2 to figure 5.25.

Scale (on figures)	Temperature (^{o}C)	Scale (on figures)	Temperature (^{o}C)
0	35.00	6	47.04
0.5	35.99	6.5	48.06
1	36.97	7	49.09
1.5	37.97	7.5	50.12
2	38.96	8	51.15
2.5	39.96	8.5	52.19
3	40.96	9	53.23
3.5	41.97	9.5	54.28
4	42.97	10	55.32
4.5	43.99	10.5	56.37
5	45.00	11	57.43
5.5	46.02	11.5	58.49

الملخص العربى

الغرض: عادة ما يتم التعامل مع سرطان الثدى عن طريق الجراحة والعلاج الإشعاعى والعلاج الكيميائى حيث ان العلاج الحرارى يعزز من تأثير العلاج الإشعاعى والعلاج الكيميائى من حيث السيطرة على الورم المحلى ومعدلات البقاء على قيد الحياة.

أيضا يتم العلاج بإستخدام الإشعاع الكهرومغناطيسى ولكن هناك اهتمام متزايد لإستخدام الموجات فوق الصوتية نظرا لعمق الاختراق وأفضل فى التركيز فى نقطة معينة . بالرغم من ذلك إلا انه لا يوجد حتى الان علاج كامل بإستخدام العلاج الحرارى ولذلك هذة الدراسة تصف التصميم النظرى لمصفوفة مراحل إسطوانية للموجات فوق الصوتية للإستخدام فى العلاج الحرارى وأيضا تم هذا التطبيق لحساب المنطة الحرارية المؤثرة على أورام الثدى وتم إيجاد النتائج.

المواد والطرق المستخدمة : نماذج الثدى التى شيدت من البيانات البشرية تم الحصول عليها من التصوير المقطعى والتصوير بالرنين المغناطيسى . حيث انه يتم تصميم المتغيرات مثل التردد، عدد العناصر الفيزيائية، عرض العنصر، الشق (التباعد بين العناصر) ، وقيمة الزاوية للحساس فوق السمعى للحصول على تركيز أصغر ما يمكن . وسوف يتم استخدام برنامج فيلد ٢ لمحاكاة الموجات الصادرة من الحساس الفوق السمعى وذلك بإستخدام الصوتيات الخطية . وسوف يتم أيضا استخدام صندوق أدوات اخر من الماتلاب ليعرض المجالات الغير خطية من الحساس فوق السمعى كيف يتم نمذجته .

تتكون هذه الرسالة من ستة فصول مقسمة كالأتى :

الفصل التمهيدى يعرض مقدمة مختصرة عن العلاج الحرارى والحاجة الى استخدام المستقبل، والهدف من هذة الرسالة، .

الفصل الثانى يشرح الخصائص الأساسية للموجات فوق الصوتية، يتم وصف نظام التصوير بإستخدام الموجات فوق الصوتية، يتم شرح أنواع الحساسات ، أنظمة التصوير، وتكوين الاشعة ودقة وضوح الصورة.

الفصل الثالث يحتوى على شرح تفصيلى لمرض سرطان الثدى من حيث علاماته وأعراضه، والعوامل الخطرة، وتشخيص المرض، والحماية منه، ونبذة تاريخية عنه. ثم يشرح العلاج الحرارى بانواعة ، والتحكم فيه، والاثار الجانبية له.

الفصل الرابع يقدم تسلسل محاكاة العمل متضمنا نماذج الماتلاب التفصيلية ، نتائج المحاكاة.

الفصل الخامس يقدم نتائج التوزيع الحرارى للحساس فوق السمعى .

الفصل السادس يقدم للقارئ ملخص كلى للنتائج المجمعة ، الاستنتاجات والتحسينات التى يمكن عملها مستقبلا فى هذا الموضوع.

"دراسة لتصميم مصفوفة مراحل اسطوانية للموجات فوق الصوتية للاستخدام في العلاج الحراري "

رسالة مقدمة من

أيمن سليمان سلمى محمد

إلى كلية الهندسة ببنها – جامعة بنها

كجزء من متطلبات الحصول على درجة ماجستير الهندسة والتكنولوجيا في تكنولوجيا الهندسة الكهربية من كلية الهندسة ببنها

اعتمدت وأجيزت من السادة الممتحنين

أ.د./ صلاح غازى رمضان **(ممتحناً داخلياً ورئيساً)**
أستاذ متفرغ بقسم الهندسة الكهربية، كلية الهندسة ، جامعة بنها .....

أ.د./ ناهد حسين سلومه **(ممتحنا خارجياً و عضواً)**
أستاذ الهندسية الطبية – المعهد القومى لعلوم الليزر – جامعة القاهرة .....

أ.د.م/ محمود فتحى محمود **(مشرفاً وعضواً)**
أستاذ مساعد ، كلية الهندسة ، جامعة بنها .....

اعتمدت من قسم تكنولوجيا الهندسة الكهربية **(رئيس القسم)**
أ.د.م/ غادة محمد عامر .....

اعتمدت من الدراسات العليا **(وكيل الكلية للدراسات العليا)**
أ.د./ هشام محمد البطش .....

اعتمدت من كلية الهندسة ببنها **(عميد الكلية)**
أ.د./ محمد السيد بسيوني .....

Benha University

Faculty of Engineering

دراسة لتصميم مصفوفة مراحل اسطوانية للموجات فوق الصوتية للاستخدام في العلاج الحراري

رسالة مقدمة من

أيمن سليمان سلمى محمد

كجزء من

متطلبات الحصول على درجة

الماجستير فى الهندسة والتكنولوجيا فى تكنولوجيا الهندسة الكهربية

تحت اشراف

أ.د.م محمود فتحى محمود

كلية الهندسة

جامعة بنها

د. وائل عبدالرحمن محمد

قسم الهندسة الكهربية

كلية الهندسة

جامعة بنها

٢٠١٤